1-1-2013

Experimental Investigation And Development Of An Extended Two Color Method (etcm) With Application To Internal Combustion Engines

Elena Florea
Wayne State University,

Recommended Citation

Florea, Elena, "Experimental Investigation And Development Of An Extended Two Color Method (etcm) With Application To Internal Combustion Engines" (2013). *Wayne State University Dissertations.* Paper 762.

EXPERIMENTAL INVESTIGATION AND DEVELOPMENT OF AN EXTENDED TWO COLOR METHOD (eTCM) WITH APPLICATION TO INTERNAL COMBUSTION ENGINES

by

ELENA FLOREA

DISSERTATION

Submitted to the Graduate School

of Wayne State University,

Detroit, Michigan

in partial fulfillment of the requirements

for the degree of

DOCTOR OF PHILOSOPHY

2013

MAJOR: MECHANICAL ENGINEERING

Approved by:

Advisor Date

DEDICATION

To my son, David A.

ACKNOWLEDGMENTS

I would like to express my sincere gratitude to my adviser, Dr. Dinu Taraza, for his constant support throughout my graduate education. With careful attention to detail, Dr. Taraza's invaluable advice steered my path in the great Sea of Engineering Knowledge. I consider myself very fortunate and blessed to have had the honor of working under his guidance.

I am very grateful as well to my professors, Dr. Naeim Henein and Dr. Marcis Jansons, for sharing their valuable insight while working with graduate students, such as myself, every day.

I would like to thank the members of my doctoral committee: Dr. Walter Bryzik, Dr. Kai Yang and Dr. Trilochan Singh. Each and every one of you had a significant contribution to my growth as a PhD. candidate.

Special thanks to Optical Engine Research Group: Dr. Marcis Jansons, Dr. Radu Florea, Kan Zha, Xin Yu, Eric Gingrich and Alex Davidson for their continued support. It was always a pleasure to work with the research team, and the friendly atmosphere always made it fun.

I will always look back with joy at the times spend with my fellow graduate students within the Center for Automotive Research with whom I shared long hours preparing for exams or setting up experiments.

Furthermore, I would like to gratefully acknowledge the financial support of the US Army TARDEC for the work conducted as PhD candidate at Wayne State University's Center for Automotive Research.

In the complexity of the PhD program machinery, every little bit helps. With this in mind, I would like to say thank you to: Rosalind Willis, Taquandra Grant and the wonderful people working at the front desk, Lidia and the machine shop staff for the daily dose of smiles and helpful attitude.

Last but not least, my sincere and special gratitude goes to my parents for their unending trust and love. And to the most important people in my life: my wonderful husband Radu and my amazing son David, you are the very reason for my life to be so incredibly beautiful.

TABLE OF CONTENTS

LIST OF TABLES

LIST OF FIGURES

NOMENCLATURE

Abbreviations

ARHR	apparent rate of heat release
AHR	apparent heat release
ARB	Air Resources Board
b/aTDC	before/after top dead center
C_2	free radical
CAFE	corporate average fuel economy
COV	coefficient of variation
CA50	crank angle for 50% heat release ATDC
CAD	crank angle degree
CARS	coherent anti-Strokes Raman scattering
CCD	charge coupled device
CH, CH*	free radical, electronically excited CH
CI	compression ignition
CMOS	complementary metal–oxide–semiconductor
CN	cetane number
CO, CO*	carbon monoxide, electronically excited carbon monoxide
CO_2, CO_2*	carbon dioxide, electronically excited carbon dioxide
DCN	derived cetane number
DEF	diesel exhaust fluid
DEM	dimethyl ether
DI	direct injection
DOC	diesel oxidation catalyst
DPF	diesel particulate filter
ECU	engine control unit

EGR	exhaust gas recirculation
EPA	Environmental Protection Agency
eTCM	extended two color method
FSN	filter smoke number
GHG	green house gas emissions
HCCI	homogenous charge compression ignition
HD	heavy-duty
HTHR	high temperature heat release
ICCD	intensified charge coupled device
IMEP	indicated mean effective pressure
IR	infra-red spectral range
JP8	jet propellant 8
LIF	laser induced fluorescence
LPPC	location peak premixed combustion
LRS	laser Rayleigh scattering
LTC	low temperature combustion
LTHR	low temperature heat release
M	flame molecule
MK	modulated kinetics
MMF	multi-mode fiber
NOx	sum of nitric oxide and nitrogen dioxide
NVH	noise – vibration – harshness
O	oxygen atom
OEM	original equipment manufacturer
OH, OH*	free radical, electronically excited hydroxyl radical
PE	potential energy

PCCI	partially-premixed charge compression ignition
PIC	pre-injection chemiluminescence
PMT	photomultiplier tube
PPC	partially premixed combustion
RCCI	reactivity controlled compression ignition
RCM	rapid compression machine
SCR	selective catalytic reduction
SI	spark ignition
SMF	single-mode fiber
SNR	signal to noise ratio
SOI	start of injection
SRS	spontaneous Raman scattering
TCM	two color method
TDC	top dead center
UHC	unburned hydrocarbons
ULSD	ultra-low sulphur diesel
UV	ultra violet spectral range (10nm to 400nm)
UV-Vis	ultra violet and visible spectral range (10 nm to 800nm)
VCO	valve covered orifice injector nozzle
VIS	visible spectral range
YM	year model

Symbols

A	area viewed by the detector
A_{cal}	aperture area for the blackbody calibration source
A_{cloud}	area of the soot cloud

B_λ	blue flame
C_1, C_2	model coefficients
$C_{(1)}$, $C_{(2)}$, $C_{(3)}$	coefficients obtained during the calibration process
C_λ, C_λ'	calibration constant for the optical setup
E_b	blackbody emissive power
E_s	soot emissive power
f_{12}, f_{23}	ratio of two detector signals
h	Plank's constant ($h=6.626069\text{x}10^{-34}$ Js)
H_λ	detector transfer function
I	pixel count (intensity)
K	coefficient proportional to the soot volume concentration
KL factor	is proportional to the soot volume fraction
L	the mean beam length for the considered volume of soot
L_{cal}	optical length from the detector to the blackbody calibration source
L_{exp}	optical length from the detector to the soot cloud
P	pressure
R^2	coefficient of determination
T	temperature
V_λ	detector signal
α	continuous function that characterizes the sooty diesel combustion
ε	emissivity of soot
ϕ	Equivalence ratio
λ	wavelength
Ω	solid angle subtended by the active area of the detector

Chapter 1. Introduction

Two major factors are driving today's internal combustion engine towards improved efficiency: the need to reduce the greenhouse gas emissions thought to be responsible for the global warming phenomenon [1, 2] along with increased fuel economy standards introduced by a number of national governments partially in response to increasing fuel demand, higher energy costs as well as national security considerations related to the current energy supply availability [3, 4, 5, 6, 7].

According to the prevailing scientific view, transportation related gaseous emissions are a major factor contributing to human health [8, 9] as well as climate change [8]. In the United States the Environmental Protection Agency (EPA) has been tasked by the US Congress with the authority of regulating these emissions and, over the last several decades, it has set increasingly strict emissions standards. In order to comply with these regulations OEM's and engine manufacturers applied in general two approaches: one is focused on improving the combustion process for a cleaner, more efficient combustion [10] and the second is focused on improving the efficiency and reducing the cost of aftertreatment devices [11, 12, 13, 14, 15, 16, 17, 18, 19].

In the following section details regarding the evolution of the combustion process improvements are presented along with the driving forces behind them.

The work presented here focuses mostly on the Diesel combustion technology, due to its high energy efficiency potential which will most likely be required to meet future Green-House Gas (GHG) emissions regulations [2] as well as higher fuel economy mandates (such as CAFE – Corporate Average Fuel Economy) [20]. Given the dominant role played by the heavy duty diesel engine in the US diesel market, the following emissions related discussion will focus on the heavy duty requirements, although the light-duty sector is facing similar challenges which are expected to result in similar engine architectures and combustion strategies.

First, in order to meet EPA's pre-2010MY heavy-duty NO_x emissions standards, most engine manufacturers have pursued the use of exhaust gas recirculation (EGR) without NO_x aftertreatment technology. A number of manufacturers relied on combustion strategies falling within the broad classification of Low Temperature Combustion (LTC) [21, 22, 23, 24, 25, 26, 27, 28, 29, 30, 31, 32] which is generally characterized by relatively long ignition delays and high degrees of premixed combustion. With ever increasing EGR rates, smoke became an issue [18, 33, 34, 35, 36, 37, 38, 39, 40, 41, 42, 43, 44, 45, 46], driving injection pressures higher, combustion phasing later in the cycle and lower engine system efficiency.

Subsequently, following EPA's 2010MY heavy-duty (HD) emissions standard decreasing the allowable limits for both tailpipe soot (0.01 g/bhp-hr) and NO_x emissions (0.2 g/bhp-hr) [47], most engine manufacturers adopted exhaust aftertreatment technologies such as Selective Catalytic Reduction (SCR) [13, 17, 18]. As a result of changing tradeoffs between the engine system and the aftertreatment system, the combustion strategy has shifted yet again. Lower EGR rates were employed [28, 36, 38, 39, 48, 49, 50], as the engine-out NO_x emissions were permitted to increase, allowing the recovery of some of the engine efficiency previously lost to emissions control constraints.

In regards to future engine emissions regulations, California's ARB (Air Resources Board), who is in charge of defining the state's emission standards, is indicating intent to further reduce the NO_x emissions by an order of magnitude compared to current (2010 emissions year) limit. ARP's decisions are generally viewed as precursors to regulations at federal level, thus the expectation of significantly tighter NO_x emissions standards in the future. However, given current SCR efficiency limitations [13, 17, 18] as well as increased Diesel Exhaust Fluid (DEF) requirements, the proposed standard will likely require a combination of high efficiency SCR with relatively high EGR rates, shifting the combustion strategy focus back toward a higher degree of premixed combustion with increased emphasis on the NO_x-soot tradeoff. It is thus expected that at least a fraction of the engine manufacturers will select one of the LTC combustion strategies to meet the future emissions targets.

Given the expected future trend of combustion system development, it is of interest to improve the application range of diagnostic tools such as the two color method (TCM) typically used in evaluating the properties of engine soot, such as temperature and volume fraction. This optical diagnostic method relies on the use of the light emitted by the soot particles along with a soot emissivity model in order to estimate the temperature T and optical thickness KL characterizing the soot cloud of interest in the engine development process. This assumption is reasonable for the "traditional" diesel combustion, where low degrees of premixed combustion result in very low amounts of blue-flame light emission compared to the soot related radiation. However, for LTC combustion modes this assumption is no longer applicable, especially for combustion strategies characterized by very large premixed combustion phases, such as the Partially-premixed Charge Compression Ignition (PCCI) strategies.

For these combustion modes soot is still of concern, as the mixture is not perfectly homogenous, but the application of TCM may be restricted by the presence of large amounts of blue flame radiation. The current work is focused on addressing this limitation of TCM and extends its range of applicability to highly premixed combustion regimes.

The aim is to obtain more information related to the combustion process and specifically on the soot formation and oxidation process. For this reason, the present research can be divided in two major sections.

The first section focuses on the development of a combustion optical probe and the optical experimental setup necessary for conducting the experimental work. On one hand, the optical probe developed is needed for providing information related to the combustion process from within the combustion chamber. Information regarding the soot formation and oxidation processes may be inferred from the measured signal. This provides complementary cycle resolved information regarding the soot evolution beyond the more widely employed engine-out soot measurements such as AVL's filter smoke number (FSN) which provide engine-out soot data. The benefits of applying the additional insight of in-cylinder soot evolution to combustion system development is well documented in literature [51, 52, 53, 54, 55, 56, 57, 58, 59, 60, 61, 62, 63, 64, 65, 66, 67, 68, 69, 70] and allowing the extension of the range of applicability of the TCM to partially premixed combustion modes could prove useful for future combustion system development needs.

With the engine development cycle in mind, the current work focuses on applying the soot measurements with an optical probe which requires minimum intrusiveness associated with the optical access. The specifics of the hardware implementation have been detailed in a number of previous publications [51, 52, 53, 54, 55, 56, 57, 58, 59, 60, 61, 62, 63, 64, 65, 66, 67], thus the focus of this work is on the development and evaluation of the optical technique.

The objective of the second section of the current research is to provide the theoretical background and experimental evidence needed to describe the proposed optical diagnostic tool, the extended two-color method (eTCM). This method attempts to extend the domain of applicability of the classical two color method within the area of strong CO continuum interference as well as providing a method of testing the validity of the conventional two-color method. Further, it provides additional information regarding the strength of the radiation associated with the CO flame continuum.

Towards this goal, the work was conducted on a fully accessible optical engine, which allowed the use of multiple synchronous optical measurements targeted towards the evaluation of the proposed optical diagnostic tool.

Chapter 2. Literature review

In the first part of the literature review, a short overview of the internal combustion engine is presented with focus on the diesel combustion strategy along with its advantages and challenges; following, other combustion strategies are introduced, with an emphasis on low temperature combustion (LTC). Furthermore, the topic of optical diagnostics is introduced along with a description of their applicability to the investigation of practical combustion systems.

This chapter is focused on reviewing previous work related to combustion sensing as well as engine applied investigations of the two-color method targeted towards soot temperature and optical thickness measurements.

The second part of this chapter outlines several optical-fiber based techniques developed for combustion monitoring.

Furthermore, the third part of the literature review chapter concentrates on the research that has been carried out in the field of two-color method technique. A discussion is presented with regards to the details of the two-color method implementation in practical combustion systems, while a description of the method itself is presented in a subsequent chapter (3.1).

2.1 Combustion engines

For the past 100 years the internal combustion engine maintained its lead as the main propulsion system for the ground transportation and marine applications. Detailed information regarding the history and progress of the combustion engines is presented by Heywood [71].

In its early days, the engine had to overcome challenges such as increased power density and efficiency followed later on by the need for reduced emissions.

Recognizing increased environmental concerns within their respective societies, an increasing number of governments are proposing legislation aimed towards reducing green-house gas (GHG) emissions of which the main contributor is CO_2. Carbon dioxide is an unavoidable by-product of hydrocarbon-based fuels; as such, a significant tool available in enabling nations to meet the proposed reduction in GHG emission is the improvement of the fuel efficiency of future combustion systems. Among the engine subsystems, the combustion chamber has significant potential for efficiency improvement and much research and development efforts are being dedicated towards achieving that potential now and in the foreseeable future.

Thus the importance of investigating the details of the combustion process with all engineering tools available, including optical diagnostics of combustion.

2.1.1 Internal combustion engine classification

Traditionally the internal combustion engines have been classified based on the ignition method. Two broad classes are typically identified based on this criterion as spark ignition engines and compression ignition engines. The spark ignition (SI), engine also known as Otto engine, is characterized by ignition of the fuel air mixture with the aid of a spark generated by a sparkplug. At the same time, the compression ignition engine (CI), commonly referred to as a Diesel engine, uses the heat of compression to autoignite the fuel that is direct-injected in the combustion chamber. Over the past decade a significant amount of combustion research targeted towards attaining the maximum efficiency with minimum emissions has yielded several other combustion modes (such as HCCI, PCCI and dual-fuel strategies) which blur the lines between the aforementioned combustion modes.

Given the focus of this work on self-ignited combustion modes, the next subchapter provides more information regarding the characteristics of diesel engines.

2.1.1.1 Diesel engines

Diesel engines are known for their high efficiency, partly due to the high compression ratio achievable in this kind of engine. The transportation sector is claiming 28% of the total energy usage in the United States (see Fig 2.1) out of which Diesels contribute to more than 20%, mostly through heavy duty applications, such as class 8 trucks. The rest is divided by gasoline fuel 61% and aviation 12% [72].

Modern diesel engine technology has improved considerably with respect to previous generations in terms of NVH (Noise – Vibration – Harshness), engine cold-start and emissions with particular highlight on PM (Particulate Matter/Soot) and NOx reduction. The diesel engine still maintains unsurpassed thermal efficiency, which makes it attractive in an economic environment in which energy costs are expected to grow over time.

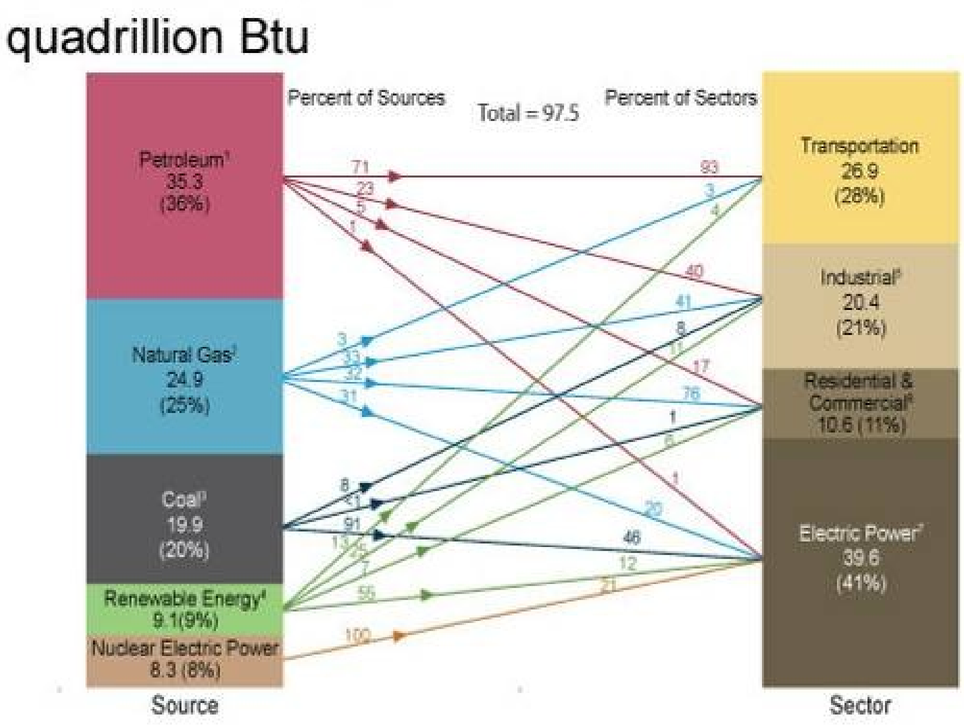

Fig 2.1 – US energy usage consumption by sector 2011 [73]

This has been accomplished largely through the use of the common-rail injection system, which allows more precise control of fuel metering, timing, injection pressures and the number of injection events. Improved control of engine parameters such as exhaust gas recirculation (EGR) rates, injection timing and pressure, further allow the diesel engine to operate in conditions which minimize pollutant formation while maximizing efficiency. The successful application of such diesel engine controls requires knowledge regarding spray formation, and especially, ignition characteristics. The currently reported work aims towards providing an additional tool for the development of the future high-efficiency internal combustion engine by providing quasi real-time combustion information regarding in-cylinder soot quantity and temperature as well as characterization of the premixed, smokeless phase of the combustion process.

2.1.1.2 Low Temperature Combustion – LTC

Low temperature combustion (LTC) is a type of combustion that has been previously shown to combine the advantages of both spark ignition combustion and compression ignition combustion by increasing the degree of premixed combustion of a compression-ignited engine. LTC attempts to operate within the low-PM and low-NOx regions of the well-known Φ-T map (see Fig 2.2) while maintaining good thermal efficiency. LTC is generally achieved by lowering the compression ratio as well as by employing higher rates of EGR [25, 28].

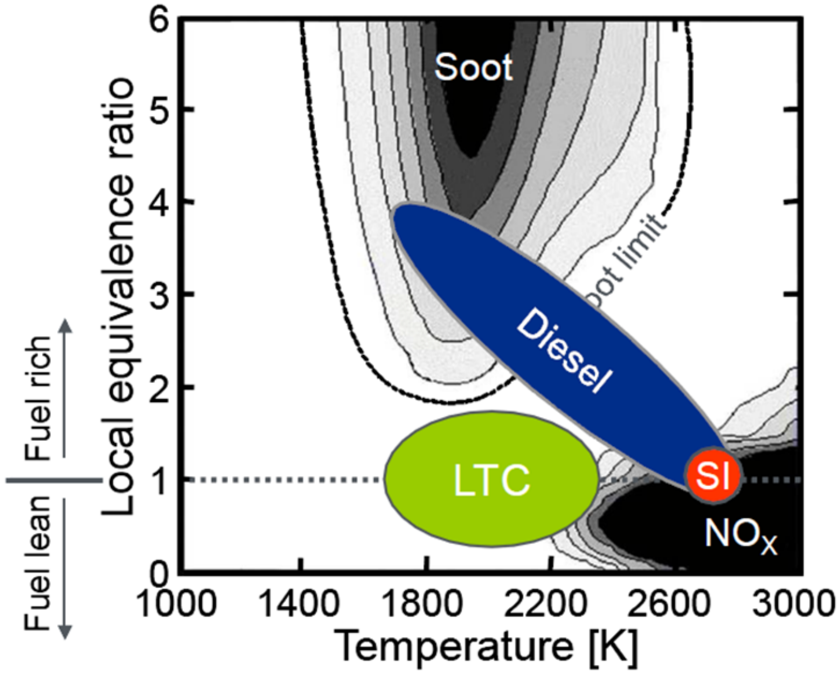

Fig 2.2 – LTC enables high efficiency with low emissions [74]

Among the most important combustion modes falling within the LTC category include: Homogeneous Charge Compression Ignition (HCCI) [29], Premixed Charge Compression Ignition (PCCI) [23], Modulated Kinetics (MK) [26], and Reactivity Controlled Compression Ignition (RCCI) [31].

Because the combustion is not initiated with the aid of a sparkplug but it rather employs the autoignition of the mixture as a diesel engine does, some of LTC combustion modes (such as HCCI) face the additional challenges in controlling the combustion phasing [21, 24, 32]. Another constraint is placed on the maximum load and/or minimum EGR rate that can be utilized in order to avoid unnecessarily high rates of pressure rise [22, 30].

In the end, combustion phasing and duration can be controlled by varying different parameters such as charge dilution, injection timing [24], air intake temperature or through different chemical compositions of the fuels [22, 31]. Another option of dealing with the combustion control at high loads was proposed by

Walter [32] with what the author called a dual mode engine application, where for part load the engine has an HCCI combustion mode while for the full load it switches to conventional diesel.

2.2 Optically accessible engines

In order to gain the knowledge regarding the details of the combustion process required to address the challenges facing the internal combustion engine, optical diagnostics of combustion have seen increasing application in different areas of internal combustion engine research. The set of tools typically includes visualization of sprays, mixture formation processes, auto-ignition, combustion, and pollutant formation within the combustion chamber. As a result, a number of research engines have been modified or developed to facilitate optical access. Depending upon the degree of intrusiveness of the optical access required, several types may be distinguished.

At one end of the spectrum are the production-grade engines with minimum modifications required to insert either a small optic-fiber access or a small endoscope attachment. These relatively small modifications maintain the integrity of the combustion system and the combustion process may be investigated in a highly-realistic environment. Typical issues associated with this approach are related to the size and quality of the optical access as well as the limited range of optical diagnostic that may be employed.

At the other end of the spectrum are model combustion systems, such as constant volume reactors and rapid compression machines (RCM). Typically these combustion systems are suitable for experiments where precise and elaborate optical experiments are needed and the combustion conditions may be simplified significantly compared to the actual combustion system being modeled.

Somewhere between these two extremes lies a range of dedicated research engines typically called “optically accessible engines” which provide a compromise between the quality of optical access and the level of modifications brought to the combustion system. As a result, there are unavoidable differences between the optically accessible research engine and the metal engine in terms of materials, cooling, heat transfer within the combustion chamber, blow-by gases, exhaust gas recirculation (EGR) composition as well as emissions [49, 75, 76].

To start with, pressure and heat release are affected by the slightly larger TDC clearance volume of the optical engine due to larger crevice volumes. For the same reason, greater fueling rates are necessary in order to attain the same load as an all metal engine. Also to counteract the lower compression ratios encountered in the optical engine, higher intake pressures and temperatures are employed [49].

Secondly, in order to lower the temperature in the combustion chamber due to modifications of the cooling system as well as different thermal conductivity of the optical materials used, a skip fire operation of the engine is applied during testing [77], [78].

However, these modifications brought to the engine in order to gain optical access are necessary in order to collect significant information for the optimization of the combustion process for production engines.

For this purpose, Colband et al. [49] have conducted a comparison between an optically accessible engine and a similar geometry all metal engine. The authors have looked at combustion performance and engine out emissions, analyzing the effect of injection strategy and fuel consumption for the same load and thermodynamic conditions. The results show that unburned hydrocarbons (UHC), carbon monoxide (CO) and soot emissions follow the same trend for the two types of engines just that for the optical engine the values were slightly higher.

In order to have optical access to the combustion chamber, one can employ one of three ways: access through the cylinder head, cylinder liner or piston. The optical access can be a full optical access or partial optical access. Also the materials the windows are made of can be made of: optical glass (fused silica, fused quartz) or crystals (sapphire). These two types of materials are most suitable due to their resistance to high temperatures and pressures as well as having a good transmission in the UV region of the spectrum. Additionally, a history of optically accessible engines: two stroke engines, SI engines and CI engines with different designs for the windows is presented by Zhao et al. in [76].

2.3 Sensors for monitoring combustion parameters

For one thing, the internal combustion engine of the 21 century is a complex system that continues to be enhanced in order to offer increased performance, better fuel economy, and lower emissions. In order to improve these engine parameters there is a necessity to monitor and better understand the combustion process. However, diesel combustion is a complex process; additionally, the combustion chamber is a challenging thermal and mechanical environment for a sensor.

Several classes of combustion sensing technologies may be distinguished. For instance, sensors that measure the in-cylinder combustion pressure can be classified as: sensors for direct in-cylinder pressure measurements or indirect cylinder pressure measurements.

The category of direct in-cylinder pressure sensors includes piezoelectric, piezoresistive and optical-based pressure measurement (deflected membrane sensors). Indirect pressure measurements include cylinder head deflection and change in cylinder head sealing gap measurement sensors as well as engine-speed based cylinder pressure reconstruction.

However, the most common sensor used for measuring in-cylinder pressure of combustion in engines is the piezoelectric transducer. Its wide use is due to its advantages, such as: dynamic and continuous measurement of the combustion pressure based on the crank angle, resistant to radiation interference, stable repeatable operation and long service life.

On the other hand, the pressure transducer is facing disadvantages as well. One of the most concerning is the measurement accuracy affected by thermal shock [79, 80, 81, 82] for certain operating conditions. One option to this problem is the use of water cooled pressure transducers but this introduces another degree of complexity to the system. Other disadvantages include: high costs and difficult mounting.

The indicated data provided by a pressure transducer has been a fundamental tool for the diagnostic of the combustion system for several decades now. It is currently employed for both research and development purposes. However, most applications would benefit from additional information beyond the indicated data, such as optical-based measurements mentioned in the previous paragraphs.

Subsequent sections will provide a description of the main classes of optical-based sensors available commercially or previously described in literature.

2.3.1 Optical fiber sensors

An optical fiber is a transparent, flexible fiber that transmits light along its axis operating on the principle of total internal reflection. The transparent core is surrounded by a transparent cladding material that has a lower index of refraction (see Fig 2.3 and Fig 2.4). That is to say, the fiber operates as a waveguide.

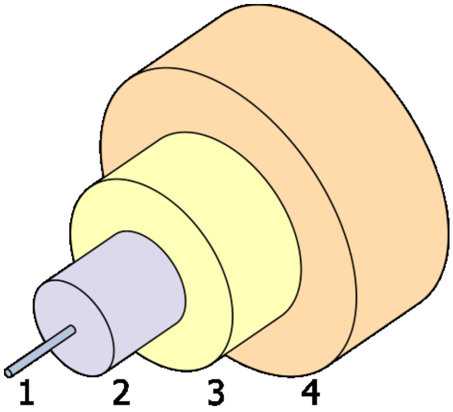

Fig 2.3 –Single mode optical fiber structure (Author: Bob Mellish)

Where: 1 – core; 2 – cladding; 3 – buffer; 4 – jacket

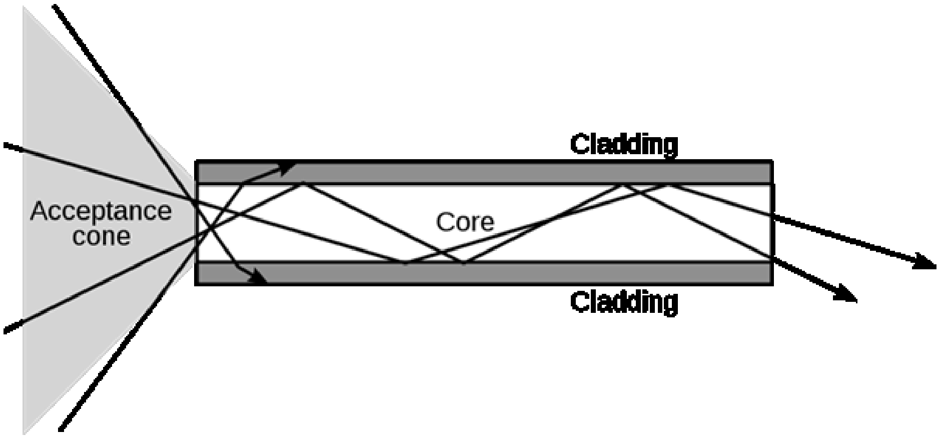

Fig 2.4 – Optical fiber [83]

Depending on the number of propagation paths, optical fibers can be divided in single-mode fibers (SMF) that supports a single mode or multi-mode fiber (MMF) that supports many propagation paths. Also, the acceptance cone is the maximum angle at which light can enter the fiber in order to propagate in the core without light leakage (see Fig 2.4 – Optical fiber). The sinus of this maximum angle is called numerical aperture (NA) of the fiber.

A typical optical fiber is made of glass, plastic or sometimes sapphire. Optical fibers have been historically developed for signal processing applications, such as high-bandwidth communication networks. However, a range of optical measurement as well as optical imaging techniques have been developed over the last several decades.

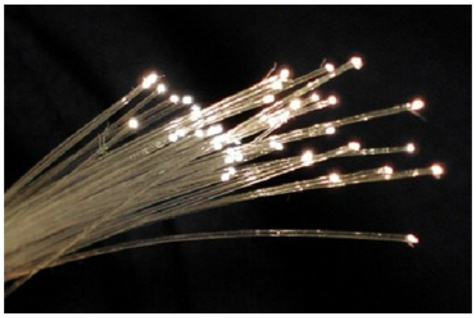

Miguel and Higuera [61] classified optical fiber sensors according to the domain and type of magnitude to be measured in the next classes: mechanical, thermal, electromagnetic, radiation, chemical composition, flow and turbulence of fluids, and typical magnitudes for the biomedical field.

On one hand, the main advantages of the fiber optic are derived from the dielectric property not to have any electromagnetic, chemical or electrical external interference. That makes it ideal for applications in hostile, corrosive environments or even environments with elevated risk of explosion. Also, due to its high fusion point optical fiber has high temperature resistance. Other advantages are the small dimension and light weight of the optical transducers. When compared to conventional sensors optical fiber has greater sensitivity, dynamic range and resolution. The signal generated or detected by the optical fiber does not deteriorate with the distance traveled due to the excellent capability as a transmission channel.

Last but not least, it is the great cost reduction of a sensor system when compared to traditional sensors.

Due to their small size and good light transmission capability, optic fibers have been employed in internal combustion engine investigations.

In 1985 Murray et al. [62] were discussing the necessity and advantages of a fiber optic sensor for in-cylinder combustion measurements. Clowater [51] developed a fiber optic imaging system with the aim of enhancing flow visualization studies. In fact, in 1994 Pendlebury and Nwagboso surveyed the available literature regarding the application of in-cylinder fiber optic measurements [64]. The authors highlight that these are the lowest cost sensors for nonintrusive measurements into the combustion chamber.

2.3.1.1 Optical fiber sensors for pressure measurement

In 1988 Witze [67] enhanced a spark plug with eight optical fibers mounted on a ring. He transmitted the light emitted by the flame through a fiber optic cable to a photomultiplier tube and to the data acquisition system. In order to obtain the average flame velocity, the time elapsed between ignition and detection of flame by the sensor was measured.

Other studies have been conducted using fiber optic sensors integrated in a spark plug such as the ones by He [53], Jie [54], Poorman [65] and Kawa [55] . The author [53] emphasized the small size and low cost system that can provide valuable information regarding the initial flame development. Jie [54] reports data related to flame propagation used to optimize fuel injection timing. Poorman [65] has conducted tests on a single cylinder gasoline stationary gen-set engine. He is also stressing the low cost, good performance and durability of the sensor developed.

2.3.1.2 Optical fiber sensors for temperature measurement

Yan et.al. [84] described an optical radiation probe that consisted of an trifurcated optical fiber bundle component exposed to the combustion chamber through a 0.25 inch diameter sapphire rod window. The rest of the components used in the optical setup are: condensing lenses, bandpass filters and photodiode detectors as it can be seen from Fig 2.5. The experiments reported were conducted on a single cylinder Cummins diesel engine. The engine cross section illustrated in Fig 2.6 shows the optical window positioning as well as the 14° field of view of the optical radiation probe employed by the authors for the experimental testing. A second design had the capability of a 180° field of view but the downside of the respective probe was the fouling of the window due to soot deposits.

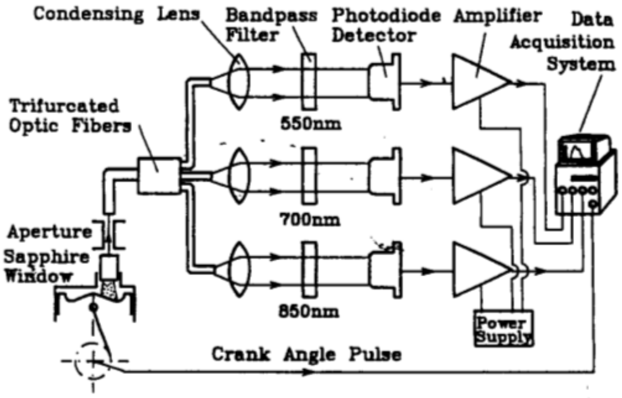

Fig 2.5 – Yan and Borman's schematic of the optical setup [84]

Different designs were employed until one design was able to sustain a clean window even for full load conditions. This optimum design is shown in Fig 2.7 and it consists of a well defined gap between the window surface and the bottom of the restriction sleeve of 1.27 mm.

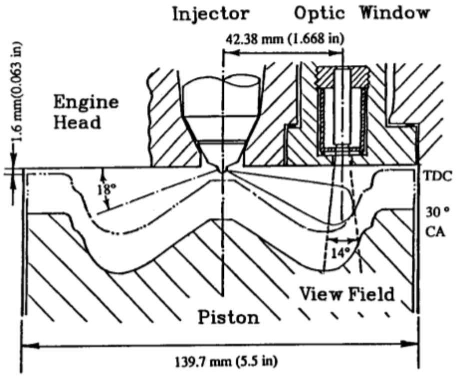

Fig 2.6 – Cummins engine cross section and optical window positioning [84]

The authors were interested in obtaining direct information related to flame temperature, soot concentration and radiative heat transfer through the use of the two-color method [85]. This optic measurement technique is described in detail in a later section (3.1). The three detectors were receiving light that was filtered for the 550 nm, 700 nm and 850 nm. However, the authors have chosen the 550 and 850 nm wavelengths for the comparisons presented in the paper [84].

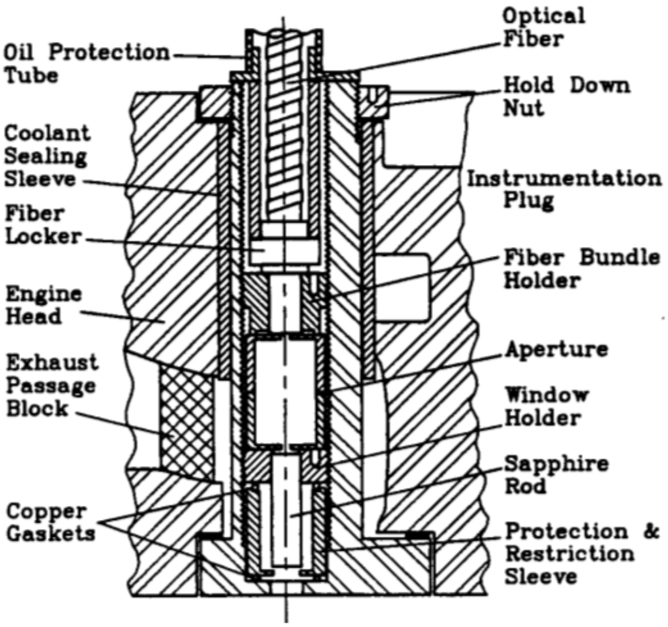

Fig 2.7 – Optimum design of the radiation probe that keeps the window clean [84]

Also, another approach was investigated by Shakal and Martin [86]. In order to gather information from a large area of the combustion chamber, they used an optical setup with a fiber optic bundle and acquired photographs during the combustion cycle. Subsequently the two-color method was applied to the photographs in order to determine the soot temperature and optical thickness factor KL. The full field optical setup consisted of a coherent fiber-optical bundle, a microscope objective lens with a 10x magnification, an image doubler and an intensified charge injection device (CID) camera. The experimental optical setup is presented in Fig 2.8. Two wavelengths were selected: 550 and 650 nm. And the optical access to the two-stroke direct injection diesel engine combustion chamber was provided through a sapphire window mounted in place of a pressure transducer.

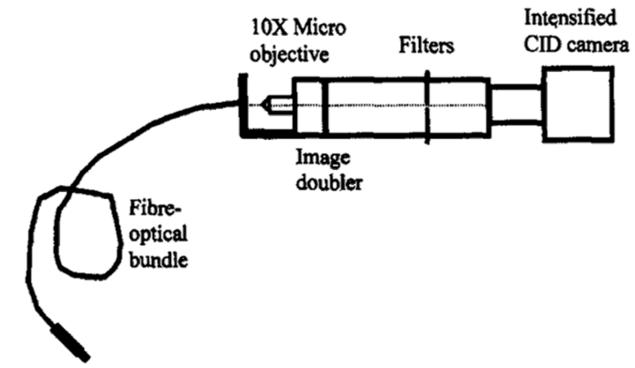

Fig 2.8 – Experimental optical setup for soot temperature and concentration measurements [86]

Li and Wallace [87] were also interested in investigating soot temperature and optical thickness in a diesel engine. They used three optical probes with direct access to the combustion gases through the cylinder head for their experimental work.

Also, Struwe in 2003 [88] used two radiant probes to measure total hemispherical in-cylinder radiant heat transfer. The probes were used one at a time and were mounted in the cylinder head in place of one of the exhaust valves. The design was based on the optical radiation probe developed by Yan and Borman [84]. Again, the self-cleaning feature of the probe played a major role in the design process as well as data analysis.

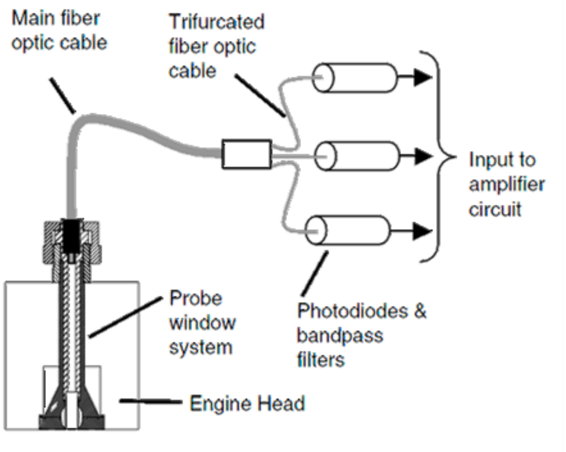

Fig 2.9 – Components of the optical system [88]

Fig 2.9 represents the components of the optical system. Also, the three wavelengths selected by the author were: 750 nm, 830nm and 1000 nm.

Additionally, Hall et al. [52] employed a fiber optic infrared spectroscopic sensor to measure the residual fraction of burned gas. Furthermore, Kawahara et al. [56, 57, 58] developed a fiber optic sensor as part of a heterodyne interferometry system to measure in-cylinder temperature of burned and unburned gases on an SI engine. The optic sensor has a sapphire window and a metal mirror. Even though the authors have used an SI engine for their tests they call attention to the benefits of the sensor that can be mounted on any engine in place of the pressure transducer. The same system was used by Lee [60] to obtain transient measurements for unburned gas temperatures.

Also, as a part of a spectroscopic system, Lan [59] has used a fiber optic sensor to measure the H_2O mole fraction and gas temperature in an HCCI engine. This all fiber laser sensor system was capable to provide real time in-cylinder temperatures but the authors faced the challenge of improving the system in order to eliminate the measurement errors.

Fig 2.10 – AVL sensor installed in glow plug adapter [89]

Another sensor developed for combustion monitoring with a fiber optic cable component is the one from AVL. The sensor, installed in a glow-plug adapter, is shown in Fig 2.10 and is part of flame analysis system designed for diesel engines. The field of view of the sensor is of 90°. The system has the capability to monitor soot evolution, formation and oxidation. The working principle is based on measurement of the emitted radiation coming from soot. Then the information is evaluated using the traditional two-color method for the 600 nm and 950 nm wavelengths [89]. The classical interpretation of the two color method (TCM) will be described in the following section

2.4 In-cylinder gas temperature measurements

When it comes to temperature measurements one thinks to thermocouples. However, for the case of in-cylinder gas temperatures thermocouples fall short when it comes to durability and time response. That is why this type of measurements has been dependent until recently by optical techniques.

The line-of-sight techniques used for this type of temperature measurements can be classified as radiation thermometry and spectroscopic techniques.

In recent years, laser based diagnostics have been developed such as spontaneous Raman scattering (SRS), laser Rayleigh scattering (LRS), coherent anti-Strokes Raman scattering (CARS), and laser induced fluorescence (LIF).

With the exception of two-color method the techniques mentioned above do not constitute the subject of the current work and so no comprehensive explanation is going to be provided here; however, detailed information can be obtained from multiple sources including the book published by Zhao [76].

2.5 Two-color method

The two-color method is a technique that has been developed in order to obtain information related to flame temperature and soot concentration in a diesel engine.

The two-color method looks at the soot spectral radiation intensity and measures the soot temperature and optical thickness by performing optical measurements at two discrete wavelengths. In order to better understand the process, some elementary information related to spectra of flames is presented in the next paragraphs.

Gaydon and Zizak [90, 91] classified the flame emission spectra in two basic types of spectra: discontinuous and continuous spectra. The first category of discontinuous spectra includes atomic spectra or line spectra characterized by isolated lines emitted or absorbed by free atoms experiencing electronic transitions from one energetic level to another; and molecular spectra or band spectra described by transitions in between energetic levels of molecules. Band spectra of free radicals such as CH, OH and C_2 are the most well-known and well studied band spectra in hydrocarbon flames.

In the second category are the continuous spectra such as the spectra radiated by the sun or the spectra emitted by a candle. The spectrum of a typical flame covers the ultraviolet (UV), visible (VIS) and infra-red (IR) regions of the electromagnetic spectrum.

Now, considering the structure of flames, two major types are generally observed: premixed flames and the non-premixed flames [90, 92]. In the case of premixed flames, the fuel and air or oxidant are well mixed prior to combustion. For the non-premixed flame or diffusion flame, little mixing generally takes place before combustion starts. The main mixing mechanisms of the fuel with the surrounding air are convection and diffusion. As the diffusion process is generally slower than the kinetically driven combustion process, it is constraining the rate at which the combustion process is evolving.

In practice premixed flames can be observed to be blue to bluish-green in color. As an example, the blue color of the carbon monoxide flame is caused by the emitted photon resulted from the chemical reaction of carbon monoxide with oxygen. This will be addressed in further detail in section 3.5. At the same time, diffusion flames appear as bright yellow. In this case the color is due to the blackbody-like radiation associated with the hot soot particles.

With respect to the topic of interest in this work, the classical diesel combustion starts with a small amount of partially premixed combustion followed by the main phase, the diffusion control combustion.

The roots of the soot optical thermometry technique are based on the two-color method initially developed in the 1940’s by [93]. The two-color method proposed by the researchers works by measuring the soot radiation intensity at two different wavelengths, hence its name. The method describes the equations and the assumptions for computing the soot temperature T and soot optical thickness factor KL (see equation (3.9) below for further details). Also, soot volumetric fraction and gravimetric density can be obtained by considering an additional set of assumptions regarding the optical properties of the associated soot particles, such as it complex index of refraction.

The classical two-color method described here is restricting the field of view of the detector to a small, well defined area. In this way, the spatial resolution is increased whereas the instrument sensitivity is reduced due to the fact that less radiation emitted by the soot is reaching the detector. Another reason for reducing the field of view is to increase the probability of having it filled with a soot cloud of homogenous properties. Should the soot cloud not fill the entire detector area, the estimated temperature would be underestimated.

In their review of the optical techniques for in-cylinder temperature measurement, Zhao and Ladommatos [94] offered a discussion regarding the selection of parameter α (see section 3.1 for further details) as well as regarding the selection of the two measurement wavelengths for both the visible and the infrared spectral regions. Several previous publications described the details of the experimental technique, including the calibration requirements.

The KL factor is sensitive to cycle-to-cycle variations, while there is a lower impact of these factors on the estimated soot temperature. The typical solution to this high KL sensitivity is the application of extensive temporal averaging. In consequence, as the traditional two-color method increases the expected accuracy by targeting a smaller area of the emitting soot cloud, the accuracy is negatively impacted by the temporal averaging process, as no two soot clouds are expected to be perfectly identical.

Thus, it is postulated here without further proof that the temporal and spatial averaging processes yield similar accuracies.

With regard to the temporal averaging, there are two methods to obtain T and KL On an average basis. According to the first method, used by Matsui [95], the measured detector signals are averaged for each crankangle and then the corresponding T and KL values are calculated. While according to the second method, T and KL are computed first for each crankangle for every cycle followed by averaging. Yan and Borman [84] have compared the two methods and concluded that there is no significant difference in the results obtained for T and KL for the combustion systems the authors investigated. However, in practice the first method is preferred for two reasons. One is that it is faster, as a the solution to the non-linear system of equations is obtained for a vastly reduced number of points. The second reason is associated with the improvement of the signal to noise ratio of the analog signals used for computing T and KL.

Another concept that should to be discussed with regard to the two-color method is related to the source of the radiation used in estimating T and KL. The method assumes that the radiation is generated only by soot, with the reflections and scattering being ignored. However, in a real combustion system, the detected signal is influenced by radiation emitted by the combustion chamber walls as well as radiation reflected by the same walls.

Whenever the two-color method is applied, as it is in this work, in the visible spectral range, the radiation emitted by walls can be safely ignored, as the surface temperature of the walls is much lower than that of soot [94]. However, the effect of the radiation reflected by the walls is significantly higher, Matsui [96] showing that for the case of low soot concentration the KL error is as much as 10% for high soot concentration. The KL estimation error is accompanied by a temperature estimation error of about 2 – 3 K. In a typical application of the two-color method is largely impossible to perform a direct measurement of the amount of radiation reflected by the combustion chamber walls and, as a result, these errors are accepted as unavoidable and contribute to the total measurement uncertainty.

On the other hand, one of the advantages of the two-color method is that it is easy to implement and can provide valuable insight through sensitivity analyses (i.e. comparison against data obtained using the same experimental setup). For example such analyses have been performed to measure the differences between fuels [97, 98, 99] or different injection techniques [100]. A second benefit is that it does not require an external light source, as the method relies on the light emitted by soot particles. Finally, by taking advantage of the fast response detectors, as in the case of the current research, real time monitoring of the soot concentration and distribution can be achieved.

There are some challenges as well. One such challenge is that TCM it is a line-of-sight method. The third dimension, the depth, is compressed and accounted for in the 2D image that is being analyzed. The non-uniformity in temperature and concentration of soot within the soot cloud is going to influence the calculated flame temperature and KL factor. Also, the flame closer to the detector is going to have a greater influence on the measured temperature than the flame further away mostly due to light absorption effects. The gradient distribution in soot concentration along the line-of-sight has a smaller influence on the measured temperature than the gradient dispersal of soot temperature [84, 94, 101].

The method assumes that the temperature is spatially uniform along the line of sight. Consequently, the information related to the temperature and optical thickness is obtained when evaluated against a calibration light source for the same wavelengths. More details related to the mathematical background of the two-color method are provided in subchapter 3.1. Also, the specifics regarding the calibration procedure of the optical setup used in the current research are presented in subchapter 0. In fact, the classical two-color method is a "line-of-point" measurement. In order to expand the field of view from a small area to a two dimensional image, the two color method can be used in conjunction with high-speed cameras or CCD cameras.

The two-color method was used by Hottel and Broughton [85] in 1932 on an open flame application and Uyehara [93] used it in 1946 for diesel flame temperature measurements. These results were reported from a single point measurement within the combustion chamber. Matsui *et al*. [96] extended the method to a full view, 2D high speed images to obtain both temperature and soot concentration with results obtained from a direct injection diesel engine. Other applications of the technique include studies regarding the effect of fuel properties on in-cylinder soot concentration [102], the effect of multiple injections [86] on the combustion process and soot emissions [100], the effect of the injection strategy and injection timing on soot and NO_x formation [103]. The full field two-color method application for 2D temperature and KL factor determination covers a wide range research areas. A few examples include the work of Kobayashi [104] in his research on a single cylinder, optically accessible diesel engine, Miyamoto [105] studied the effect of oxygenated additives on the combustion process and emission formation, Arcouomanis [46] analyzed the effect of EGR on flame temperature, Winterbone [106] examined the effect of swirl on combustion and Shiozaki [50] gained more insight on the reliance of OH radical emissions on flame temperature.

Of particular interest for the current research is the work published by Musculus [101] at Sandia National Laboratory. The author applied the two-color method in order to measure the temperature and heat transfer with the goal of correlating the soot radiative heat transfer to NO_x formation.

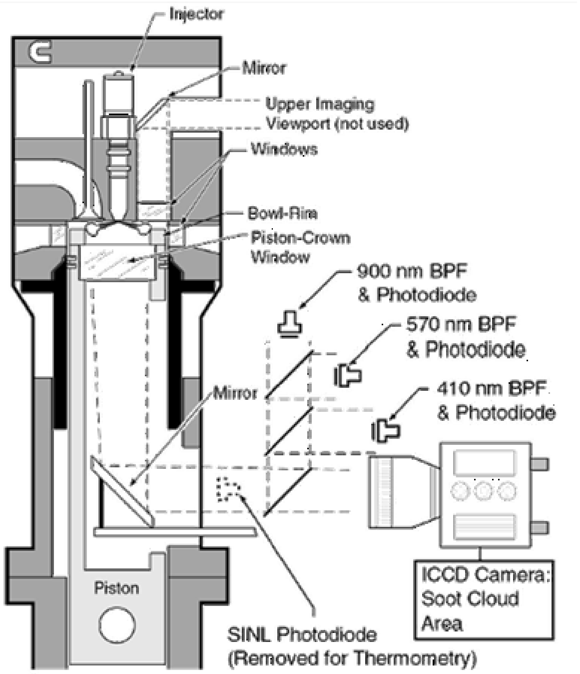

Fig 2.11 – Optical setup for temperature and heat transfer measurements – Musculus [101]

The optically accessible, single cylinder, direct injection (DI) diesel engine is shown in Fig 2.11. Similar to the classical Bowditch arrangement, a mirror is placed under the extended piston at a 45° angle and it offers optical access through the piston crown window into the combustion chamber. Soot thermometry is performed with the help of an ICCD camera and three photodiodes. Elements of the optical setup are three beam splitters as well as three bandpass filters placed at 410 nm, 570 nm and 900 nm. The ICCD camera is used by Musculus to estimate the surface area of the soot cloud. Experiments were carried with different start of injection (SOI) timings and the corresponding engine out NO_x emissions were recorded at the same time. The author concludes that at late SOI and with a corresponding increase of the premixed burning phase, the NOx emissions were also increasing. This behavior was shown to be influenced by the reduced quantity of soot that is being formed. Less soot formed less radiation emitted by the soot and thus an increased flame temperature which farther can be translated as higher NO_x emissions.

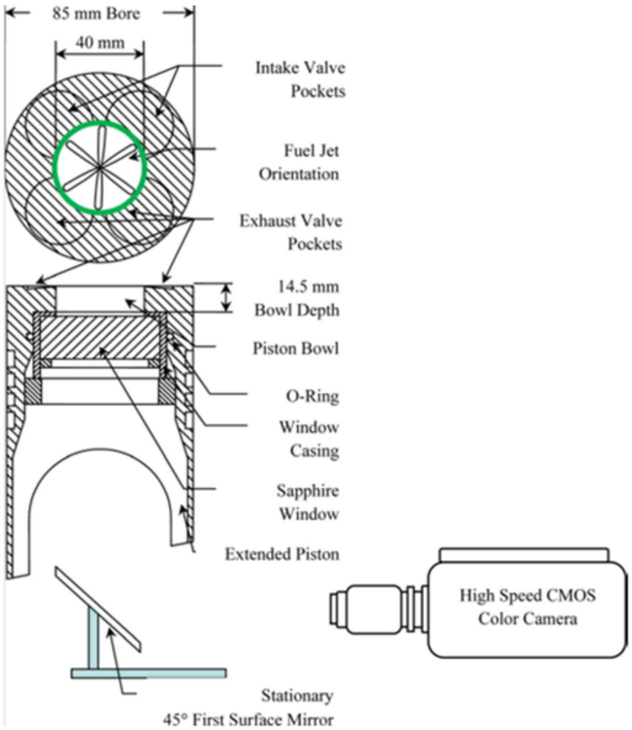

Fig 2.12 – Experimental setup for the optically accessible diesel engine [98]

Recent papers focused on the in-cylinder soot evolution, employing the technique of two color method, are the ones from Wayne State University's Center of Automotive Research group [97, 98, 99]. The authors are using the same optically accessible diesel engine (see also Fig 2.12) that has been employed in this work. The experimental setup is described in detail in Chapter 4.

Yu *et al.* [97] compared the in-cylinder soot evolution of two fuels, JP-8 (a kerosene based jet fuel widely used by the US Military) and ULSD. Yu has employed three approaches for his comparison. First, engine out soot measurements were obtained by using an AVL MicroSoot Sensor. Second, for his optical set-up the author used the high speed CMOS color camera in order to obtain images from which temperature and optical thickness factor KL information can be extracted. And third, a chemical kinetic-coupled CFD model was developed and utilized for understanding the third dimension that was not available experimentally. Also, the line-of-sight integration was applied to the 3D model with the aim of attaining equivalent images for comparison with the images obtained experimentally.

According to the research of Yu, fuels with higher volatility such as JP-8 show a lower engine out soot emissions. This behavior was attributed to the better fuel mixing. For the same testing conditions, it was confirmed that JP-8 exhibits lower in-cylinder soot formation. The lower KL factor, as well as the reduced number of high temperature zones exhibited by JP-8 were reproduced by the CFD line-of-sight integration results.

Zha *et al.* [98] published the results of an investigation regarding the effect of a biodiesel blend on soot formation and oxidation during combustion. The authors used ULSD as a baseline fuel and performed the tests on the optical engine whose schematic is presented in Fig 2.12. For the optical setup the high speed CMOS color camera was used in order to obtain crank angle based combustion images. The camera is a visible range camera with a Bayer color filter array for the CMOS sensor.

The authors focused on gathering data for light load engine operating conditions, in the low temperature combustion regime. For different fuel injection pressures, the soot evolution was analyzed for the two fuels. It was showed that B20 produces more soot earlier in the cycle, in the premixed burning phase; however, owing to the higher soot oxidation rates for B20, lower engine-out soot emissions were measured for the biofuel compared to baseline fuel, ULSD. Also, for higher injection pressures the author showed that B20 as well as ULSD have lower late cycle soot formation.

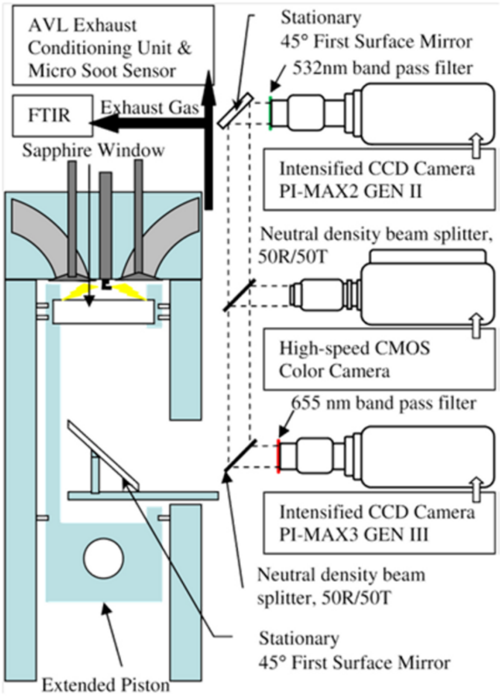

Fig 2.13 – Optically accessible single cylinder diesel engine with optical setup for two-color thermometry [99]

In a subsequent publication, Zha *et al.* [99] continued their research by extending the optical setup to the one presented in Fig 2.13 where two more intensified CCD cameras were added alongside the high-speed CMOS camera. The goal of the research was to extend the dynamic range of the two-color method towards the lower intensity regions of the cloud (i.e. low temperature or low optical thickness). In this experimental setup, the light detected by the ICCD cameras is wavelength restricted with the aid of two narrow bandpass filters for 655 nm and 532 nm respectively. These two cameras are used for soot temperature and KL optical thickness factor measurement for low intensity soot clouds while the high-speed CMOS color camera is focused on the same measurements for the high intensity soot clouds. As in the previously reference paper, Zha used two fuels for the experimental investigation: ULSD and a 20% by volume blend of soybean biodiesel and ULSD, B20.

The extended capability of the optical setup allowed the authors to make some interesting data comparison. First, the data collected by the high-speed CMOS camera was analyzed, followed by data collection with the two ICCD cameras. Finally, the ICCD camera information was integrated into the high-speed camera data to yield an expanded camera dynamic range.

The authors concluded that the high speed color camera is underestimating the soot formation in the early stages of combustion by about 30% compared to the results obtained using the three camera setup and also predicts lower temperature because it omits the low intensity soot clouds. On the other hand, the use of the ICCD cameras alone, with unchanged sensitivity levels, overestimate soot temperature and underestimate KL factor by about 70%, due to omission on high intensity soot clouds as a result of pixel data saturation.

2.6 Blue flame

While blue flames have been extensively investigated in open, atmospheric pressure flames for well over a century, relatively little blue-flame data is available for high-pressure environments such as internal combustion engines. A possible explanation for the relative lack of experimental data in this field of spectroscopic measurements could be due to the relatively low direct application of such techniques towards the development of internal combustion engines.

In 1926 Clark *et al.* [107] described the blue-flame emission of different motor fuels through spectroscopic techniques. Similarly, in 1957 Pipenberg *et al*. [108] performed spectroscopic investigations of n-heptane on an ASTM supercharged method engine. The authors focused on studying the radiation phenomena and the accompanying preflame reactions for n-heptane in the UV, VIS and IR spectral regions.

By collecting spectrums throughout the entire combustion cycle, the authors were able to identify some of the chemical species present at specific times during combustion as well as their quantity.

Also, the radiation from the preflame was used to identify three types of flames: the cool flame, the blue flame and the intense blue flame. From the experimental data it was shown that the blue flame reactions preceded the autoignition and that with an increase in compression ratio (CR) there was an increase in the blue flame as well.

In 1991 Ohta *et al.* [109] reported data regarding the identification of cool and blue flames in CI engines with the help of emission spectroscopy. As means of identifying the blue flame the authors have used the HCO molecule emitted at 330 nm wavelength as well as the emitted blue color.

Additionally, Lawn *et al.* [110] investigated in chemiluminescent emissions from premixed flames. However, the authors focused on the UV region OH chemiluminescence intensity relation to heat release.

Later studies performed by Griffiths *et al.* [111] on a rapid compression machine to study knock occurrence confirmed that blue flame appearance is signaled by the emerging HCHO* followed by CH* and then CO2* covering the UV and VIS regions of the electromagnetic spectrum.

Both Yao *et al.* [112] and Arcoumanis *et al.* [113] studied the applicability of dimethyl ether (DME) as a candidate fuel for compression ignition engines. While Arcoumanis performed experimental studies to investigated DME’s chemical properties compared to diesel fuel, Yao carried a numerical study to explore the chemical reaction mechanism in the HCCI process of DME. It was noted by

Arcoumanis that DME burns with a visible blue flame, while Yao explained that the blue flame reaction of the high temperature reaction is the moment when DME is oxidized rapidly and there is a sharp increase in the CO concentration.

More information on the chemistry of blue flame is provided in subchapter 3.5. An attempt at emulating the reaction mechanism of CO_2* (electronically excited carbon dioxide, the main source for the blue-flame radiation) was realized by Kopp *et al.* [114] concurrent with experimental results performed in a shock-tube.

2.7 Conclusions

The internal combustion engine is on a continuous path of improvement to reduce exhaust gaseous emissions and improve fuel economy. While recent trends in diesel engine development have lowered the EGR requirements, future regulatory pressure will likely result in a reversed trend in the future. Highly premixed combustion modes generally falling within the LTC category are typically accompanied by the occurrence of blue-flames. The stronger the degree of premixed combustion, the stronger the CO_2* emitted blue-flame radiation. This may result in a significant inference in the application of the two-color method which, at the most fundamental level, needs to be understood and ultimately compensated for. This chapter summarized previously published studies relevant for the current research, with a focus on the details of the application of the two-color method.

Chapter 3. Development of extended two color method (eTCM)

3.1 Two color method – theoretical background

The two color method is a method used in soot optical thermometry for determining the temperature and volumetric concentration of a soot cloud. This method is of interest for characterizing the soot formed and oxidized in a diesel engine. Following, a description of the mathematical background is presented.

The dependence of the blackbody emissive power on temperature and wavelength is given by Plank's equation:

$$E_b(\lambda,T) = \frac{C_1}{\lambda^5\left(e^{C_2/\lambda T} - 1\right)} \tag{3.1}$$

where E_b is the blackbody monochromatic emissive power [W m^{-3}], λ – wavelength [nm], T is the blackbody temperature [K], C_1 and C_2 are model coefficients given by $C_1 = 3.7418\text{x}10^2$ [W nm^2] and $C_2 = 1.4388\text{x}10^7$ [nm K]

Citing the work of Hottel et.al. [115], Siegel and Howell [116] considered an empirical equation describing the emissivity of soot in the following form:

$$\epsilon(\lambda) = 1 - e^{-\frac{KL}{\lambda^\alpha}} \tag{3.2}$$

where the wavelength λ is expressed in μm even though for this empirical equation the term λ is regarded as unitless, K is a coefficient proportional to the soot volume concentration and L is the geometric thickness of the flame along the optical axis of the detector . The product between K and L is called KL factor and is used for quantifying the soot concentration. Also, the value of the wavelength exponent coefficient α depends on the optical and physical properties of the soot present in the flame. This includes variables such as wavelength range and fuel used. Due to the fact that the three wavelengths selected for the current research are in the visible range of the spectrum the value of α is less critical for evaluation of flame temperature and KL factor [94]. In 1963 Siddal and McGrath [117] have developed a continuous function to characterize the wavelength exponent coefficient ɑ. Following their work, Matsui et al. [96] used this alpha function to characterize sooty diesel combustion. As a result of the experimental work conducted they came up with different constants for the ɑ function as it can be seen from the following equation:

$$\alpha = 1.22 - 0.245 \ln(\lambda) \tag{3.3}$$

To be noted that ɑ is a dimensionless number; however, the value of λ used in the equation should be in µm. Subsequently, the results obtained by using equation (3.3) are in conformity with the findings of Siegel and Howell [116], and Hottel and Broughton [85]. They suggest the use of $\alpha = 0.95$ for infrared measurements ($\lambda > 800$ nm) and $\alpha = 1.39$ in the visible range ($300\text{nm} < \lambda < 800$ nm). Other values for the ɑ coefficient have been suggested over the years by numerous authors and are summarized by Zhao and Ladammatos [76]. Thus, based on equations (3.1) and (3.2), the soot emissive power is given by:

$$E_s(\lambda, T) = \varepsilon(\lambda) \cdot E_b(\lambda, T) \tag{3.4}$$

Also, the equation for the signal received from an optical detector that looks at a radiating soot cloud can be expressed by [101, 118]:

$$\mathrm{V}_\lambda = \int_\lambda \int_\Omega \int_A \mathrm{H}_\lambda \cdot \varepsilon_{\mathrm{soot}}(\lambda) \cdot \mathrm{E}_\mathrm{b}(\mathrm{T}, \lambda) \mathrm{d}A \mathrm{d}\Omega \mathrm{d}\lambda \tag{3.5}$$

Where V_λ is the signal that comes from the detector; H_λ is the detector transfer function; A is the area of the soot cloud and Ω is the solid angle subtended by the active area of the detector.

Typically, under the two-color method described previously, a requirement for a narrow field of view of the detector must be imposed in order to simplify the form of equation (3.5) and avoid the triple integration. So in this narrow cone associated with the field of view, the temperature and composition are assumed to be constant.

While this is a convenient mathematical simplification, it reduces the amount of signal that can be received by the detector. More importantly, the two-color method becomes quite sensitive to cycle-to-cycle variation in the position of the soot clouds, thus requiring extensive cycle-averaging (as much as 1000 cycles)[76] (see Fig 3.1). In seeking to alleviate this issue, one may remove the requirement for a narrow field-of-view and replace it with a set of assumptions. It is assumed that for a cloud of soot of arbitrary shape and size, there exists an equivalent temperature and KL factor which closely approximates the behavior of the soot-cloud temperature and concentration. This assumption is necessary due to the lack of spatial resolution of this type of measurement and it has been used implicitly in equation (3.6). The term H_λ is considered a constant. Let ε_{soot} and E_b be the equivalent average function such that ε_{soot} times E_b equals the equivalent of the triple integral.

It can be argued that the assumption used does not increase the error in soot temperature measurement when compared to the classical two-color method as described by Zhao and Ladammatos[76]. While the two-color method measures the incident radiation in a much smaller field of view of the detector and the gradient of soot temperature and concentration may be assumed to be relatively small, the averaging needed in order to remove the cycle-to-cycle variation introduces actually a "gradient" in time of the two variables. Thus, the errors in determining the soot temperature and concentration of the two-color method and the extended two color method are expected to be of the same order.

The effect of temperature and soot concentration non-uniformity has been studied for the two-color method by Matsui et.al.[119],[120] and by Yan et.al.[121] whose work was cited by Zhao and Ladammatos [76]. It has been observed that a severe variation of the temperature distribution results in the underestimation of the KL factor while a variation in the soot concentration has a milder effect on the measured temperature. Additionally, the measured temperature will have a higher value than the arithmetic average due to the exponential nature of the light emission as a function of temperature.

$$V_{\lambda} = C_{\lambda} \cdot E_{s}(T,\lambda) \cdot \frac{A_{cloud}}{L_{exp}^{2}} \tag{3.6}$$

Equation (3.6) is the equation used for describing the optical detector signal received during the experiment. Where C_{λ} is the calibration constant, A_{cloud} is the area covered by the soot cloud during the experiment and L_{exp} is the length from the detector to the soot cloud during the experiment. More information related to the calibration constant is going to be presented in the next subchapter on

Method calibration.

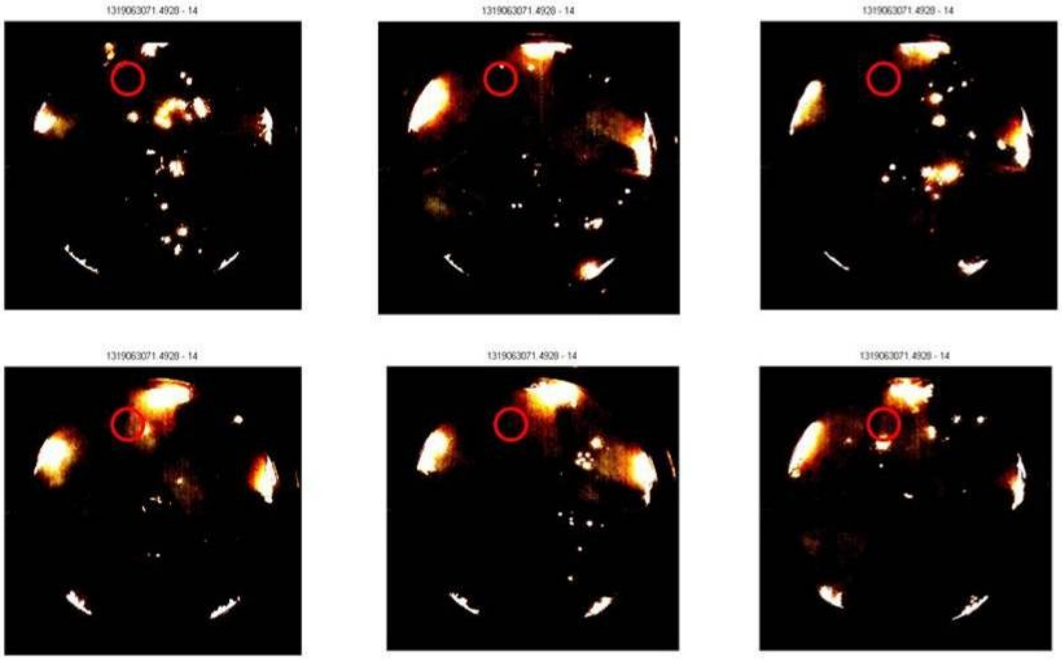

Fig 3.1 –Detector's field of view for the two color method case with high speed visible range images

3.2 Development of the combustion optical probe

The need to obtain more information related to the combustion process with a sensor system that has small dimensions when compared to traditional sensors has driven the author to develop the enhanced chemiluminescence-based combustion optical probe. A picture of the instrument layout is shown in Fig 3.2.

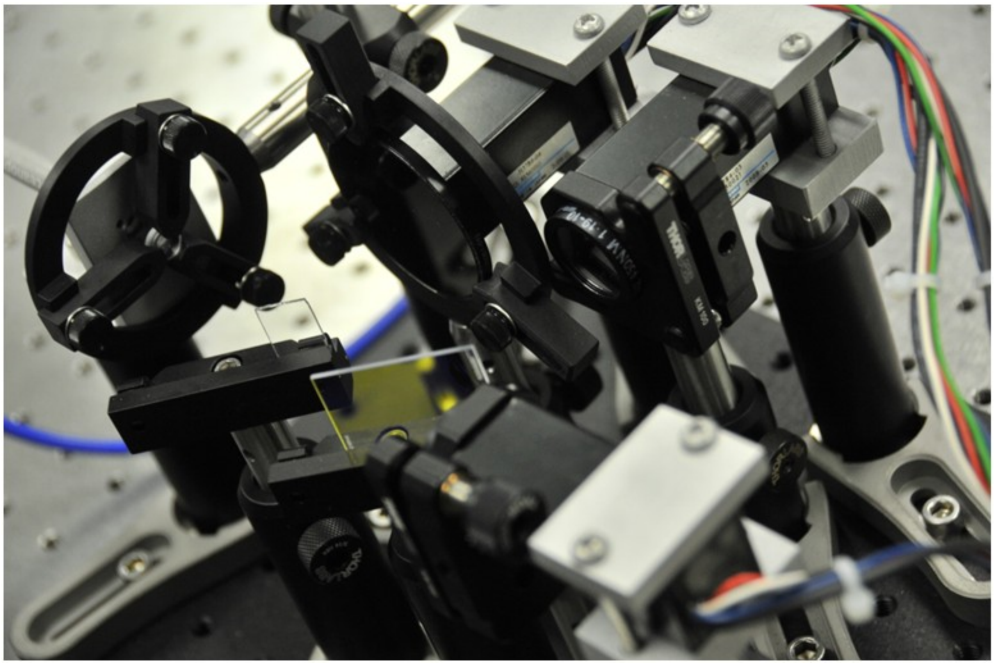

Fig 3.2 – Optical components of the combustion probe

With its aid, essential information is gathered and analyzed. More details on data analysis are presented in Chapter 5. This subchapter however, is focused on the development of the combustion optical probe.

Specifically, Fig 3.3 illustrates the schematic of the combustion optical probe. The light emitted during the combustion process is collected with the aid of a focusing lens and directed to the collimating lens through an optical cable. Next, the collimated beam of light encounters the first beam splitter where light in the 446-500 nm range is reflected while light in the 513-723 range is transmitted. The reflected light passes through a 450 nm bandpass filter and reaches the first photomultiplier tube. Then, the once transmitted beam of light encounters the second beam splitter. The reflected light in the 499-555 nm range passes through a 532 nm bandpass filter and arrives at the second PMT. In the same way, the transmitted light in the 569-730 nm range is delivered to the third PMT through a 640 nm bandpass filter. At the PMT level light intensity is translated into voltage output that it is collected further on by the data acquisition system with a resolution of 0.1 CAD.

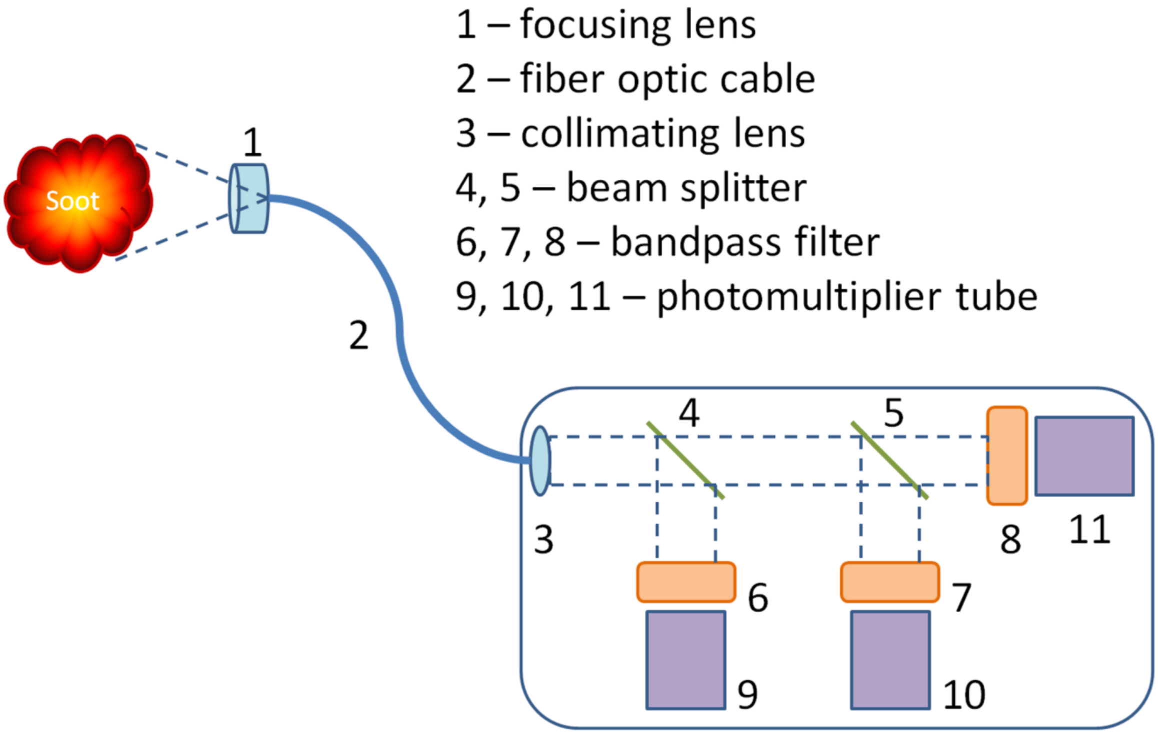

Fig 3.3 - Schematic of the combustion optical probe

Detailed information related to every component used for the optical probe development is presented in the next subchapters.

3.2.1 Lenses and optical fiber components

First, in order to obtain accurate data, as much light as possible is collected from within the combustion chamber. The Ocean Optics 74-UV collimating lens plays the role of a focusing lens and is connected to one end of the optical fiber. The 74-UV lens is adjusted for UV-VIS setup and specifications are offered in Table 1.

Table 1 – 74-UV collimating lens specifications [122]

74 UV collimating lens	
Lens diameter	5 mm
Lens length	10 mm
f-number	f/2
74-UV material	Dynasil 1100 quartz (200 nm – 2 μm)
Range	200-2000 nm

Second, the optic fiber cable used for this application is a 1mm diameter, solarization resistant (UV grade) cable from Ocean Optics, model # P1000-2-UV-VIS. It comes at a standard length of 1 m, it is made of acrylate and it is most efficient in the 300-800 nm wavelength range.

Next, the plano-convex lens from Edmund Optics is connected to the other end of the optic fiber. The lens is manufactured using research-grade synthetic fused silica and offers excellent transmission characteristics as well as having the capability of operating at high temperatures. The lens is employed as a collimating lens that converts divergent beams of light into a parallel beam. More information related to the NT48-804 model lens is presented in Table 2 while geometric specifications are illustrated in Fig 3.4 and transmission characteristic is plotted in Fig 3.5.

Table 2 – Specifications of the UV plan-convex lens [123]

NT48-804	
Diameter	6 mm
Clear aperture	≥90% of diameter (mm)
Effective focal length EFL	9 mm
Back focal length BFL	7.29 mm
Radius R1	4.13 mm
Edge thickness ET	1.21 mm
Center thickness CT	2.50 mm
Centering	3-5 arcminutes
Design wavelength DWL	587.6
Coating	UV-VIS

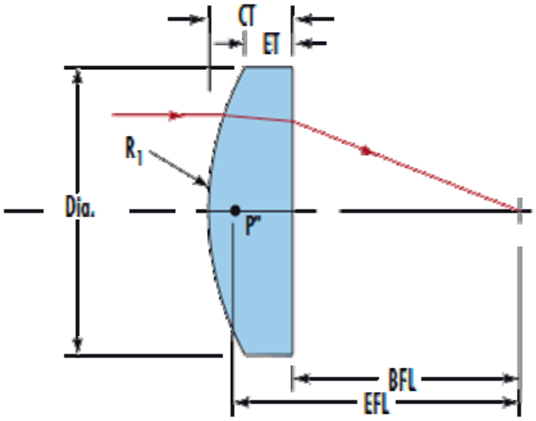

Fig 3.4 – Geometric specifications of the UV plan-convex lens [123]

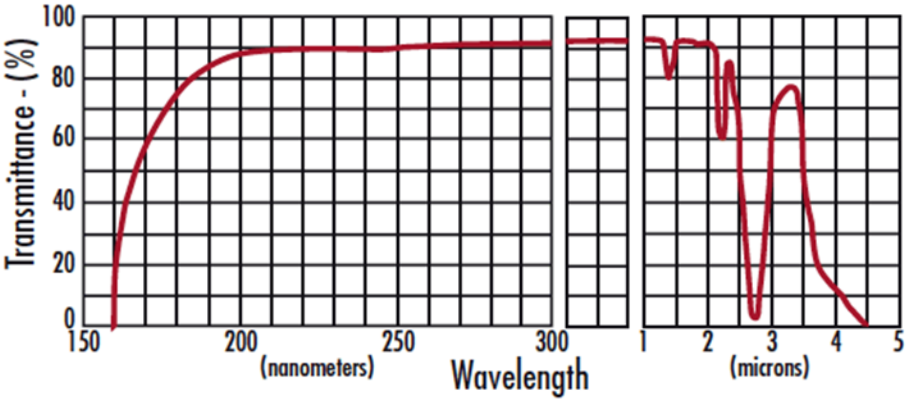

Fig 3.5 – Transmittance UV grade fused silica [123]

3.2.2 Beam splitters

As it can be seen from Fig 3.3, two beam splitters were used for the optical probe development. Both are dichroic beam splitters from Edmund Optics, model # NT47422 and NT47423. A dichroic beam splitter is an optical device that splits a beam of light in two beams (one reflected and one transmitted) with different wavelengths. How much is transmitted and how much is reflected depends on the application and the properties of the beam splitter. For these particular beam splitters the main characteristics are presented in Table 3.

Table 3 - Beam splitter specifications [124]

	NT47422	**NT47423**
Color	Blue-green	Green-orange
Dimensions	25.2 x 35.6 mm	25.2 x 35.6 mm
Thickness	1.1 mm	1.1 mm
Angle of incidence	45°	45°
Reflection wavelength	446-500 nm	499-555 nm
Transmission wavelength	513-723 nm	569-730 nm
Cut-off wavelength	508 nm	565 nm
Substrate	UV grade fused silica	UV grade fused silica

Also, in Fig 3.6 the transmission wavelength range can be seen for the blue-green dichroic beam splitter. Same thing is plotted for the green-orange dichroic beam splitter in Fig 3.7

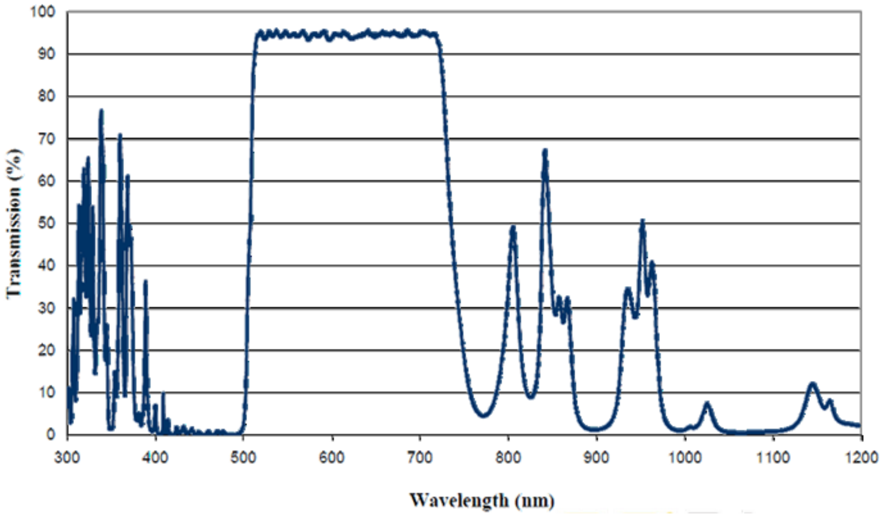

Fig 3.6 – Blue-green dichroic plate beam splitter coating performance [124]

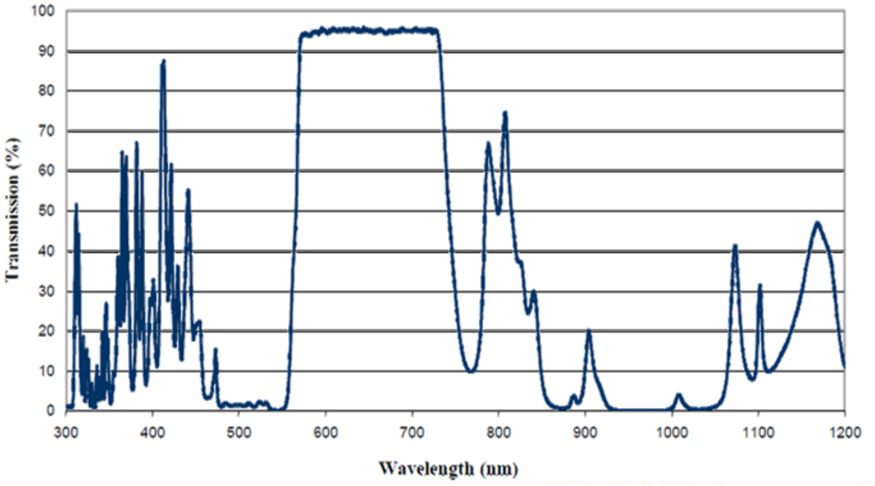

Fig 3.7 – Green-orange dichroic plate beam splitter coating performance [124]

3.2.3 Bandpass filters

Next, three bandpass filters from Thorlabs were used for the optical probe set-up. Each filter has a diameter of 1" and is mounted in a block anodized aluminum ring. Using a bandpass filter is a simple way to transmit a well defined wavelength band of light, while rejecting unwanted radiation. The three wavelengths of interest that were chosen for this application are 450, 532 and 640 nm.

The plot shown in Fig 3.8 displays the transmission characteristics for the three bandpass filters selected and more specifications are presented in Table 4.

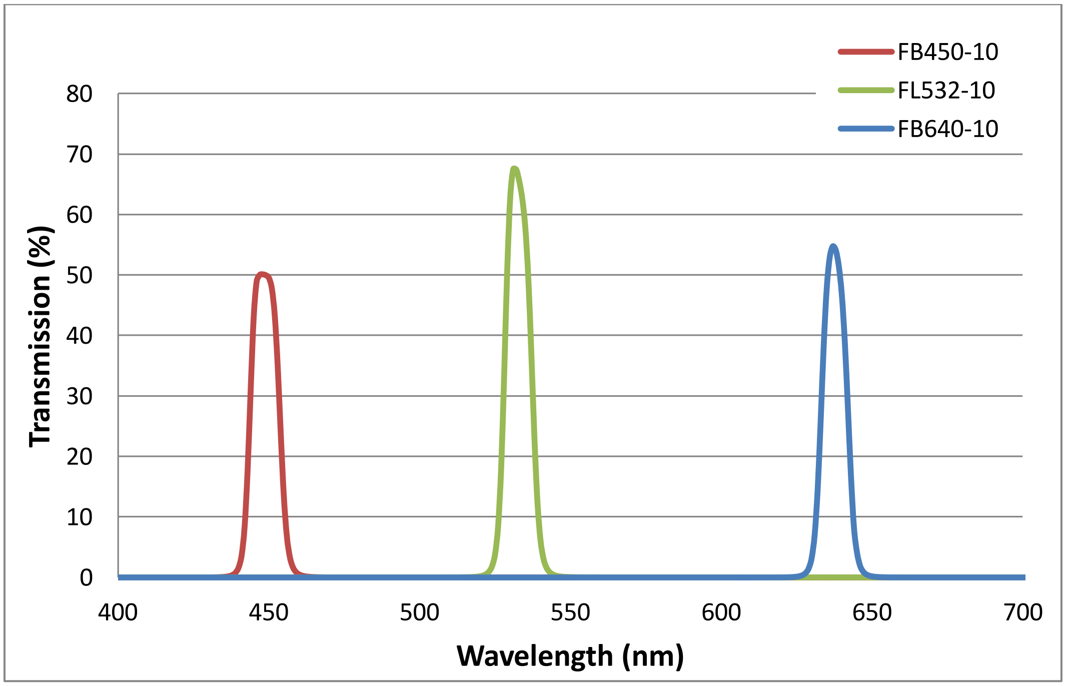

Fig 3.8 – Transmission data for the bandpass filters [125]

Table 4 - Bandpass filters specifications [125]

Item #	CWL	FWHM	T(min)	Size
FB450-10	450±2 nm	10±2 nm	45%	Ø1"
FL532-10	532±2 nm	10±2 nm	70%	Ø1"
FB640-10	640±2 nm	10±2 nm	50%	Ø1"

Where CWL – center wavelength; FWHM – full width half maximum; T(min) – peak transmission

A discussion is essential at this point in order to explain why the three specific wavelengths have been chosen for this particular research. As mentioned before in the literature review part of this thesis, soot emits a continuous spectrum in the infrared and visible regions of the electromagnetic spectrum. The two wavelengths, λ_2 and λ_3, should be chosen in such a way that minimum to no radiance interference from other species should exists. On the other hand λ_1 has been chosen on purpose in the maximum range of interference from the CO continuum. Another reason for choosing visible wavelengths over infrared ones is due to the larger rate of change of the spectral radiance with respect to temperature for a given wavelength. In this way, greater signal sensitivity can be achieved. Following, by having a larger difference in the signal output from the two wavelengths λ_2 and λ_3 signal to noise ratio is improved. Next, having $\lambda_{1,}$ λ_2 and λ_3 in the visible range makes the estimation of temperature and KL factor less sensitive to the value of parameter α. A detailed explanation for KL and α is provided in the following section 3.1. To continue the discussion for the choice of λs another advantage of visible over infrared is given by the fact that combustion chamber wall reflections and radiation are insignificant when calculating the temperature and KL factor with the two-color method. Overall, it can be said that using the wavelengths in the visible region of the spectrum increases the reliability of the two-color method.

3.2.4 Photomultiplier tubes

Lastly, the photomultiplier tubes used in the combustion probe development are from Hamamatsu, model # H5784. A photomultiplier tube (PMT) is a vacuum tube and a very sensitive detector of light in the ultraviolet and visible range of the electromagnetic spectrum. The main components of a PMT are: an input window, a photocathode, focusing electrode, an electron multiplier and an anode. Table 5 offers more details related to the H5784 PMT specifications.

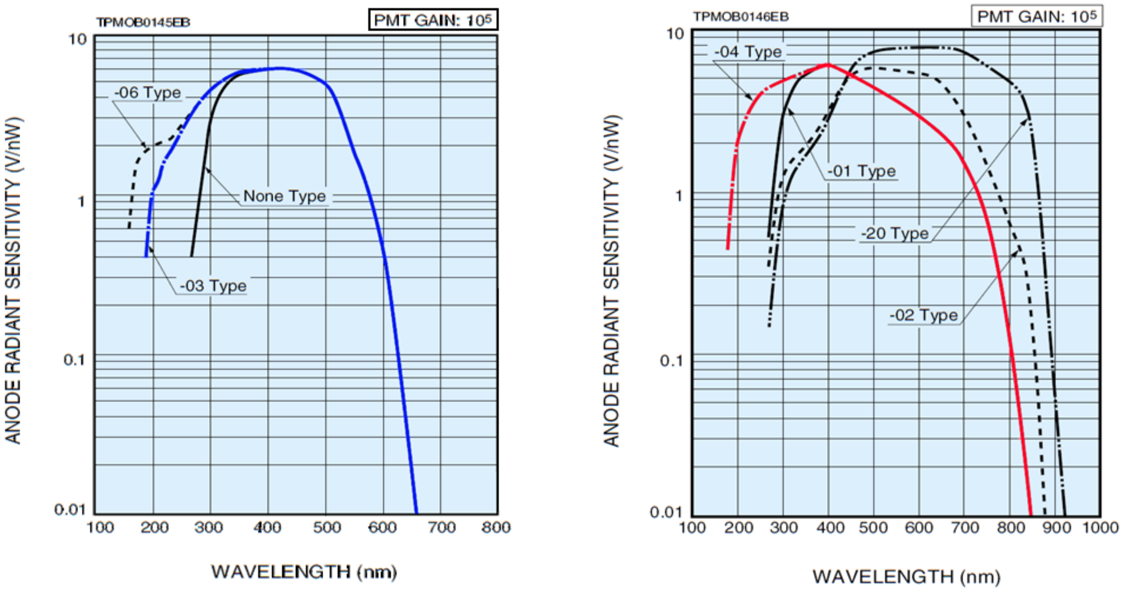

Fig 3.9 – Sensitivity of Hamamatsu photomultiplier tubes, type -02, -03 and -04 [126]

Table 5 – Hamamatsu H5784 PMT specifications [126]

H5784 PMT	**Type -03**	**Type -04**	**Type -02**
Effective area	8 mm	8 mm	8 mm
Cathode type	Bialkali	Bialkali	Bialkali
Peak wavelength	420 nm	400 nm	500 nm
Peak radiant sensitivity	62 mA/W	60 mA/W	58 mA/W
Window material	Borosilicate glass	Borosilicate glass	Borosilicate glass
Min wavelength	185 nm	185 nm	300 nm
Max wavelength	650 nm	850 nm	880 nm

Cathode luminous sensitivity	70 uA/lm	150 uA/lm	250 uA/lm
Cathode blue sensitivity	8 A/lmb		
Red white ratio		0.2	0.25
Anode luminous sensitivity	5.0E+07 A/lm	7.5E+07 A/lm	1.25E+08 A/lm
Dark current	0.2 mV	0.4 mV	2 mV
Output type	Voltage output	Voltage output	Voltage output
Amplifier	Y	Y	Y
Amplifier gain	1.0E+06	1.0E+06	1.0E+06
Amplifier bandwidth	2.0E+04 Hz	2.0E+04 Hz	2.0E+04 Hz
Power supply	C7169	C7169	C7169
Replaced by	H10722	H10722	H10722

3.3 Method calibration

A transfer function is a function that relates the input measured variable to the output variable. When this transfer function is determined experimentally it is known as calibration curve.

3.3.1 Source calibration

During the calibration of the experimental setup, a blackbody source is used (Mikron M330), characterized by a known spectral emissivity equal to one. The blackbody simulates the flame temperatures estimated to be encountered within the combustion chamber. Thus, equation (3.6) during the calibration process becomes:

$$V_\lambda(T\_object) = C_\lambda \cdot E_{bb}(\lambda, T\_blackbody) \cdot \frac{A_{cal}}{L_{cal}^2} \qquad (3.7)$$

And then C_λ can be expressed as:

$$C_\lambda = \frac{V_\lambda(T\_object)}{E_{bb}(\lambda, T\_blackbody)} \cdot \frac{L_{cal}^2}{A_{cal}} = C_\lambda^{'} \cdot \frac{L_{cal}^2}{A_{cal}} \qquad (3.8)$$

where a distinction has been made between the temperature detected optically – T_{object} – and the one measured by the blackbody source thermocouple - $T_{blackbody}$. Under ideal conditions of blackbody thermal stability and emissivity, T_{object} and $T_{blackbody}$ are equal. During the calibration procedure sufficient time should be allowed before measurement for thermal equilibrium to be reached.

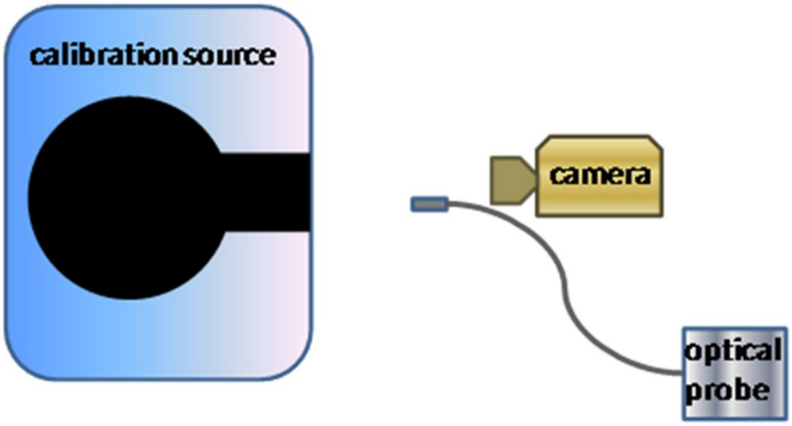

Fig 3.10 – Optical probe calibration setup with a blackbody source

Equation (3.7) uses the form of the blackbody function shown in equation (3.1), along with the voltage V_λ measured experimentally at the three different wavelengths λ = 450, 532 and 640 nm. The resulting value of $C_\lambda^{'}$ is calculated for different blackbody temperatures; $C_\lambda^{'}$ is shown as a function of T in the figure below. It can be observed that $C_\lambda^{'}$ can be considered independent of temperature, which is an expected outcome of equation (3.7). The markers are representing the experimental data collected for each pair of wavelengths while the lines are showing the linear fit. By averaging the obtained values, the three coefficients are:

C(1) =78.24303, C(2) = 17.199917 and C(3) = 4.04148.

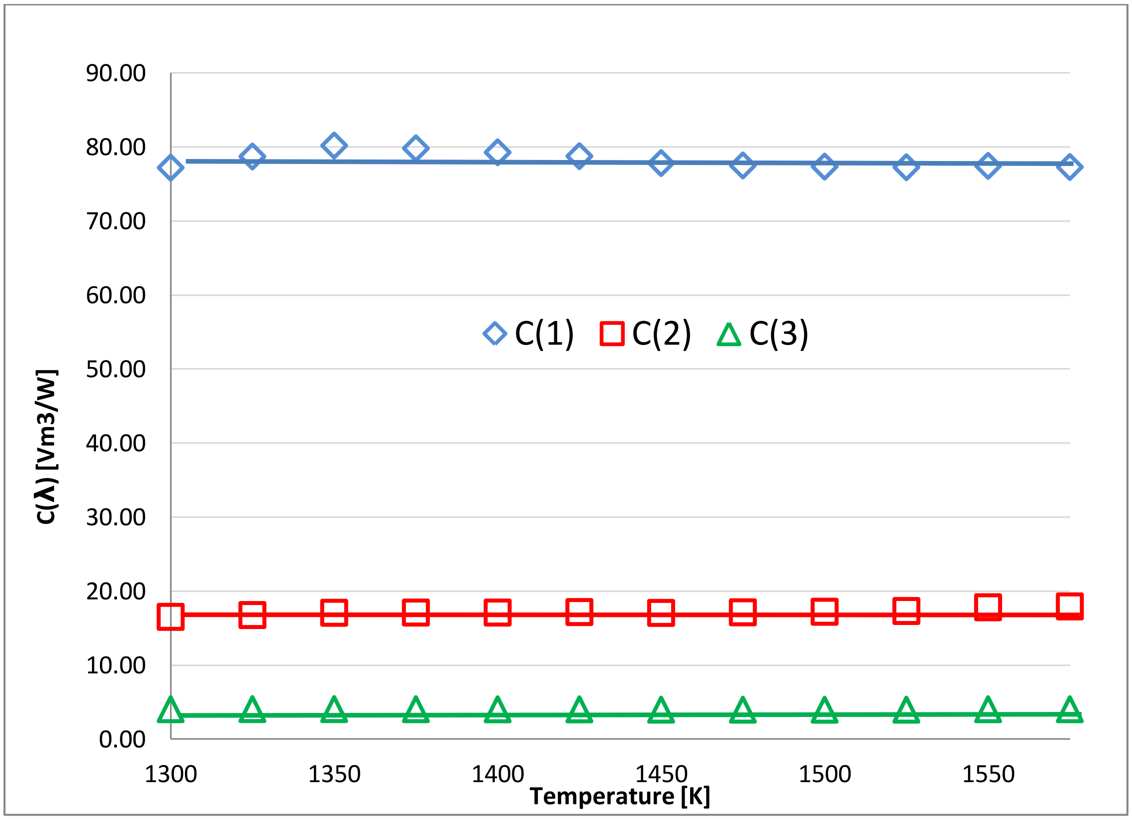

Fig 3.11 – Scaling coefficient calculated for different blackbody temperatures

3.3.2 High speed camera image calibration

For example, in order to compare the two signals, one coming from the optical probe and the other one from the high speed Phantom camera a new calibration needs to be performed. The Phantom camera does not have an angular effect. No matter where the soot position is within the combustion chamber its intensity is recorded in the same way on the Phantom image. However, with the optical probe this angular effect is present and has to be accounted for.

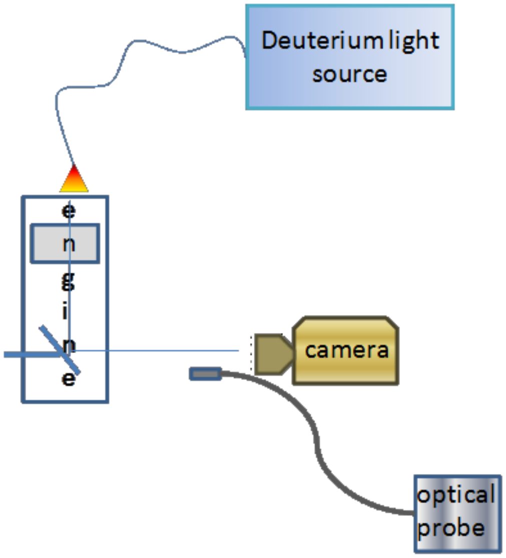

Fig 3.12 – Optical probe setup calibration

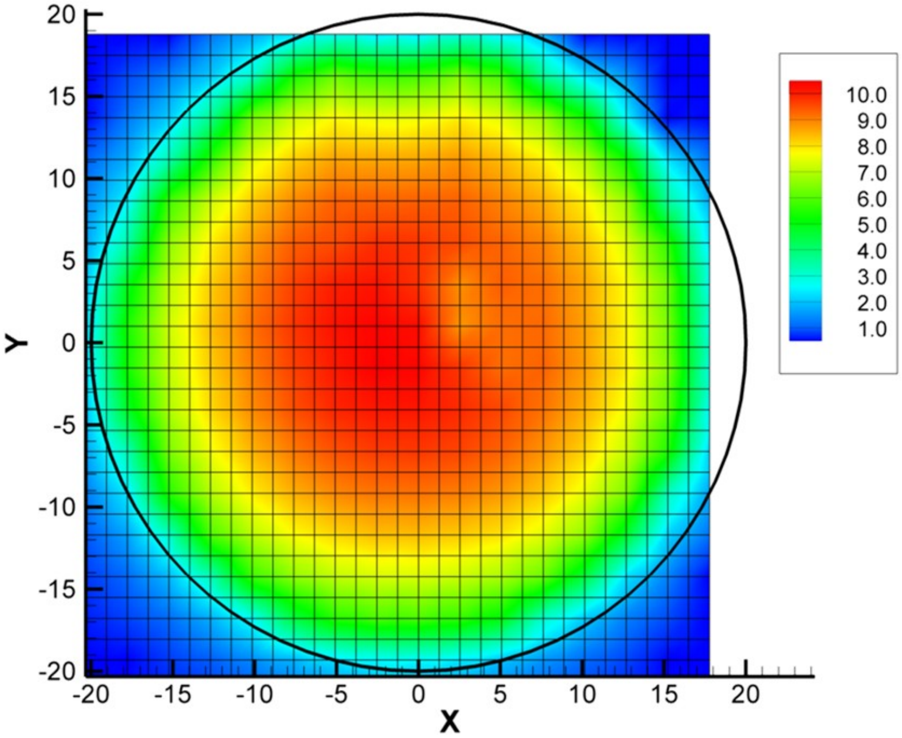

Fig 3.13 – Angular effect calibration results

In Fig 3.12 the calibration setup is shown. The Phantom camera and the optical probe were positioned in the same way as during the experimental setup. One deuterium light source was moved within the combustion chamber on a Cartesian grid. The results are plotted in Fig 3.13 and it can be seen that the intensity coming from the sides of the combustion chamber is less important than the intensity coming from the center. That being the case, in order to correlate the two signals one has to apply on the phantom images the obtained transfer function.

Next, by repeating the same procedure presented above but translating the XY plane on the Z axis a second function is obtained. This information from Z axis is lost when the Phantom camera is used because the image obtained is integrated on the line of sight. The results are plotted in Fig 3.14. As it can be seen there is an effect from the Z positioning within the combustion chamber but it is not that significant. So, an assumption it is made. One can use the previously determined transfer function at a certain Z positioning within the combustion chamber and can say that it is valid for the entire combustion chamber.

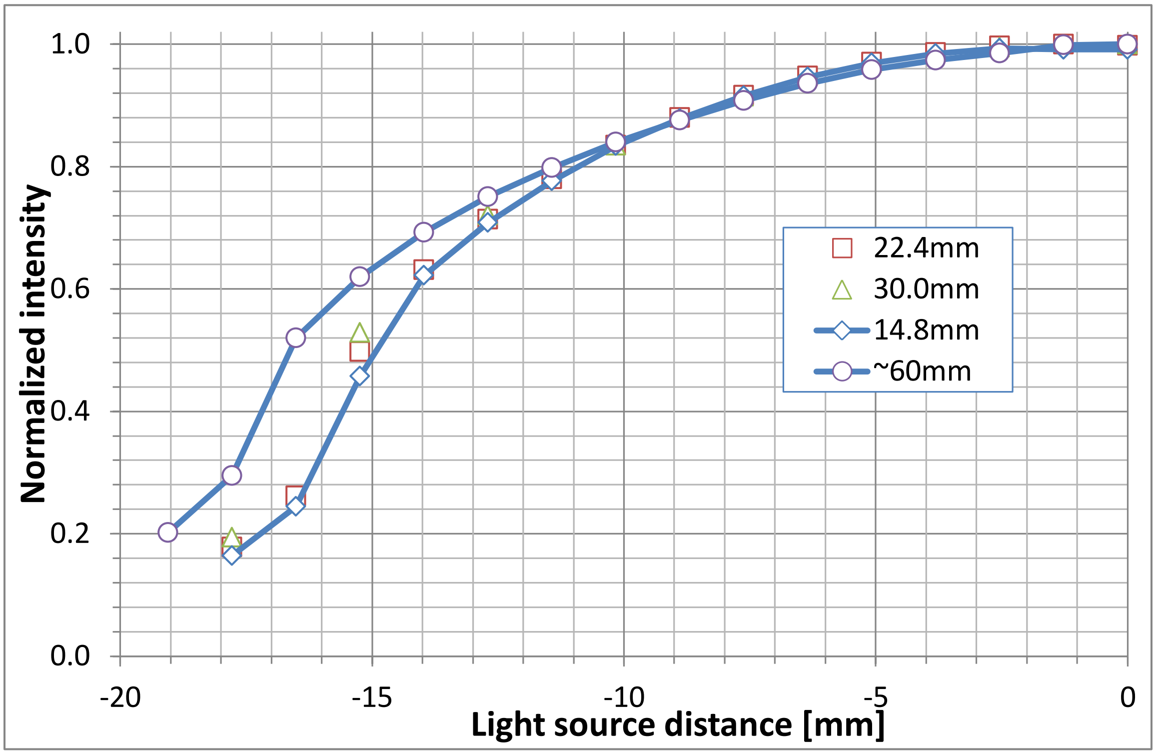

Fig 3.14 – Optical probe calibration. Effect of light source on Z position

3.4 Numerical solution

To resume, by inserting equation (3.8) in (3.6), one obtains:

$$V_\lambda = C'_\lambda \cdot E_s(\lambda, T) \cdot \frac{A_{cloud}}{L_{exp}^2} \cdot \frac{L_{cal}^2}{A_{cal}} \tag{3.9}$$

Equation (3.9) actually represents a system of two equations with two unknowns, KL and T. In this system of equations, although T_{soot} is not known, voltages V_λ are determined experimentally and thus available. The system of equations is non-linear and the most reasonable approach to solving it is to seek the roots numerically. While many options for solving this system numerically are available, the `fsolve()` function, part of the MATLAB© [127] computing language, has been chosen due to ease of implementation, algorithm efficiency and flexibility of seeking either the actual root or a minimum of the function, as it will be shown later.

The function that is being solved for is directly obtained from (3.9), and has the following form:

$$F(KL, T, \lambda) = (1 - e^{-\frac{KL}{\lambda^\alpha}}) \cdot \left(\frac{C_1}{\lambda^5 (e^{\frac{C_2}{\lambda T}} - 1)} \right) \cdot C_\lambda \cdot \frac{A_{cloud}}{A_{cal}} \cdot \frac{L_{cal}^2}{L_{exp}^2} - V_\lambda \tag{3.10}$$

This can be written as a system with two equations, two unknowns. In order to visualize a potential surface associated with this function, the following procedure has been applied. First, all V_λ have been evaluated using the soot emissive power described by equation (3.4) for given values of KL_{soot} and T_{soot}, in order to generate input data for the classical two color method which is not affected by measurement errors. This approach is quite useful in assessing the error behavior, which will be presented later. Next, the value of the function:

$$PE(KL, T) = \sqrt{F(KL, T, \lambda_2)^2 + F(KL, T, \lambda_3)^2} \tag{3.11}$$

is calculated for different values of the T, KL, λ2 and λ3 provided earlier. Its values are shown in the figure below. The solution, which in the ideal scenario, without input errors, would mean that the function F reaches zero, is achieved when the potential surface reaches zero. As PE ≥ 0 due to the form chosen, it means that the solution is also a minimum for the potential surface. Indeed, that can be observed in Fig 3.15 for the conditions chosen.

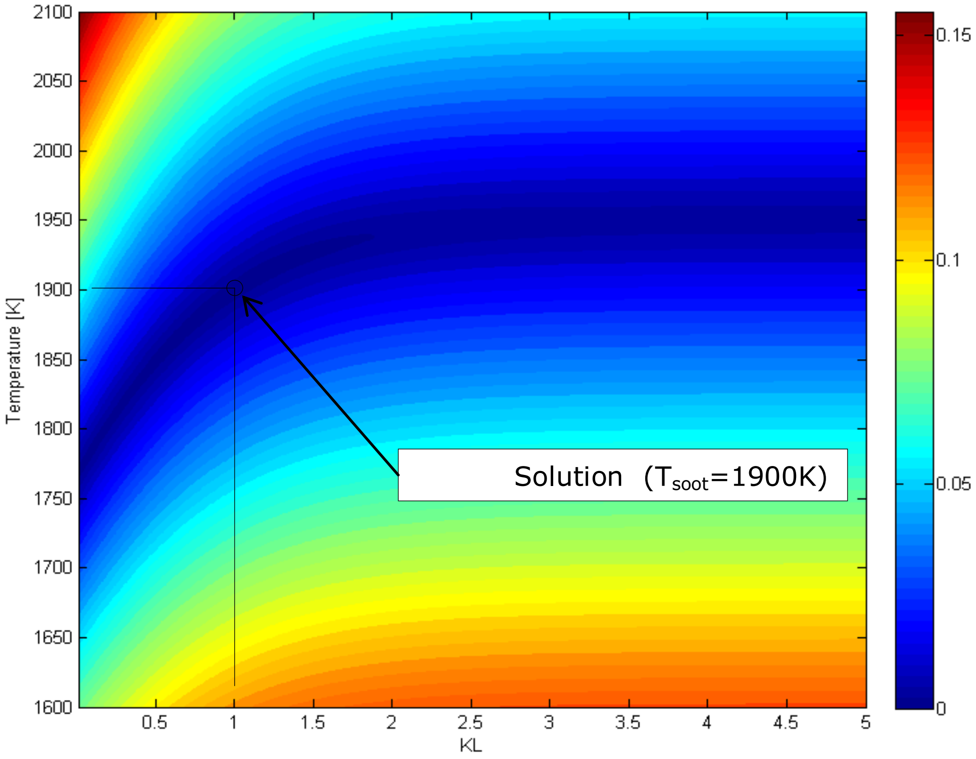

Fig 3.15 – Solution for T and KL

3.5 Theoretical background for extended two-color method

Previously, in this chapter, the traditional two color method was used to solve a system of two equations (see (3.9)) for two wavelengths λ_2 = 532 nm and λ_3 =

640 nm. In this way solutions for T and KL can be found. By following the same steps in the reverse way, from T and KL one can calculate the signal that should be received from the first detector at the 450 nm wavelength. This signal denoted by "V_1 calculated" is compared with the actual measured signal, V_1 measured.

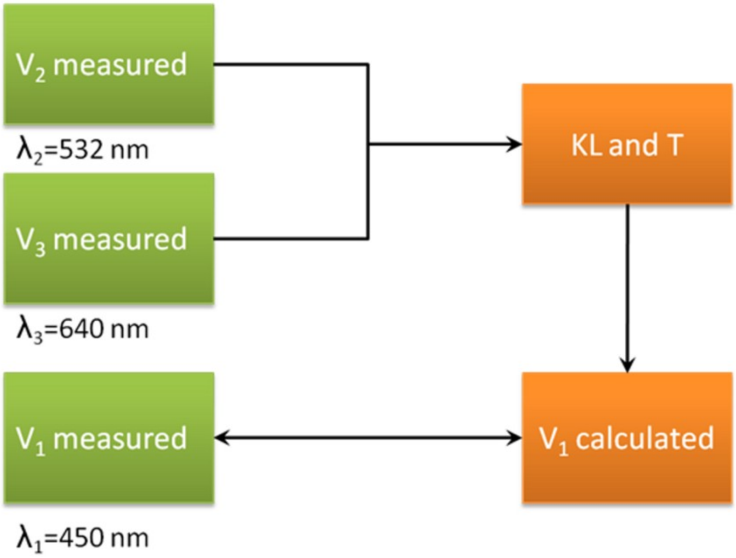

Fig 3.16 – Schematic diagram of numerical solution

Following the comparison one would expect for the two signals to coincide. In the case when the two signals overlap this comparison would confirm that the calculations for temperature and KL are correct and the two color method is validated. However, by looking at Fig 3.17 it can be observed that V_1 calculated is different from V_1 measured at least for the first 20 CAD for this particular cycle. In the first part of the cycle the temperature is reaching high unphysical values.

It appears that the CO flame information is "encoded" in the available signals V_1, V_2 and V_3. Should a relationship exist between the spectral components of the CO flame signal at the sampled wavelengths, it could be exploited to infer both the intensity of the CO flame as well as provide an accurate estimate of the soot temperature and optical thickness factor KL. So, the difference between V_1 measured and V_1 calculated is a strong indicator of the error introduced in the two color method by the CO flame.

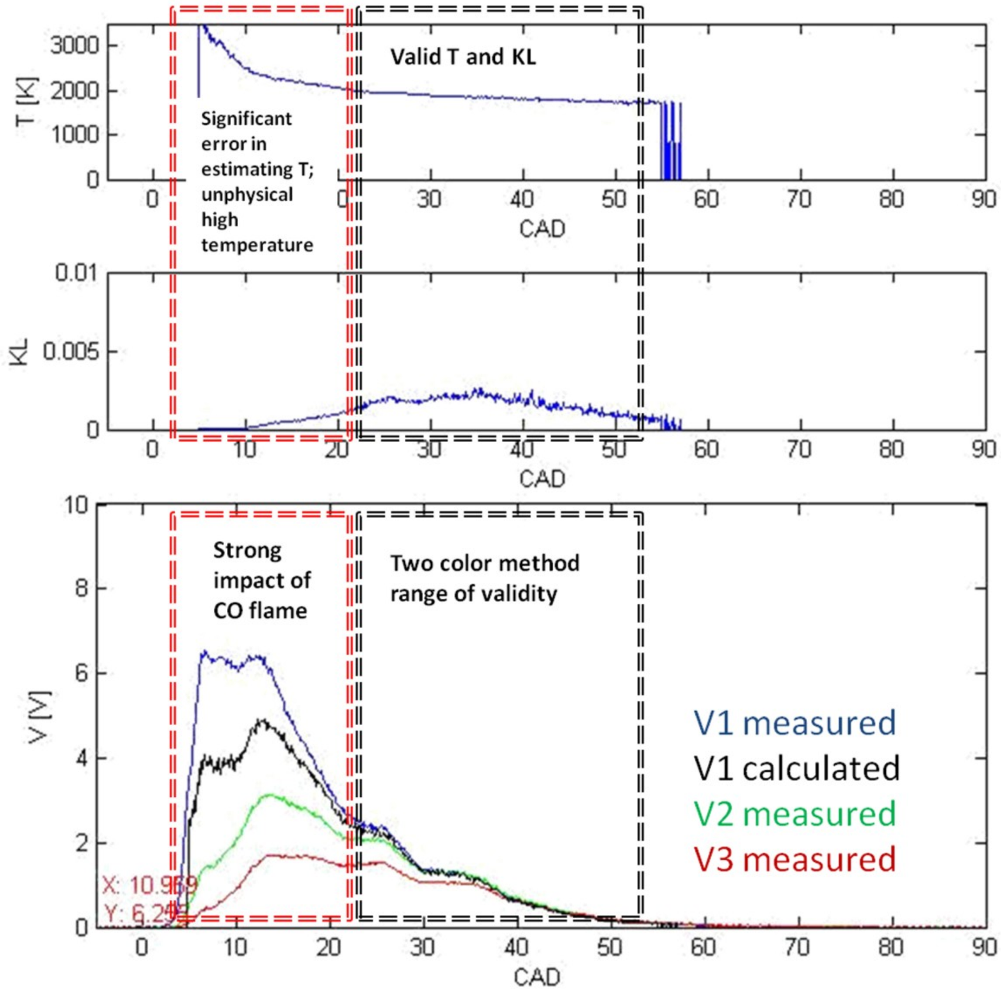

Fig 3.17 – Calculated T and KL; measured signals V_1, V_2 and V_3; and calculated signal V_1

Next, by understanding the CO flame behavior an attempt is made to experimentally determine and quantify this phenomenon.

Looking at Fig 3.18 the orange line is describing the soot continuum for the 300-900 nm range that includes the visible spectrum domain as well. The blue line is representing the CO flame continuum. At the three wavelengths of interest a signal V_λ is measured that can be used to determine the characteristics of the soot cloud within the combustion chamber. It can be seen that there is a disparity between the orange line and the blue line. This difference is denoted by B_λ and is the signal measured by the detectors additional to the signal proportional to the soot radiation intensity. So B_λ is the signal attributed to the chemiluminescence reaction called "blue flame".

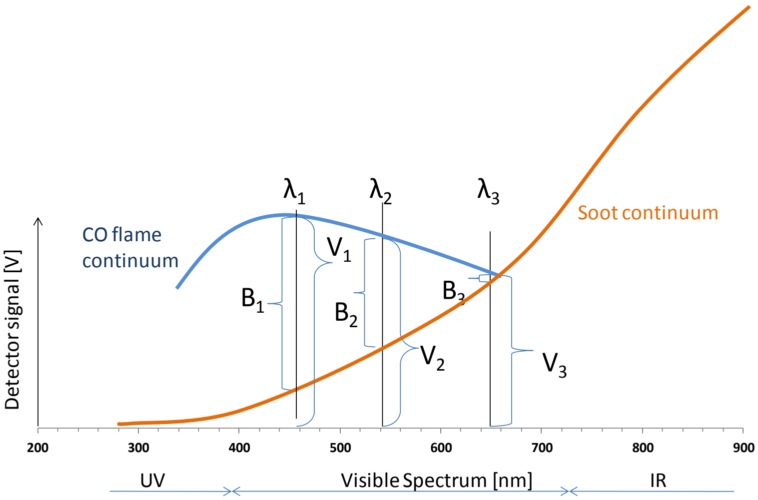

Fig 3.18 – CO flame continuum and soot continuum

According to Gaydon [90, 128] carbon monoxide combustion generates a spectrum of the blue flame that can be described as a continuum with the strongest peak in the 350-450 nm region. However, the continuum extends into the ultraviolet region as well as the visible region of the electromagnetic spectrum approximately from 340 nm to 650 nm.

A detailed reaction mechanism for the formation and destruction of CO2* is not well understood as of today but this is not a limited factor because it can be addressed through experimental measures [114].

The processes generating the blue flame continuum was initially described as a result of the interaction:

[128, 129]

$$\mathrm{CO}+\mathrm{O}\rightarrow\mathrm{CO}_2+h\nu \tag{1}$$

Where CO is carbon monoxide molecule, O is oxygen atom, CO_2 is carbon dioxide molecule, h is Plank's constant and υ is the frequency of the emitted photon.

While the CO band system is attributed to the three body collision:

[128]
$$\mathrm{CO}+\mathrm{O}+\mathrm{M}\rightarrow\mathrm{CO_2}^{*}+\mathrm{M} \qquad 2$$

Prominent bands of CO are mentioned by Gaydon [128] to be present at 434.3 nm, 455.2 nm and 464.4 nm. While regions clear from the band structure can be found at: 435 nm, 453.9 nm and 465.4 nm. This fact is important as the optical combustion probe developed is set up with one detector at the 450 nm wavelength which was selected due to the lack of CO band spectrum interference. Additionally, measurements done by Gaydon and Kaskan [128, 129] show that the absolute intensity of the bands remains unchanged with the temperature increase.

However, in a later publication, Gaydon [90] updates the hypothesis related to the origin of the CO continuum, reporting that either reaction 1 or the set of reactions 3 [90, 114] are possible explanations:

[90]
$$\begin{aligned}&\mathrm{CO}+\mathrm{O}+\mathrm{M}\rightarrow\mathrm{CO_2}^{*}+\mathrm{M}\\&\mathrm{CO_2}^{*}\rightarrow\mathrm{CO_2}+\mathrm{h}\nu\\&\mathrm{CO_2}^{*}+\mathrm{M}\rightarrow\mathrm{CO_2}+\mathrm{M}\end{aligned} \qquad 3$$

According to the chemical reactions presented above, CO_2* will relax to ground state by emitting a photon or it will dissipate the energy by colliding with a third body M.

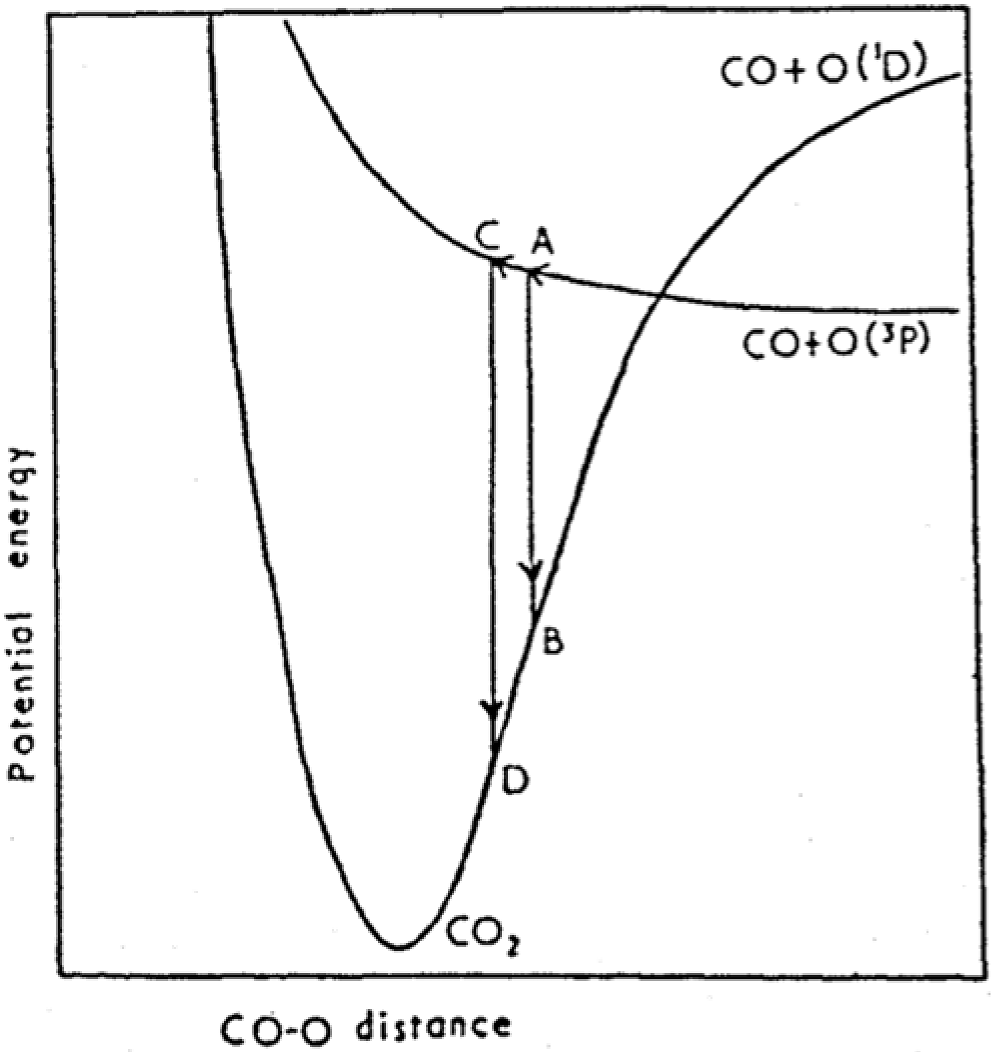

Fig 3.19 – Theoretical potential energy curves for the CO and O interaction to form CO_2 [128]

At this time, as the author is not aware of any other publically available research regarding this topic, reaction 1 will be considered to be responsible for the CO continuum in an attempt of describing the CO continuum behavior. This explanation relies on work by Gaydon [128]. However, consideration of system (3) is not expected to have a significant impact on the conclusions presented later.

The goal is to understand the impact of temperature and pressure on the relative spectral intensity of the CO continuum. Towards this goal, let us consider the molecular potential energy model proposed by Gaydon [128] and shown in Fig 3.19.

Along the *X* axis is represented the distance between the CO molecule and O atom as they collide within the combusting mixture, while the *Y* axis corresponds to the potential energy resulting from the balance of attractive and repulsive forces occurring between the atomic nuclei. Two curves are depicted: one for the reaction of CO with O in the singlet D state (^{1}D) and the other one for CO and O in the triplet P state (^{3}p). The CO2 dissociation reaction is expected to follow the CO + O(^{1}D) path.

According to Gaydon's model, in the case when enough kinetic energy is available to the CO molecule and O(^{3}P) atom at the time of their collision, it is probable that the CO+O(^{3}P) system will reach state A or lower. Due to repulsive characteristics of the CO+O(^{1}D) system, it is not possible to form a CO_2 molecule unless a transition occurs from CO+O(^{1}D) to CO+O(^{3}P). A certain probability distribution will exist for all the possible transitions occurring from energy state A or lower, which may be translated into a certain spectral intensity distribution as measured experimentally by a spectrometer. As the temperature of the system is increased, providing CO and O with higher kinetic energy at the time of the collision, the highest energy state achieved by the CO+O(^{1}D) system increases from state A to state C. The resulting transition to state D will yield higher energy photons, characterized by shorter wavelength. This in turn skews the probability distribution towards shorter wavelengths, which was indeed observed experimentally.

In other words, if CO continuum intensity measurements are performed at two wavelengths, the ratio of the shorter wavelength intensity to the longer wavelength will increase with an increase in temperature.

At the same time, increased pressure for the environment in which the CO+O collisions are taking place will increase the probability of collision (i.e. absolute blue flame light intensity) but will not have an impact on the photon energy probability distribution (i.e. ratio of CO continuum light emission at different wavelengths).

However, while Gaydon's conceptual model for CO continuum light emission is based on scientific data available through spectral measurements as well as good understanding of the quantum-mechanics behavior of the atoms and molecules involved, it is not validated by direct measurement or computation of the potential energy surfaces suggested in Fig 3.19.

With the aid of modern tools, such as numerical Schrödinger equation solvers (e.g. *ab initio* solvers such as Gaussian [130]), the model could be validated by computing the potential energy surfaces associated with the CO+O(^{1}D) and CO+O(^{3}P) systems. Additionally, it is possible that this understanding of the potential energy surfaces would provide the means to predict the impact of temperature on the probability distribution function which governs the light emission for reaction 1 for a range of v's.

Under these circumstances, going back to eTCM equation (3.9) can be rewritten with the additional term that counts for the blue flame:

$$V_\lambda = C'_\lambda \cdot E_s(\lambda, T) \cdot \frac{A_{exp}}{L^2_{exp}} \cdot \frac{L^2_{cal}}{A_{cal}} + B_\lambda \qquad 3.12)$$

Where: B_λ is the blue flame phenomenon that influences in different proportions the signal received for the specific three wavelengths considered. This is the equation used by the extended two-color method – eTCM. The next step is how to quantify the B_λ term. This subject will be further discussed and analyzed in Chapter 5.

Chapter 4. Research engine and experimental facility

The experiments presented in this thesis were conducted on a small bore optically accessible diesel engine. The engine is part of a state of the art experimental facility at Wayne State University known as Low Temperature Research Center.

Further technical details related to the research engine and investigation equipment are presented in this chapter and a schematic of the experimental setup can be seen in Fig 4.1.

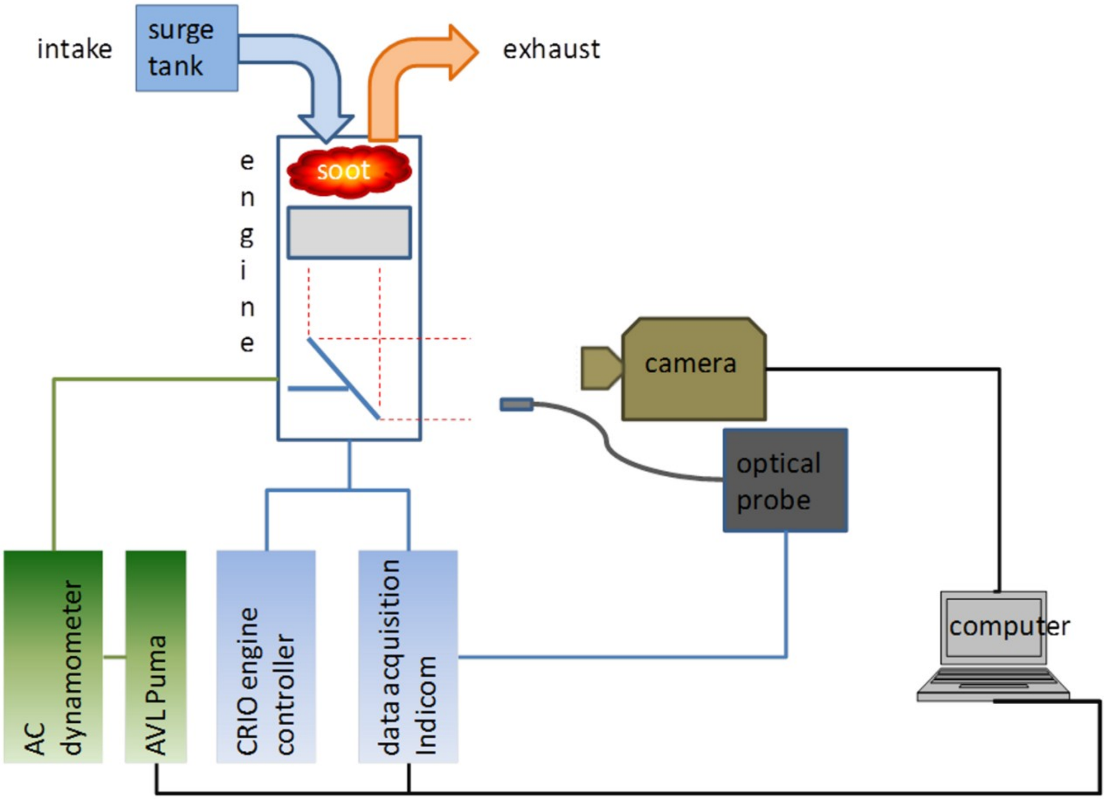

Fig 4.1 – Experimental setup

4.1 Optically accessible experimental engine

As mentioned before, the engine used for the experimental component of this thesis is a single cylinder, direct injection, model AVL 5402 research diesel engine. Pertinent information related to the engine characteristics is presented in Table 6.

Table 6 – Experimental engine characteristics

Optically accessible engine	**AVL 5402, DI**
Bore	85 mm
Stroke	90 mm
Swept volume	510 cm3
Compression ratio	15:1
Connecting rod length	148 mm
Combustion bowl diameter	40 mm
Combustion bowl depth	17 mm
Number of intake valves	2
Number of exhaust valves	2
Intake valve opening/closing	326°/594° CA aTDC
Exhaust valve opening/closing	106°/374° CA aTDC
Injection system	Bosch Common Rai (Pmax=1350 bar)
Swirl control/ratio	AVL/2.0-4.5
Rated speed	3000 rpm

The engine’s fuel injection system is a common rail, Bosch CR CP1, with a VCO design, 5 holes Bosch fuel injector. The system is capable of delivering injection pressures up to 1350 bar. Table 7 provides more details regarding the fuel injector specifications.

Table 7 – Fuel injector specifications

Injection System	**Common Rail CP1**
Model	Bosch DSLA 142 P
Design	VCO – nozzle
Injection Pressure	Variable (1350 bar max)
Injector Number of Holes, **Hole Diameter**	5 holes, 180μm dia
Hole Included Angle	142°

For instance, optical access is provided through a 20 mm thick window mounted on the extended Bowdich type piston. This window is encased in a metallic casing allowing the assembly to be removed with ease for cleaning.

As it can be seen from Fig 4.3 a fixed mirror is positioned at a 45 deg angle, with respect to the cylinder axis, underneath the piston assembly in order to grant unrestricted view of the 40 mm diameter combustion bowl.

Fig 4.2 – Elongated optical piston

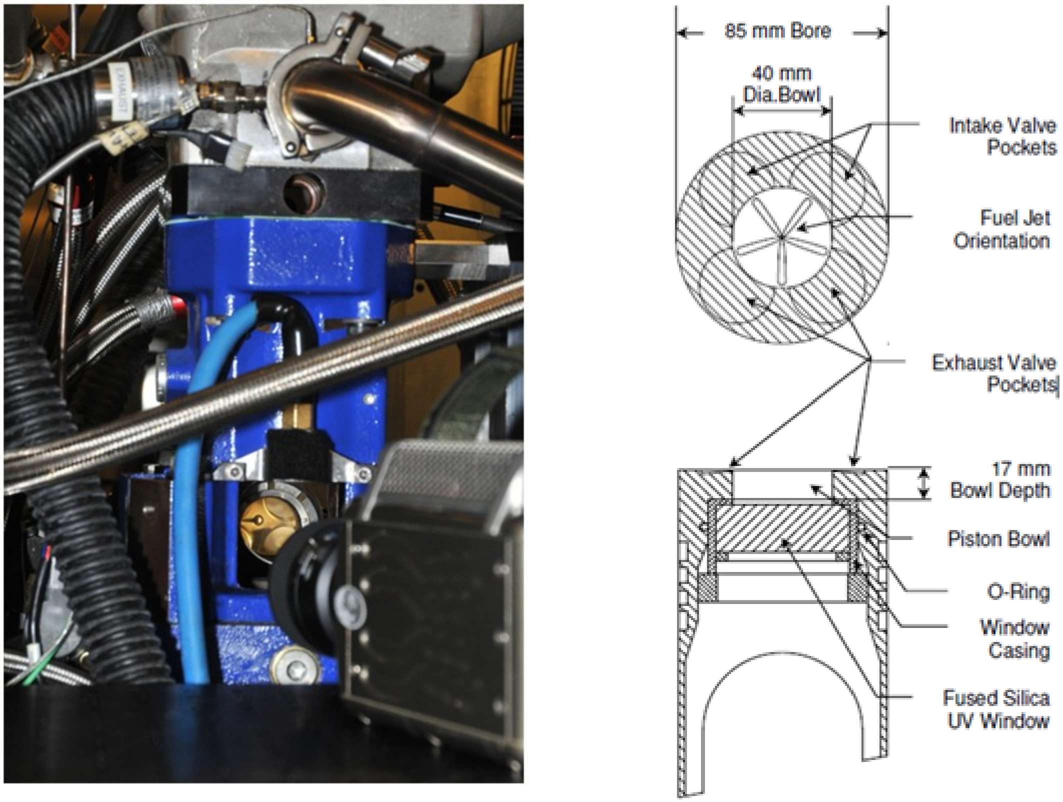

Fig 4.3 – AVL 5402 Single cylinder optically accessible research engine [131]

Additionally, there are two more optical windows mounted in the piston crown. The design of the piston and combustion chamber, while providing necessary optical access is striving to maintain the geometry as close as possible to the geometry of an all metal engine.

The combustion chamber is a high pressure, high temperature environment. That being the case, the materials utilized for the windows have to withstand these harsh conditions. Combining these mechanical properties with optical requirements two materials are most suitable for the optical windows: fused silica and sapphire. Depending on the application both materials have their advantages. On one hand sapphire has great hardness; while on the other hand, fused silica has better transmissivity in the UV-Vis spectrum. Fig 4.4 and Table 8 – Optical properties of fused silica and sapphire [133] show details related to spectral transmissivities and optical and mechanical properties of sapphire and fused silica.

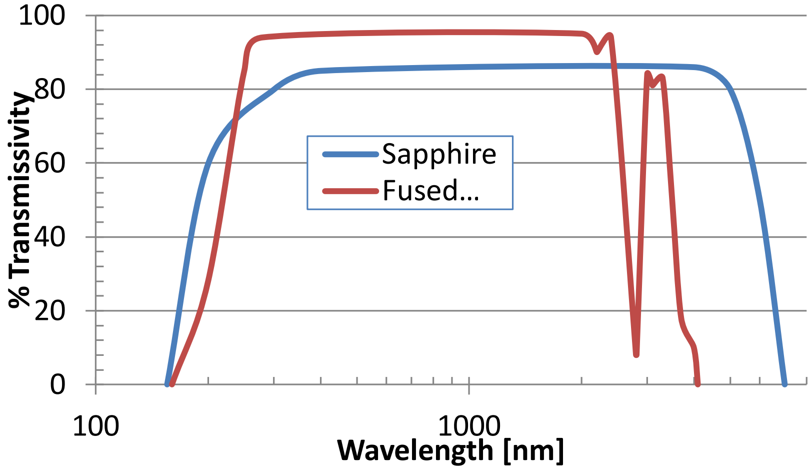

Fig 4.4 – Spectral transmissivity for fused silica and sapphire [132]

Table 8 – Optical properties of fused silica and sapphire [133]

Property	**Fused Silica**	**Sapphire**
Chemical Formula		Al_2O_3
Index of refraction @400nm	1.469	1.785
Density @293K [kg/m^3]	2.19	3.98
Thermal Conductivity @300K [W/m.K]	1.4	35.1 ∥ 33.0 ⊥
Thermal Expansion @ 293K [1/K]	0.5e-06	5.6e-06 ∥ 5.0e-06 ⊥
Specific Heat @298K [J/kg.K]	750	753
Mohs Hardness	7 (ref [134])	9
Young’s modulus of elasticity E [GPa]	72	335
Poisson’s Ratio	0.17	0.25

In order not to interfere with the optical access, oil cannot be employed for cooling the piston. The oil-less lubrication is provided by slotted graphite rings while sealing of the piston is achieved by uninterrupted bronze-teflon rings. Also, compressed air is directed underside of the piston window to cool the piston crown-window during the engine operation.

4.2 Test cell instrumentation, engine systems

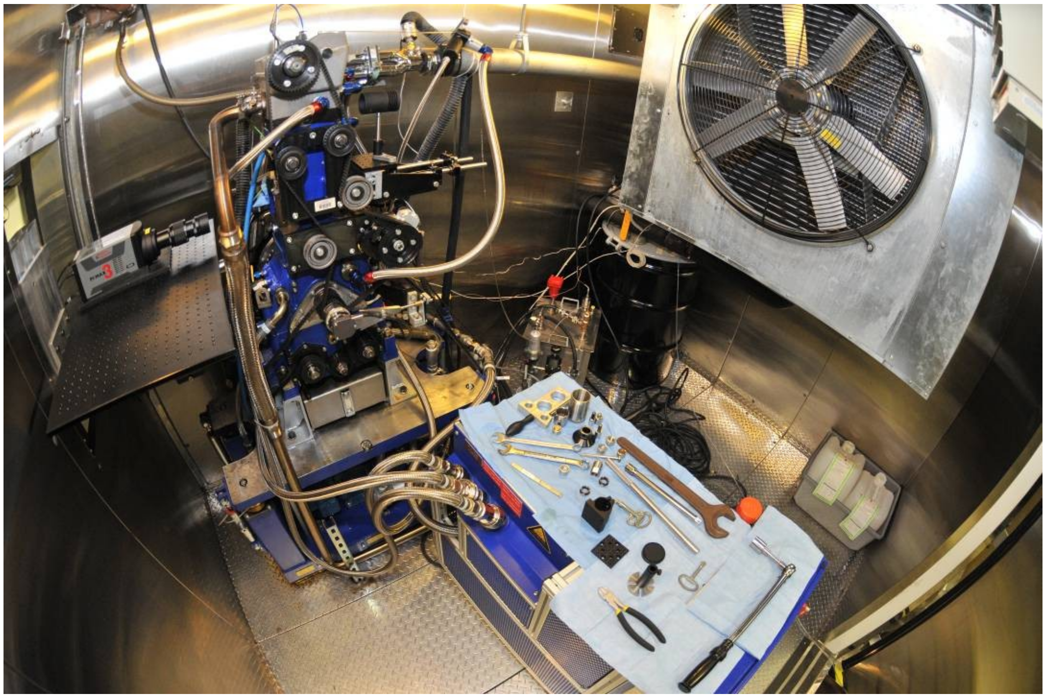

Fig 4.5 – AVL optical engine and AVL conditioning unit

The optical engine is located in a closed environment cold chamber that can lower the environment temperature up to -40°C. However, the cold starting testing of the engine is not of interest for the subject of this thesis.

For example, the AVL 577 external conditioning unit (see Fig 4.5) is used to maintain the coolant and lubricant flows at the preferred, optimum temperatures. Electric resistance heaters are used for raising the temperature to a desired, set-up value of 60°C in order to prepare the engine for the experimental testing. On the other hand, heat exchangers are used for dumping the heat from the closed system during the experiments. In case of the optical engine, the coolant and lubricant systems are separate systems and their functioning is independent on the engine speed.

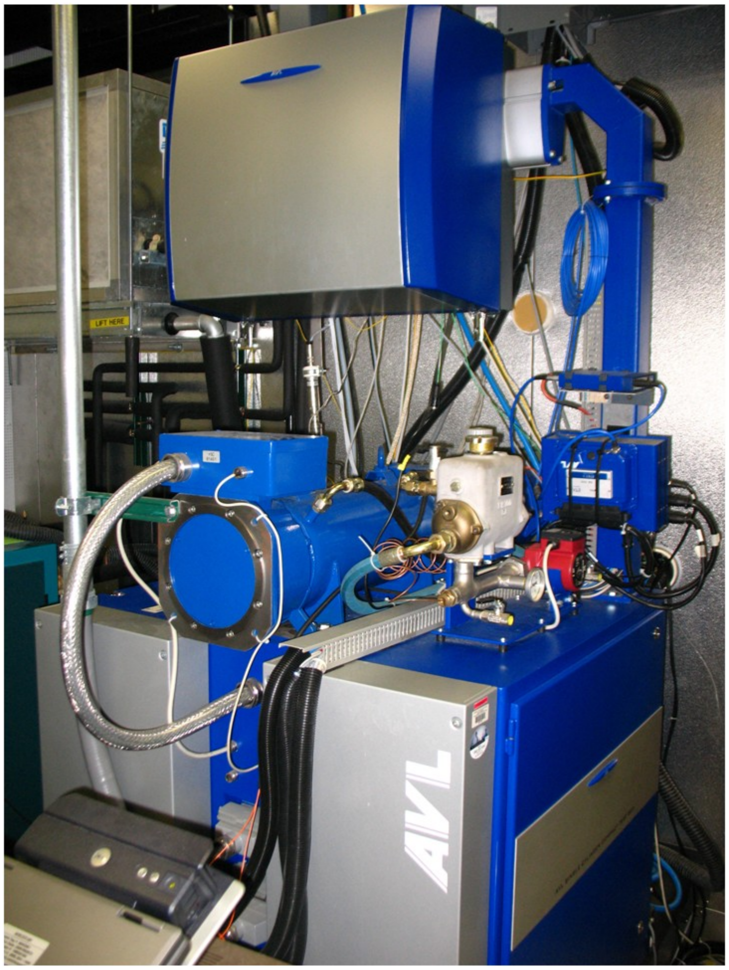

Fig 4.6 – AVL engine dynamometer

As part of the experimental setup, an AVL AMK AC dynamometer (DW13-170-4-A0W) is used for driving the single cylinder engine. The dynamometer is characterized by a 38 kW output power with a maximum torque of 120 Nm for a nominal speed of 3000 rpm.

Also, an optical encoder wheel (AVL 365) with a resolution of 720 pulses/ resolution is mounted on the crankshaft. In order to increase the angular resolution from 0.5 CAD to 0.1 CAD for the data acquisition system a pulse multiplier (AVL Model 365Z01M) is used to extrapolate the crankshaft position. A cam-shaft type TDC pulse is supplied to other equipment that require a crank angle signal for data synchronization such as NI-cRIO based engine and camera controller.

Fig 4.7 – Bosch ECU and ETAS VTK7.1

The engine’s electronic control unit is a Bosch ECU designed for diesel applications. The ECU is working together with the ETAS ETK 7.1 controller through the INCA v5.1 software to manage the fuel rail injection pressure. The National Instruments compact RIO (cRIO) real-time controller is controlling the triggering for the camera systems as well as fuel delivery parameters such as injection timing and duration.

The optical engine also has the capability of adjustable swirl. With the aid of a butterfly valve different swirl values are obtained, ranging from 2.0 to 4.5 swirl number.

4.3 Data acquisition system

Two data acquisition systems are available for use with the optical engine setup. First, is a high speed data acquisition system, AVL Indimeter, which is used to acquire cycle resolved information. It has eight channels available with a memory of 128 MB to record information for parameters of interest such as: in-cylinder pressure, needle lift and common rail pressure. This data acquisition system can operate at a maximum frequency of 20 MHz. Next, the information is handled by the AVL Indicom computer software and can be saved in an IFILE format. For post-processing a Matlab script [135] is used in order to have more flexibility for data analysis and display.

The second one is a low speed data acquisition system, AVL IFEM (Front End Module). This system is used for recording information related to slow changing parameters such as engine speed, fluid and gas temperatures. It has a maximum frequency of 100 Hz and the recorded parameters are time based instead of crank angle based.

4.4 Engine instrumentation

For information related to the combustion process such as rate of pressure raise and maximum combustion pressure the optical engine is equipped with an un-cooled piezo-electric pressure transducer (AVL GH 12 D) mounted with access within the combustion chamber through the cylinder head. A charge amplifier (AVL 621) is used for signal conditioning. The pressure transducer is characterized by a calibration constant of 16.25 pC/V.

Then, a fuel line pressure transducer is mounted between the fuel rail and injector in order to feed the high speed data acquisition system with cycle resolved rail pressure information. The transducer is an AVL SL31D-2000 strain-gage type transducer and the AVL 621 strain gage/charge amplifier is used for signal amplification. The calibration settings for this pressure transducer are 275.95 bar/V and 0.453μV/V.bar.

Also, a MicroEpsilon ES04 needle lift sensor is mounted on the fuel injector in order to detect the displacement of the injector needle throughout the injection event. The sensor is capable of measuring displacements from 0 to 0.4 mm. The amplifier (MicroEpsilon eddyNCDT 3300) used with the senor supplies a signal in the range of 0 to 10 V.

4.5 Optical equipment, high-speed camera

In addition to the optical probe developed, a high-speed camera was used for the experimental section of this thesis. The Phantom v7.3 from Vision Research Inc was found to be one of the best cameras for combustion studies; it is a visible range, high-speed CMOS digital, color camera. It has a 16 GB memory and a 14 bit dynamic resolution for each color. The CMOS sensor is using a Bayer color filter array (RGBG) covering the visible spectrum from 400 to 700 nm. The sensor’s maximum resolution is of 800x600 pixels where the pixel size is of 22 μm. Also, the camera is capable of capturing 200,000 frames per second.

During the experiment, the camera is synchronized with the engine and individual frames are recorded with a resolution of 0.5 CAD. With this high resolution the quantity of data captured is so large that in order to save memory as well as reduce the post-processing time only the frames within a 90 CAD interval are recorded. This range of interest begins with the start of fuel delivery and is signaled by the triggering of a TTL pulse from the National Instruments cRIO/Drivven Inc. controller. In this way only the frames of interest that contain pertinent information are recorded.

Resolution	Frames/s
800 x 600	6,688
640 x 480	10,101
512 x 512	11,527
256 x 256	36,697
128 x 128	88,888
128 x 64	129,032
64 x 64	148,148
32 x 32	190,476

Fig 4.8 – Phantom v7.3 (high-speed CMOS camera)

In addition, Zha *et al.* [98] has published a paper in which the normalized spectral response of this high-speed camera has been measured and the results are illustrated in Fig 4.9.

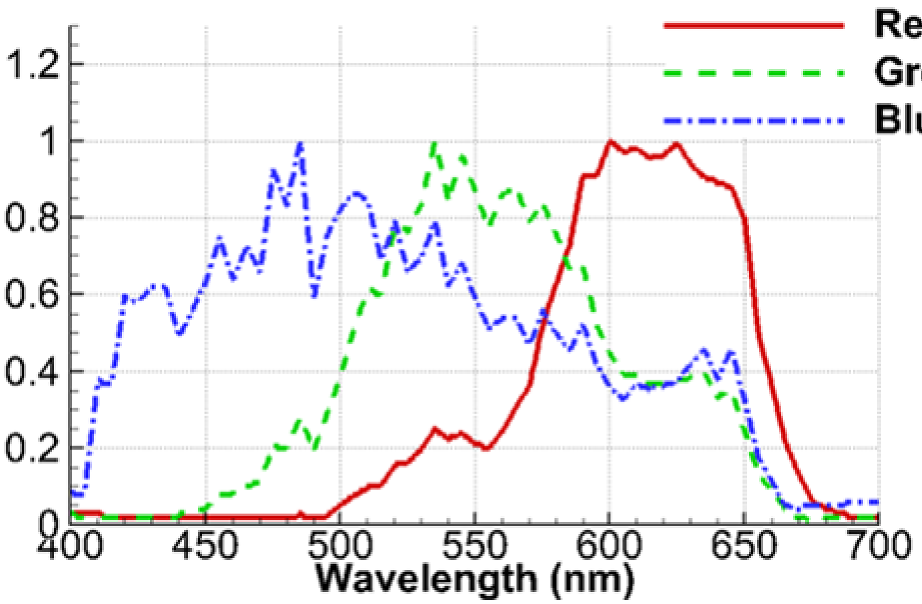

Fig 4.9 – Vision Research Phantom v7.3 optical response [98]

Due to space restrictions the camera is mounted on a custom design camera support outside the cold chamber with access to the engine through a window. Also, the camera support has the capability of x, y and z translations for high accuracy positioning.

Chapter 5. Data analysis

5.1 Experimental operating conditions and motivation

The experiments were conducted using a single cylinder optically accessible diesel engine. A complete description of the optical engine and its specifications as well as the equipment used during testing has been previously presented in Chapter 4.

Table 9 – ULSD and n-heptane fuel properties

properties	ULSD	n-heptane
cetane number	48.3 (DCN)	56 (CN)
density@15°C [kg/m3]	842	680
lower heating value [MJ/kg]	41.2	44.5
kinematic viscosity @40°C [mm2/sec]	2.479	-
Bulk modulus [GPa]	2.562	-

Two fuels were used for testing. First, ultra low sulfur diesel was selected, as it is the fuel of choice for diesel-type combustion systems. The second fuel, n-heptane, was chosen as a low-soot alternative to ULSD. While the n-heptane combustion process is quite similar to that of ULSD [136], it also has the advantage of low smoke (soot) formation propensity partially due to the lack of aromatic content. This characteristic will be taken advantage of later, during the results analysis part, when quantification of the CO flame will be necessary. Actually, similar trends can be seen for both fuels in terms of homogeneity when comparing the premixed combustion part.

In Table 9 a list of ULSD and n-heptane fuel properties is provided along with the distillation curve of ULSD presented in Fig 5.1.

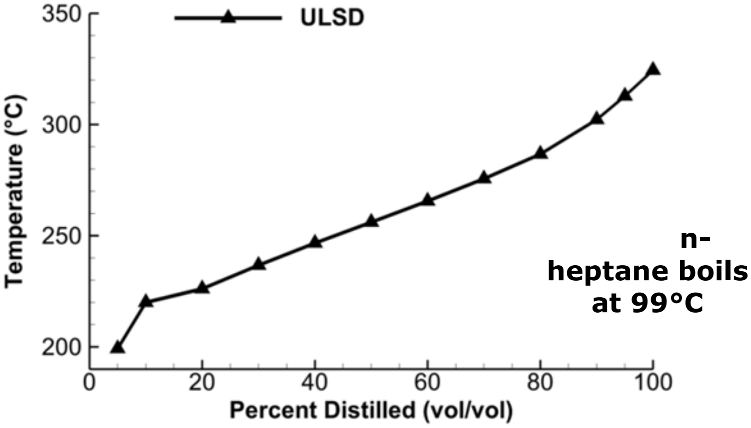

Fig 5.1 – ULSD distillation curve

In order to maintain the optical access free of impurities for as long as possible, the engine is equipped with an "oil-less" ring pack, where the production rings are replaced with Teflon-based rings. To facilitate the control the ring pack temperature and thus reduce the wear on the Teflon piston rings, the engine was skip-fired. During the skip-fired operation, fuel is injected for 3 consecutive cycles followed by a variable number of motoring cycles, ranging from 7 to 12 cycles, so that the thermal stability of the ring pack is maintained, as indicated by in-cylinder pressure measurements. Another advantage of using the skip-fire operation is that the window providing optical access within the combustion chamber is kept clean for a larger number of fired cycles. Matsui *et al*. [96] showed that, for a direct diesel engine, a 14% reduction in transmissivity influences the estimate for temperature by 1%, while the KL factor impact is 5%. In the referenced work the measurements were performed at 550nm.

Table 10 – Experimental operating conditions

Parameter	ULSD	n-heptane
Engine speed	1200 rpm	
Injection timing	9.5 °bTDC	7.5 °bTDC
Common rail injector solenoid activation time	480 μs	450 μs
Injection pressure	800 bar	
Location of peak premixed combustion	7°aTDC	
Intake temperature	306 K	
Swirl number	2	

The main parameters for the experimental operating conditions are summarized in Table 10. A single injection event 480 μs long, with a fuel rail pressure of 800 bar was chosen to yield a location of the peak premixed combustion at 7°aTDC. In addition, the engine cooling and lubricating systems were conditioned for one hour at 60°C prior to performing the experiments.

Also, images were acquired with the high speed camera (details available in the previous chapter) and each frame was synchronized with the engine crankshaft position. Individual frames were recorded with a crank position resolution of 0.5 CAD for each engine cycle.

A MATLAB script was used to calculate the apparent rate of heat release (ARHR) using the average pressure data. The ARHR calculation is based on the method described by Heywood [71] and the data shown is normalized by the engine displacement.

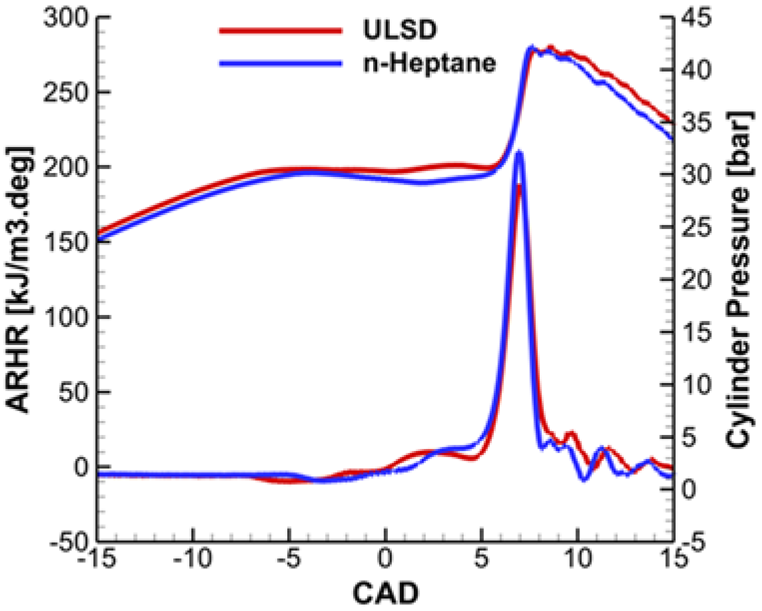

Fig 5.2 – Cylinder pressure and ARHR for ULSD and n-heptane

The combustion behavior shown in Fig 5.2 is typical of PCCI combustion, characterized by long ignition delays followed by a strong peak of premixed combustion and little to no diffusion combustion. This combustion mode is relevant for light load, high EGR, light duty engine applications as well as other combustion modes similar to the PCCI combustion. The engine was operated with no external EGR.

5.2 High-speed imaging results

In order to provide a better understanding of the single-point results, the high-speed imaging results will be described briefly in this section. Fig 5.4 shows the comparison of the combustion process of ULSD and n-heptane associated with one representative cycle. One may immediately observe a clear difference between the n-heptane and ULSD combustion: the lack of soot radiation, as indicated by lack of bright-yellow flame regions. While the combustion of n-heptane has been previously shown [137, 138] to lead to the formation of soot under certain operating conditions, is observed in this experiment to form negligible amounts of soot.

Both the ULSD and n-heptane combustion are characterized by five individual flame regions associated with each injector nozzle used in this experiment. The blue flame region is observed to occupy mostly the central region of the combustion chamber, while the soot-rich area is mostly restricted to the combustion chamber walls, close to the point of fuel jet impingement.

This combustion behavior, as documented by the high-speed color images, is significantly different from the traditional diesel combustion, where the fuel ignites and combusts during the injection process. As a result, the blue-flame radiation from the CO flame continuum is either dominant (n-heptane combustion) or of the same order of magnitude (ULSD combustion) as the soot blackbody-like radiation.

A final observation worth mentioning here is the timing of the blue-flame and soot radiation within the combustion process. The blue-flame is observed to initiate early on, as soon as the high-temperature heat release (HTHR) phase of the ARHR starts. As the local temperature increases and soot is formed, soot clouds become apparent. As the premixed combustion ends, the blue-flame radiation intensity decreases. As a result, the blue-flame radiation contribution to the two-color method decreases.

The goal of this research is to allow for the separation of the blue-flame and soot radiation effects, which in turn enables the calculation of the instantaneous gas temperature.

The topic of blue-flame interference on the soot radiation signal will be addressed in the following sections.

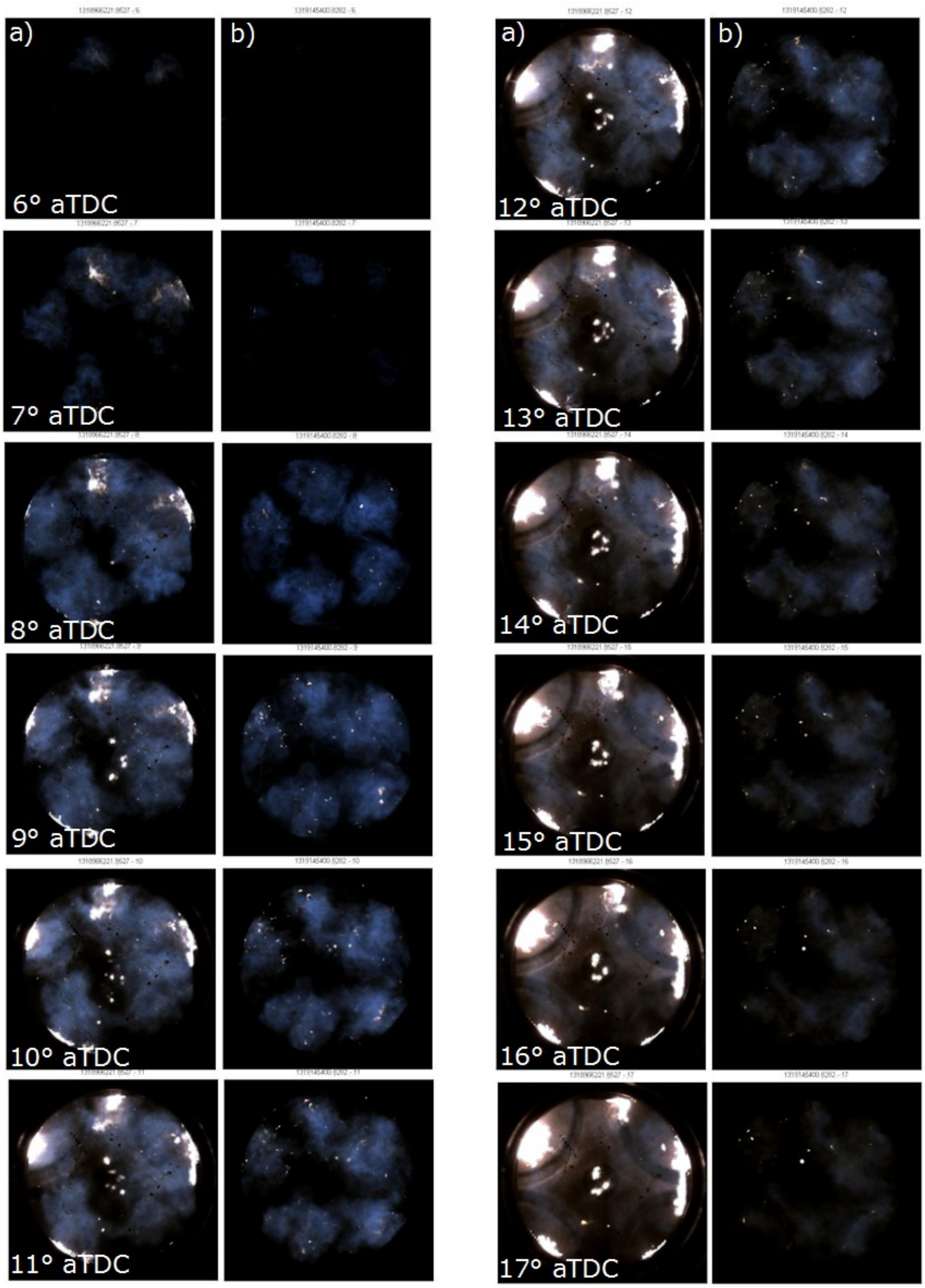

Fig 5.3 – Single-cycle high speed combustion images for a) ULSD and b) n-heptane

5.3 Fiber-optic probe measurements. Blue-flame intereference

Simultaneous measurements were performed using the fiber-optic probe described in section 3.2. The fiber-optic probe is exposed to the same radiation detected by the high-speed camera. As discussed in the previous section, the blue-flame radiation is fairly strong and may interfere with the application of the two-color method, by invalidating one of the TCM assumptions. By applying the method in its traditional form, using two detection channels, it is impossible to determine when such interference occurred except for the conditions in which the two-color method computes unreasonably high temperatures.

However, the blue-flame component of the radiation may be included in the TCM assumptions by considering a blue-flame model. As previously discussed in Chapter 3, section 3.5, the equation describing the optical detector signal received during the experiment is given by:

$$V_\lambda = C'_\lambda \cdot E_s(KL, T) \cdot \frac{A_{exp}}{L_{exp}^2} \cdot \frac{L_{cal}^2}{A_{cal}} + B_\lambda$$

where KL, T and B_λ are the unknown quantities. One may note that B_λ as defined above does not have an engineering unit and is subject to the experimental setup calibration settings.

The characteristics of the blue-flame radiation may be determined by interpreting the fiber-optic measurements associated with the smokeless n-heptane combustion. Under these specific conditions where there is no soot generated during the combustion process equation (3.12) becomes:

$$V_\lambda = B_\lambda \tag{5.1}$$

By writing equation (5.1) for λ_1, λ_2 and λ_3 and taking the ratios one obtains:

$$\frac{V_1}{V_2} = \frac{B_1}{B_2} = f_{12}$$
$$\frac{V_2}{V_3} = \frac{B_2}{B_3} = f_{23} \qquad (5.2)$$

and the ratios are denoted by: f_{12} and f_{23}.

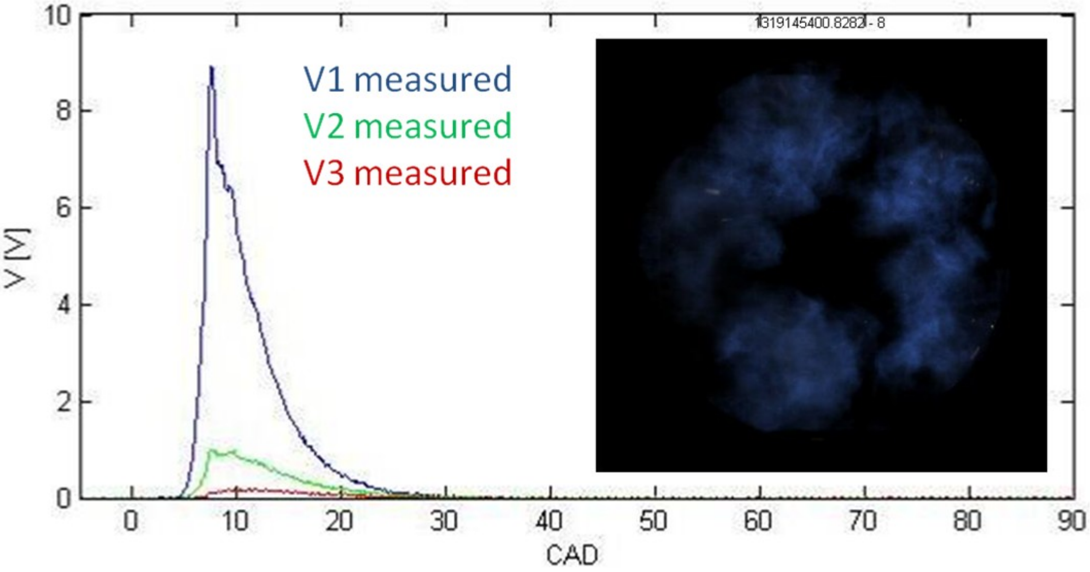

Fig 5.4 – Detector signals for one cycle and corresponding high speed camera image at 8 CAD

Fig 5.4 shows data from one engine cycle where n-heptane was used as fuel. Also, an image of the high speed camera is shown for 8 CAD of that cycle. The high-speed camera image confirms (Fig 5.4) the lack of radiation associated with soot. The assumption shown in equation (5.1) is thus reasonable.

While V_1, V_2 and V_3 are characterized by a large cycle to cycle coefficient of variation (COV), Fig 5.5 and Fig 5.6 show that f_{12} and f_{23} have a significantly lower COV, with a repeatable and constant behavior. For both figures, the average values of f_{12} and f_{23} are plotted in red. Coefficient f_{23} is observed to have slightly higher noise compared to f_{12}, which may be attributed to the lower level of blue-flame radiation at longer wavelengths [90, 128].

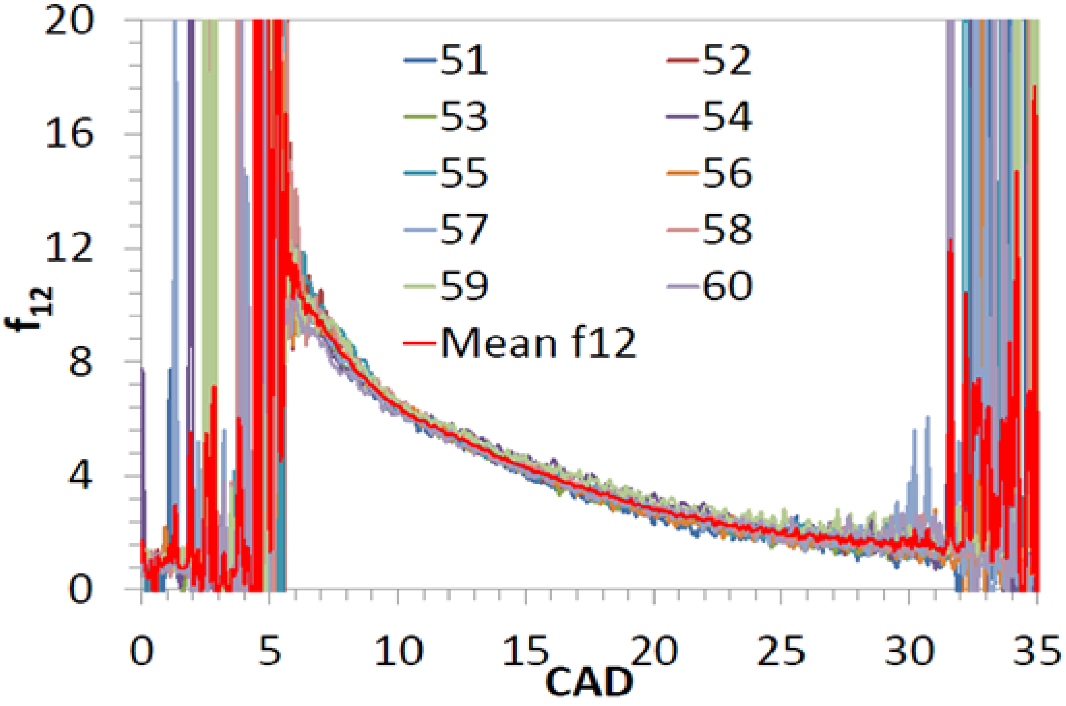

Fig 5.5 – Plot of f_{12} for 10 arbitrary, consecutive cycles

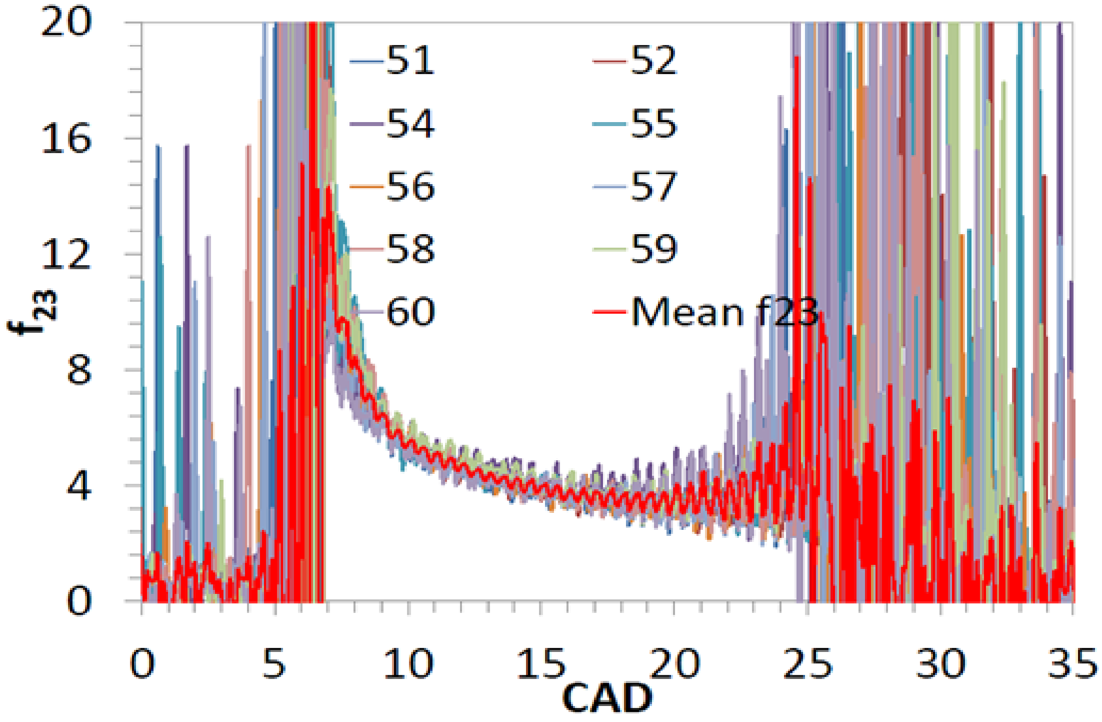

Fig 5.6 – Plot of f_{23} for 10 arbitrary, consecutive cycles

The range of interest is delimited by the range where the optical probe detectors receive a signal due to the blue flame phenomenon. Outside that range, the signal to noise ratio (SNR) is low and no useful information is available.

The fact that ratio f_{12} is not constant may lead to the assumption that the signal is influenced by aldehyde chemiluminescence. However, the fact that f_{23} has the same shape and magnitude indicates that it is less likely that this mechanism is responsible for the observed behavior.

As previously discussed in section 3.5, the author believes that with increase in pressure there is an increased probability of having collisions between the molecule of CO and the O atom that could be translated in an increase magnitude of the continuum throughout the entire spectrum. But it is supposed that there is no effect on changing the shape of the CO continuum spectrum (i.e. relative spectral intensity).

The author acknowledges the fact that, due to the complexity of the phenomenon (i.e. tri-atomic molecule responsible for the measured change in continuum relative intensity, potential contribution from CO flame bands or aldehydes and others), this hypothesis requires further testing in order to be fully validated.

On the other hand, the experimental tests performed by Gaydon [128] on preheated flames (750°C) of CO with air and CO with O2 in a modified burner showed for both cases that with increase in temperature the CO flame continuum is increasing in intensity and the short-wave end is getting stronger. Gaydon's findings have also been confirmed by Kaskan [129] who obtained the same behavior in his experimental work.

Also, formaldehyde (CH_2O) can influence the measurements because it emits in the region of interest of the CO continuum; however, it is consumed at the onset of the blue flame. This can also be a factor that influences the uncertainty of the eTCM in calculating the temperature and optical thickness factor at the beginning of the combustion cycle (see Fig 5.11).

In conclusion, based on currently available evidence from the literature, an assumption is made regarding f_{12} and f_{23} and that is that the ratios are depended only on the combustion temperature and are not a function of pressure [90, 114, 128].

5.3.1 Short wave effects – f12

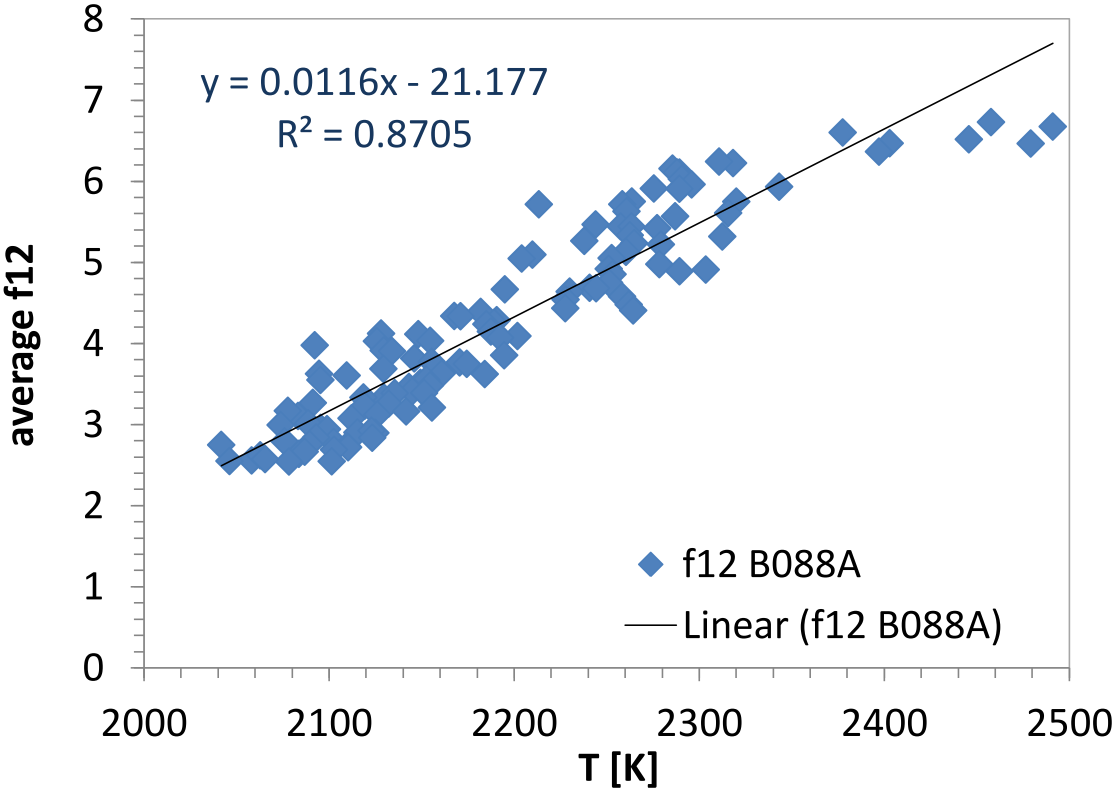

Fig 5.7 – f_{12} linear dependence of temperature

At this point a second assumption is needed. It is assumed that the n-heptane and ULSD combustion generates are characterized by similar in-cylinder temperatures. This assumption is reasonable due to the closely shared characteristics of n-heptane and ULSD, such as energy release rate and stoichiometric adiabatic flame temperature [136]. Additionally, owing to their small size, the soot particles emitting the blackbody radiation are in thermal equilibrium with the surrounding mixture, assuming the temperature of the surrounding gas. With the additional experimental data provided by a fundamental investigation of f_{12} and f_{23}, the need for this assumption would be alleviated, with potential benefits related to blue-flame intensity measurement.

A fairly strong correlation may be observed in Fig 5.7 between the quasi-average in-cylinder temperature determined by eTCM and the associated f_{12} value. The correlation appears to be mostly linear, although the linearity assumption is not completely certain due to the relatively large degree of scattering exhibited by the data. The linear regression R^2 coefficient mirrors the increased data scatter.

The physical reason behind the linear correlation is not fully understood at this time and additional data is required to fully describe it. A possible explanation could be associated with the relatively small range of temperatures explored by this experimental setup, which in turn has a linearizing effect.

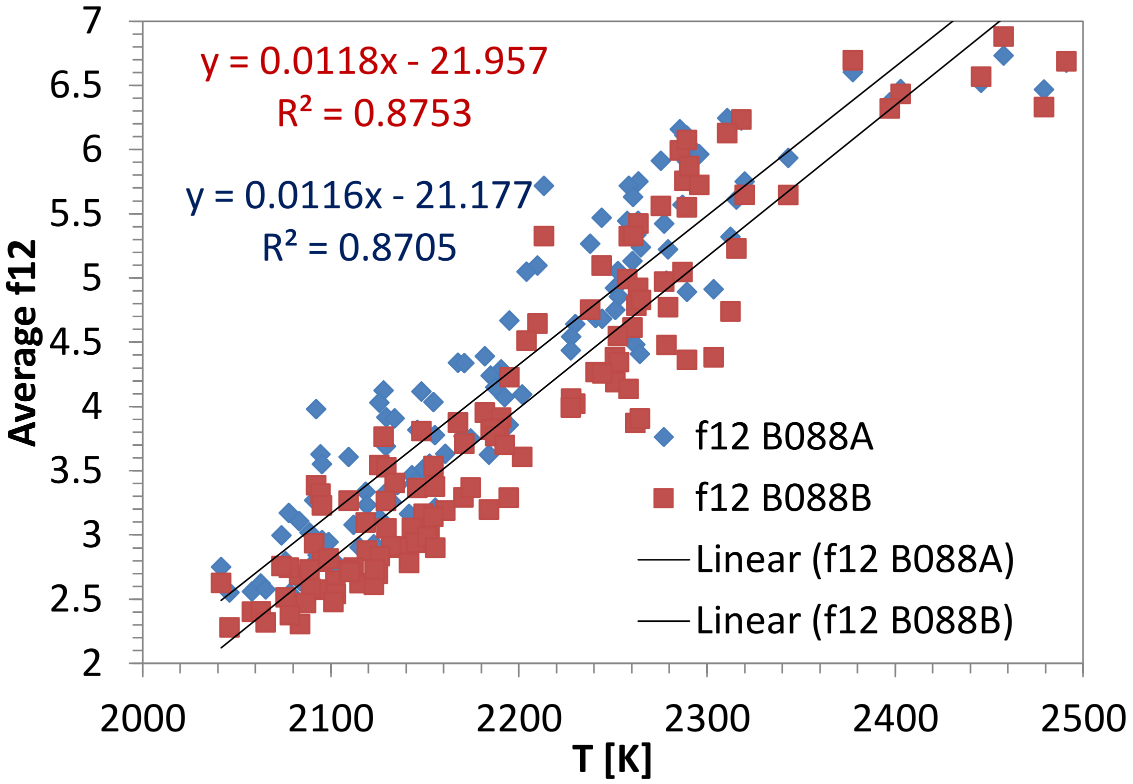

Fig 5.8 – f_{12} linear dependence of temperature for two data sets

Further, Fig 5.8 shows the f_{12} correlation for two data sets; these data sets are were sampled consecutively with no cleaning of the main optical access occurring between them. The results indicate that the correlation is replicated very well between the two tests. The slight vertical shift between the two linear regression models could be associated with window deposit effects. As is the case with the traditional implementation of TCM as well, window deposits are responsible for increased measurement uncertainty which needs to be controlled for reliable temperature and soot optical thickness estimations.

5.3.2 Long wave effects – f23

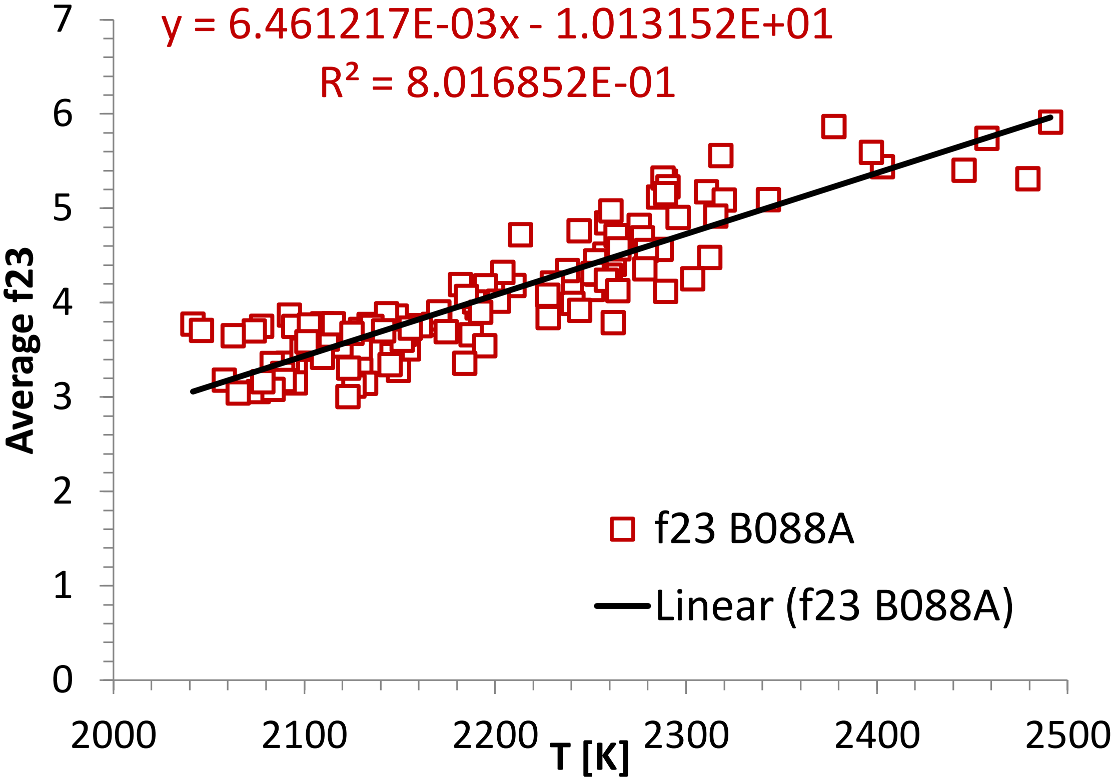

Fig 5.9 – f_{23} linear dependence of temperature

A similar correlation is observed for the intensity ratio between detectors two and three. A linear correlation is maintained, albeit the regression model exhibiting a lower slope.

The blue-flame spectral emission models f_{12} and f_{23} are now used to determine the soot temperature and optical thickness under blue-flame interference conditions. Equations 3.12 along with the empirical f_{12} and f_{23} models described previously, form a system of equations that may be solved for the unknowns T, KL and blue-flame intensity B_1. The solution algorithm is shown in Fig 5.10 below.

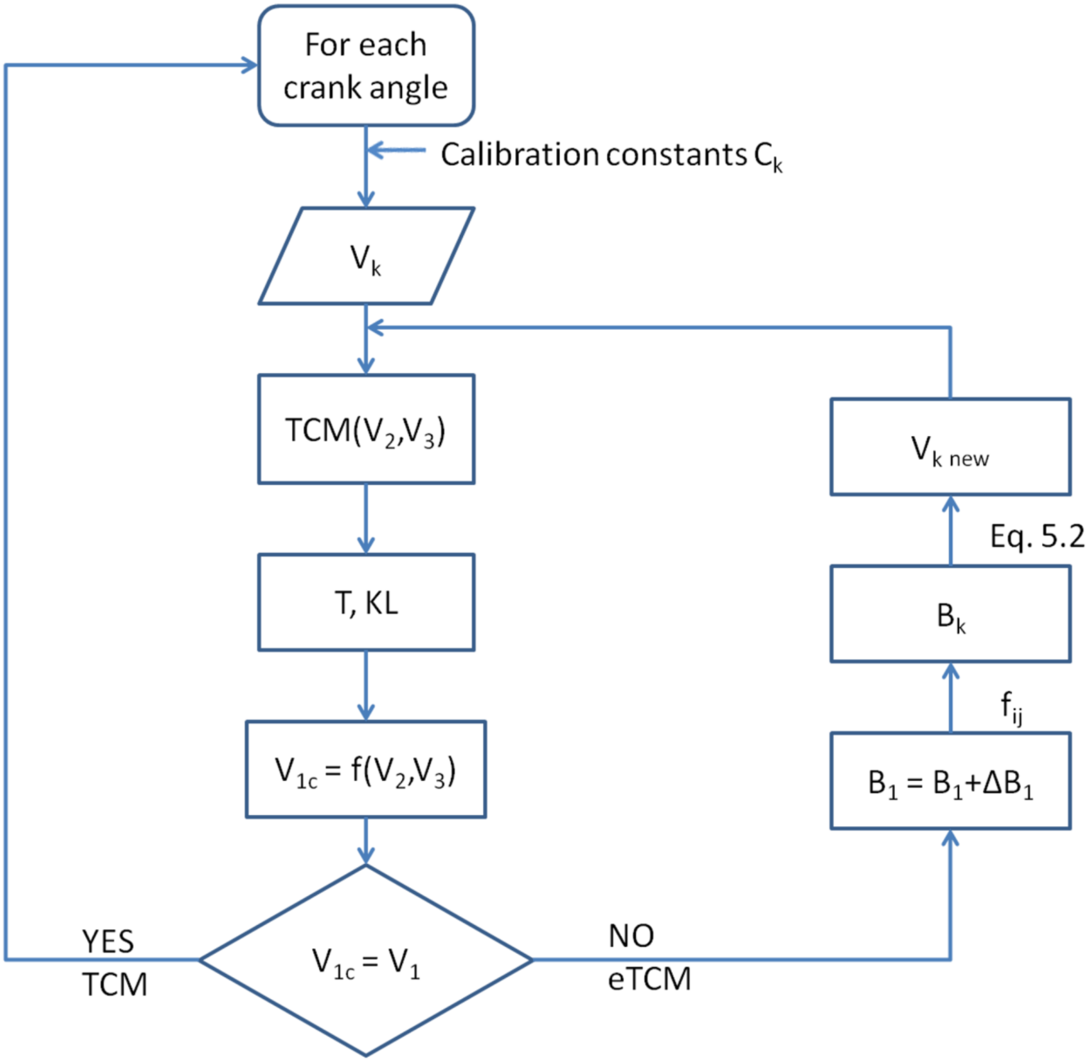

Fig 5.10 – Numerical solver – description of the iterative steps

5.4 Blue flame interference compensation. eTCM

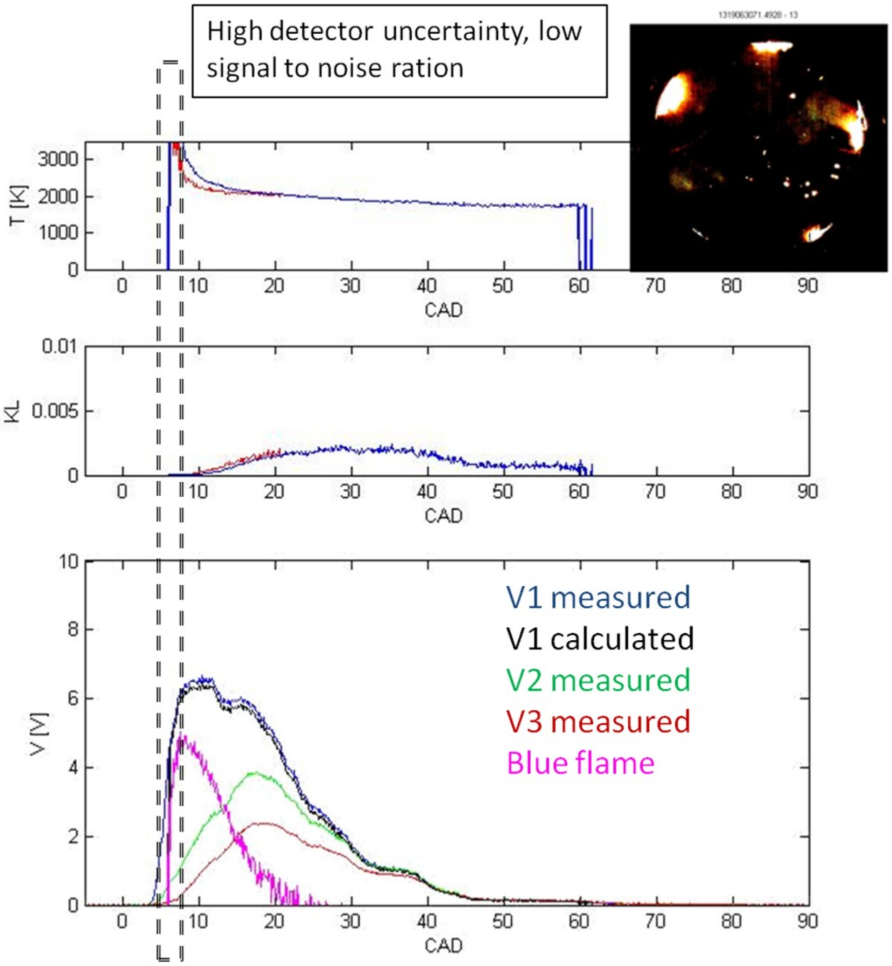

Fig 5.11 – eTCM results for soot temperature and KL factor

A sample engine cycle is shown for illustration purposes in Fig 5.11. It may be observed that the measured and calculated V_1 signals agree rather well. This is expected, as it represents one of the solver constraints, as shown in Fig 5.10. At the onset of combustion the temperature prediction is unreasonably high, well in excess of the stoichiometric adiabatic flame temperature of the selected fuels. This could either be attributed to the high detector uncertainty and low signal to noise ratio associated with the third detector signal, V3. The temperature and optical thickness results are shown as well. In blue is the temperature calculated with the two-color method while with red is represented the temperature recalculated with the extended two-color method. The optical thickness KL is computed under the assumption that the soot cloud occupies the entire combustion chamber. This assumption is rather an extreme case out of the possible scenarios. The impact of this assumption will be discussed in a subsequent section.

The eTCM solution is applied up to about 25 CAD in this case. As the blue-flame interference diminishes below detection limit, the TCM method is applied until the signal strength from the three detectors decreases below a 0.1V amplitude.

As for both methods for the first crank angle degrees of each cycle unphysical high temperatures are obtained. This can be explained by the high detector uncertainty that translates in a low signal to noise ration.

To conclude, it has been shown that the blue flame has a significant effect on the measurement of T and KL when using the traditional two-color method. A solution has been proposed to measure the strength radiation of the blue flame by employing the extended two-color method.

5.5 Extended Two-Color Method (eTCM) assumptions

Two major assumptions are part of the proposed extended two-color method. First, one assumes that the blue flame interference is significant and can no longer be ignored without incurring significant temperature and KL estimation errors. This statement was already discussed in the previous section but will be demonstrated in the section 5.6 below.

Second, the area of interest is no longer assumed to cover an infinitely small area of the soot cloud. Rather, as described in section 5.6.2, the detector is allowed to collect light from the entire visible range of the combustion chamber. This approach replaces the typical time-averaging associated with the classical TCM with space averaging. Thus, the temporal uncertainty regarding the position of the soot cloud is now replaced with the spatial uncertainty associated with the heterogeneous coverage of the combustion chamber by the soot cloud. Without proof, the two methods are expected to have uncertainties in the same order of magnitude. From this point of view, the eTCM and TCM are inter-exchangeable without loss of accuracy. However, as the measurement area is increased to the whole combustion area visible using optical techniques, the position and area occupied by the soot cloud are unknown at the time of the measurement. In order to get around this issue, eTCM assumes that the soot cloud is uniformly distributed across the entire view area. The impact of this assumption will be discussed in further detail in section 5.6.2.

5.6 Uncertainty factors

5.6.1 Temperature and optical thickness KL effects

As previously prefaced in figure Fig 5.11, the eTCM results differ from the TCM results during the blue flame interference phase. This is better viewed in an eTCM

versus TCM correlation plot. Fig 5.12 shows such a temperature correlation for five consecutive cycles. While there is some cyclic variability that may be observed in the data, all cycles exhibit similar trends. First, a high degree of correlation is observed for lower temperatures. Those temperatures occur later in the cycle, during the expansion stroke, where the blue-flame radiation drops below the detection limit. Higher temperatures, occurring earlier in the cycle have a significant deviation from the diagonal line which indicates equality between the TCM and eTCM derived temperatures. As a result of the blue-flame interference, as mentioned in section 5.4, the TCM results tend to overestimate the soot temperature. The error can be significant in this range, showing 10% higher temperatures compared to the eTCM estimation.

Similarly, the optical thickness KL results for eTCM and TCM are the same for the crank angle range where there is no blue-flame interference, while the blue-flame introduces significant errors in the KL prediction. This may be observed in Fig 5.13, where, unlike the temperature results which were overestimated by TCM, both over and underestimation are encountered. The error bound for the KL estimation is as high as 30% of the measured signal. This behavior is in agreement with previous error analyses of TCM [76] where various uncertainty factors have an exaggerated effect on KL and a relatively small impact on temperature.

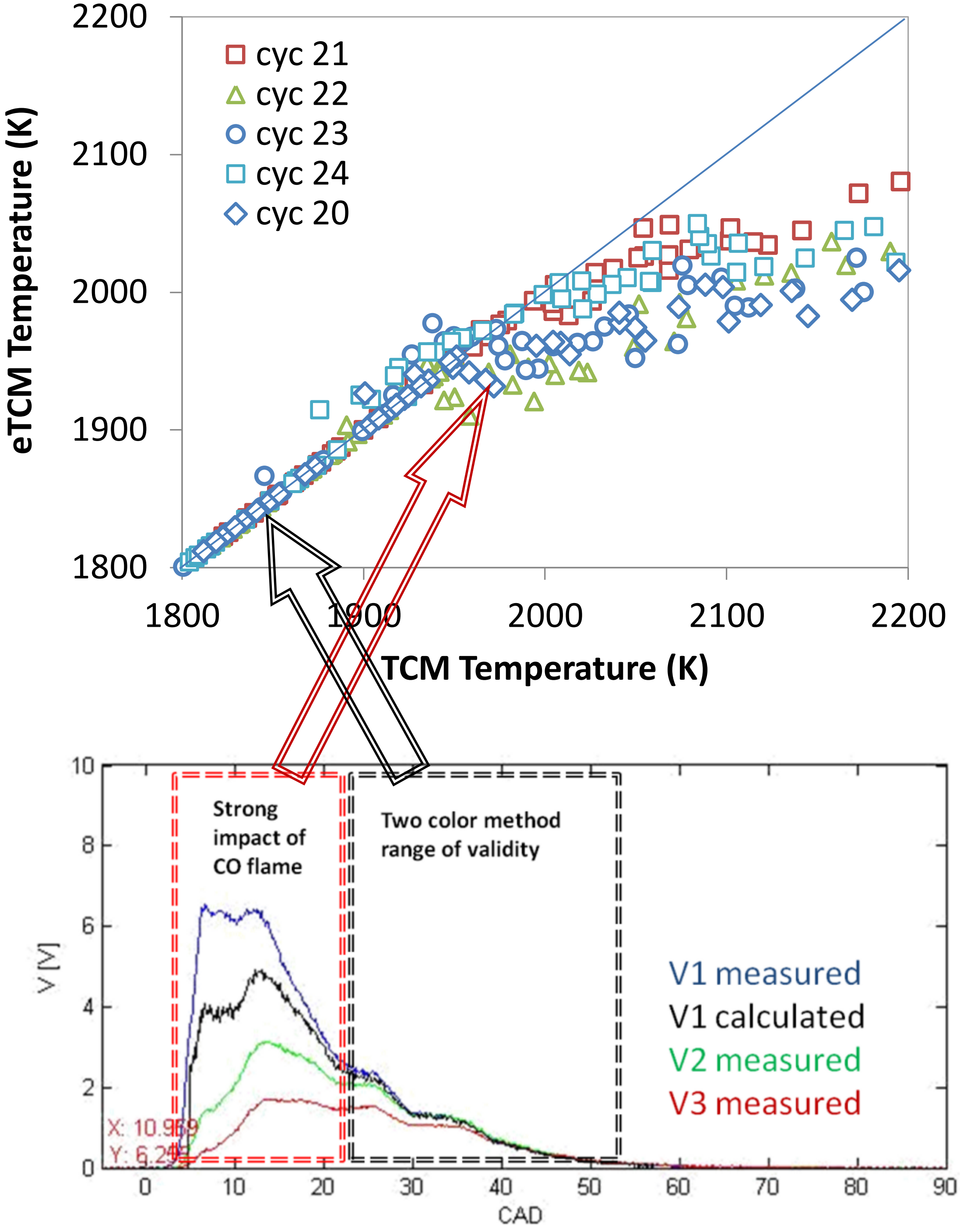

Fig 5.12 – Temperature results comparison for TCM and eTCM

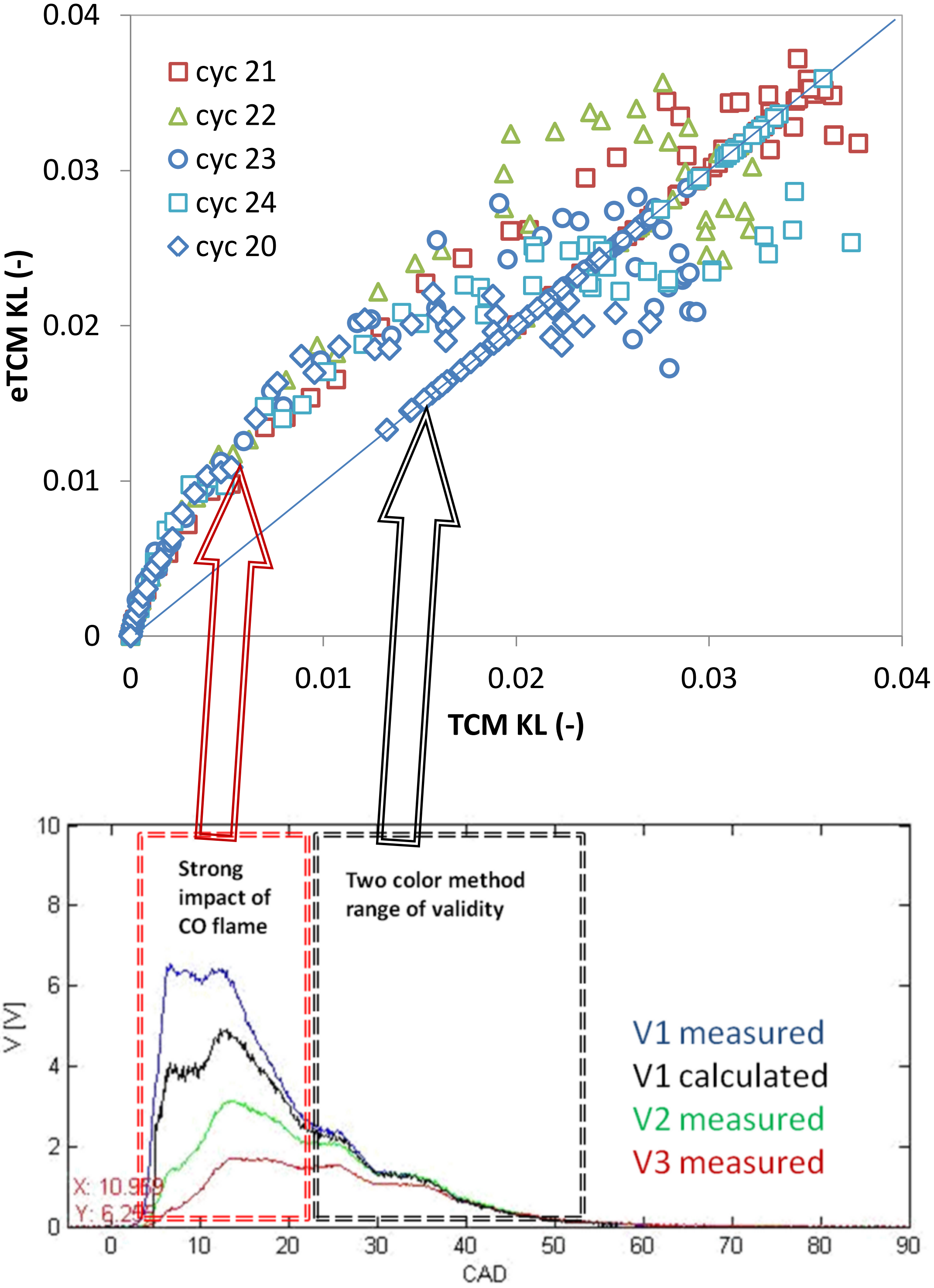

Fig 5.13 – Optical thickness factor KL results comparison for TCM and eTCM

5.6.2 Soot cloud area effects

Unlike the conventional two-color method, where a small area of the combustion chamber is sampled by the detector, eTCM proposes the use of the optical information collected from the entire field of view available. The main benefit of this approach is that single-cycle measurements are possible with a much higher degree of accuracy compared to the conventional approach, which requires significant cycle-averaging. The resulting soot optical thickness factor KL is thus a representation of the average combustion chamber soot concentration. This assumption is referred to as the "standard eTCM assumption". The assumption regarding the soot cloud sampled area is expected to have a small impact on the soot temperature estimation. The following paragraphs will describe the impact of various area assumptions on the temperature and KL estimations.

First, a cycle's worth of data has been processed under different assumptions regarding the soot cloud area. As discussed previously, eTCM assumes that the soot cloud covers the entire combustion chamber. This 100% area coverage will be considered to be the reference solution. Fig 5.14 shows the temperature difference between the 100% area coverage reference case and a range of area coverage assumptions. As a result temperature differences as high as 4K may be observed if the area assumption is off by an order of magnitude. When viewed in Fig 5.15, this temperature difference occurs at about 1900K, resulting in a 0.2% error. The contribution of this error to the measurement uncertainty is thus relatively small compared to other sources of uncertainty. Consecutive cycles, shown in Fig 5.16, have a similar behavior for the 10% to 100% coverage area temperature difference.

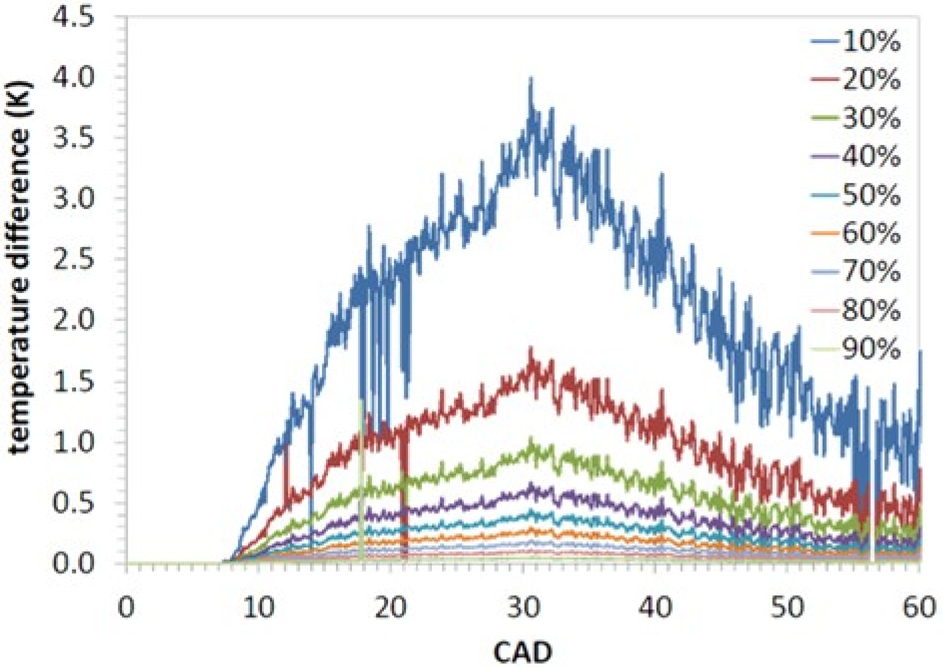

Fig 5.14 – The difference in temperature for various soot cloud areas with respect to 100% area function of CAD

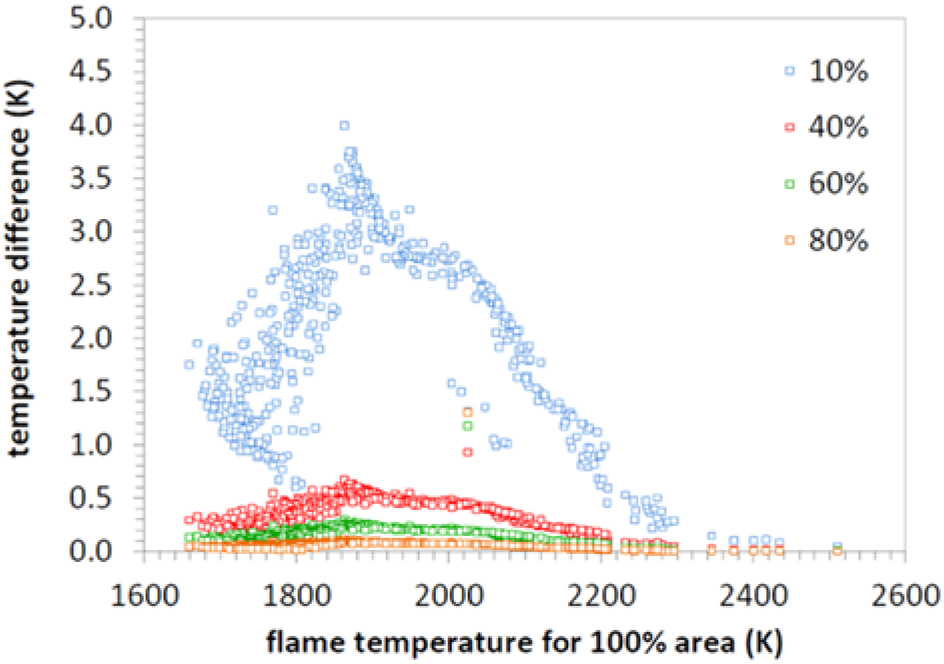

Fig 5.15 – The difference in temperature for various soot clouds area function of combustion temperatures

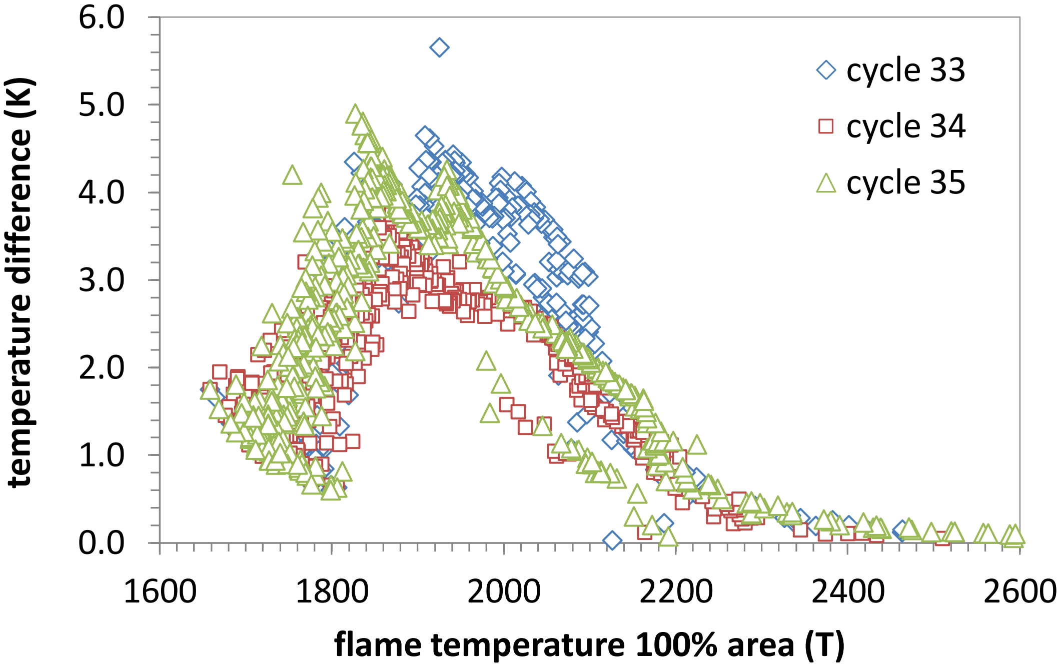

Fig 5.16 – The difference in temperature for a 10% soot cloud area for various cycles

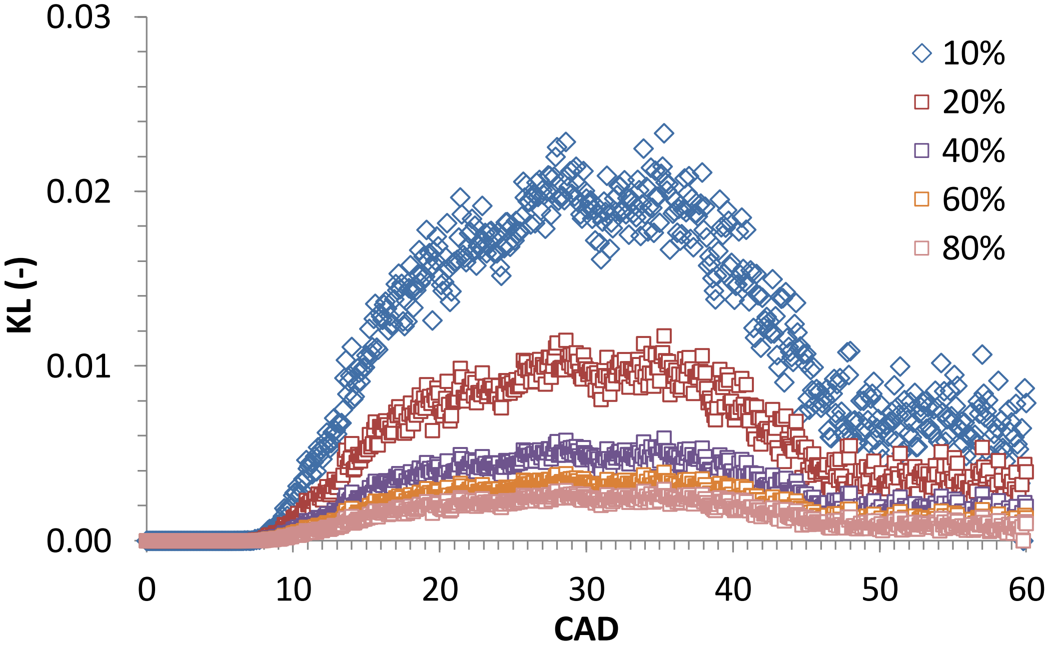

Fig 5.17 – Optical thickness factor KL evaluation for different soot cloud areas

The impact of the cloud area assumption is shown in Fig 5.17. Large “errors” are apparent, as KL halves as the cloud area increases from 10 to 20%. However, it will be argued that this is not a real “error”. Due to the large light sampling area, the optical thickness factor is now area dependent and thus its value will change as a function of the assumed area convention. As the assumed soot cloud area increases, the equivalent cloud would need to be “optically thinner” in order to match the spectral intensity characteristics experimentally measured.

5.6.3 Comparison with high-speed soot cloud area measurement

Given the increased flexibility allowed by the experimental setup available for this work, the results of the eTCM method may be compared under two sets of assumptions. The first includes the use of the standard eTCM assumption, where the entire field of view available is considered as being covered by a homogenous soot cloud of equivalent optical properties as the one available experimentally. The second set of assumptions follow the work of Musculus [101], where the area covered by the soot cloud is estimated using the available high-speed camera data. An error estimate is thus available to further quantify the impact of the standard eTCM assumption. As one may recall, the standard eTCM assumption is needed in combustion systems where a full optical access or high-speed imaging of combustion is not practical.

An additional verification of the validity of the eTCM results is available by comparing the blue flame data provided by eTCM with the blue-flame data sampled by the high-speed camera. The range of data points available for this type of work is expected to be restricted to combustion events with relatively small amounts of soot and relatively strong CO flame radiation intensity.

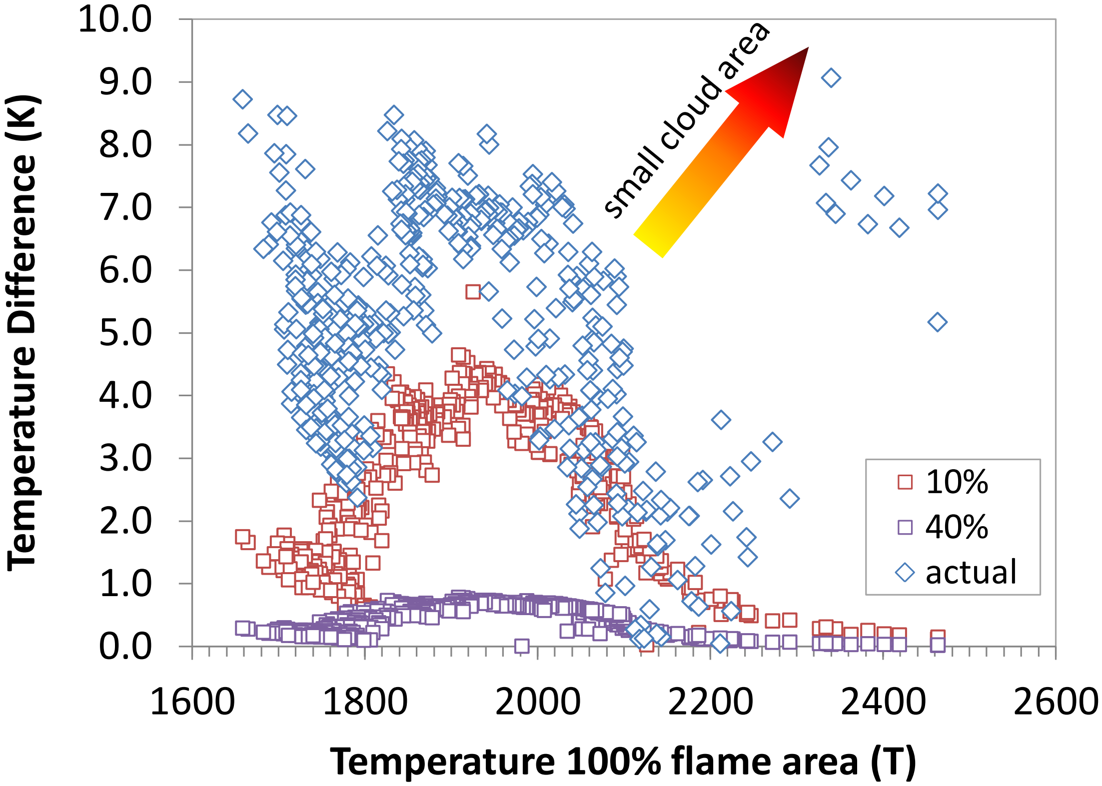

Fig 5.18 – Temperature difference for the actual soot cloud area, 10% and 40% soot cloud area assumptions function of combustion temperature

The impact of the constant area assumption is shown in Fig 5.18 above. The temperature difference between the estimation based on the standard eTCM assumption (100% of the combustion chamber is occupied by soot) and the temperature estimation based on the "actual" soot cloud area measured by the high-speed camera. The result shows that the maximum uncertainty introduced by this assumption is about 10K, or 0.5%.

5.7 Blue-flame results

Besides the improved temperature and KL estimations which relate to soot properties, eTCM provides the added benefit of quantifying the amount of blue-flame radiation. The amount of radiation emitted by CO_2* is proportional to the rate of energy release from the premixed phase of the combusting fluid. This in turn provides a useful measure of the degree of combustion homogeneity, which could provide significant benefits in both combustion research as well as development efforts, such as engine calibration.

5.7.1 Comparison with high-speed blue-flame intensity measurements

As in the case of the soot cloud area, the high-speed information may be used to provide added validation of the eTCM assumptions and hypotheses. The high-speed camera, equipped with a Bayer-type filter, allows for the spatial separation of the radiation originating from blue-flame and soot radiation. A Matlab® based script was used to identify the pixels likely occupied by blue flame and performed a signal integration. Some of the blue flame radiation will not be fully accounted for, as it originates from regions of the combustion chamber where soot is available along the line of sight. However, for the combustion mode investigated, the soot cloud area is rather small, occupying up to 10% (Fig 5.18 previously discussed). As such, the error introduced by ignoring the amount of blue-flame radiation originating in those areas will be very small.

At the same time, the results of the high-speed image integration may be compared with the blue-flame intensity estimation provided by eTCM. Such results are shown in Fig 5.19 below. Two distinct zones may be observed in this plot. First, an area of linear correlation between the camera and eTCM results is apparent, especially for higher blue flame intensities. For the linear correlation zone, the degree of scatter is well within acceptable limits, indicating a good agreement between the camera and eTCM results.

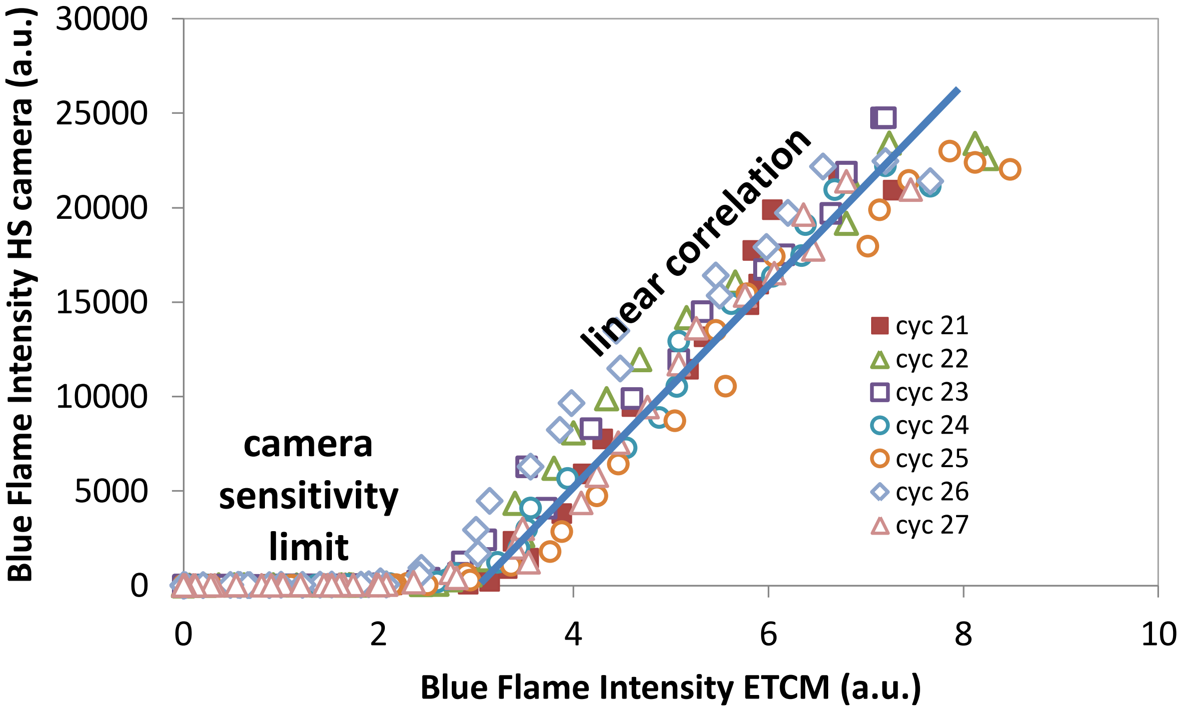

Fig 5.19 – Blue flame intensity comparison for high-speed camera and eTCM

On the other hand, for low blue-flame intensities (i.e. 3 eTCM blue flame intensity units), the high-speed camera is no longer sensitive and no data is available. The optical probe appears to have increased sensitivity compared to the high-speed CMOS chip. This increased sensitivity could be attributed to the data acquisition methodology employed for the two blue-flame measurement methods. While the CMOS chip samples the data through a large number of individual detectors, eTCM uses a much restricted number of detectors, performing the integration process within the detector hardware, prior to the digital conversion step, which significantly improves the signal to noise ratio.

It is noteworthy that the blue-flame detection sensitivity is maintained even after a significant number of computational steps required by the eTCM approach.

5.7.2 Effect of soot cloud area assumption on blue-flame intensity estimation

eTCM assumes that the soot cloud covers the entire combustion chamber area. However, as previously discussed in section 5.6.3, this is not the case. The effect of this assumption has been explored in Fig 5.20 below. Data plotted along the *x* axis is associated with the blue-flame prediction considering the actual soot cloud area, as measured from the high-speed images. At the same time, the difference between the blue-flame intensity determined using this assumption and the blue-flame estimation considering 100% soot area coverage is plotted on the *y* axis. The data indicates a reasonable impact of the 100% area assumption for high blue flame intensities. However, for lower blue-flame intensities the error quickly grows and may exceed 25%. This behavior is likely caused by the decrease in SNR associated with the lower blue-flame intensities.

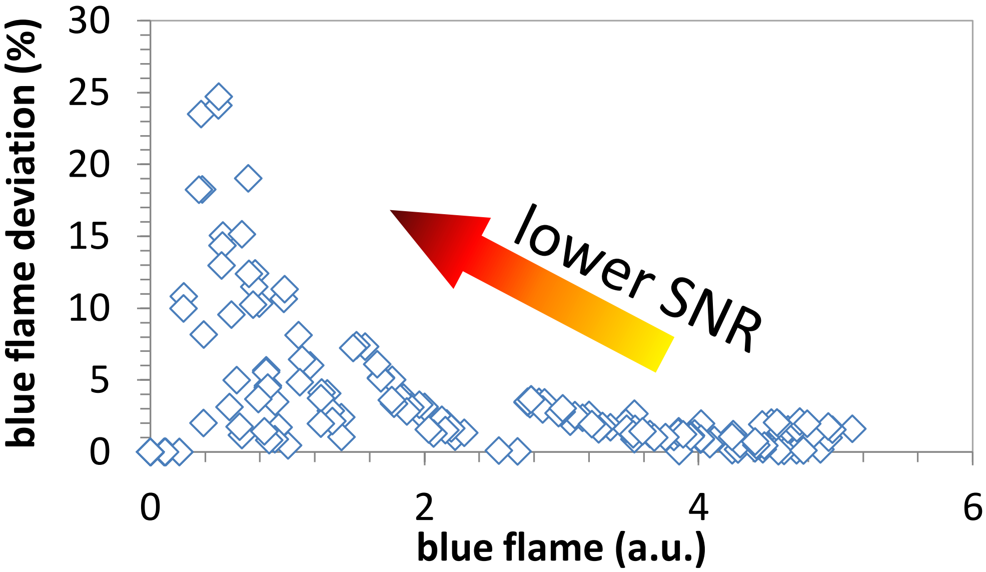

Fig 5.20 – Effect of soot cloud coverage assumption

Chapter 6. Conclusions and future work

6.1 Conclusions

In modern engines, combustion modes, such as partially-premixed charge compression ignition (PCCI), are characterized by strong premixed flames accompanied by relatively small soot-producing diffusion controlled flames.

In such situations, the application of the two-color method to determine flame temperature and soot optical thickness is strongly influenced by the contribution of the CO flame radiation. This is shown in high-speed photography collected by the author as well as numerous other publications from other research groups. As a result the two-color method assumptions break down and temperature and KL data is no longer available.

The current work presents the theoretical background and experimental evidence needed to describe a newly proposed optical diagnostic tool, the **extended two-color method (eTCM)** as well as the development and construction of an original **optical probe** designed to provide the required experimental data.

The optical combustion probe is capable of providing information regarding the soot formation and oxidation processes calculated from the measured signal. Three detectors are used to collect information from the 450 nm, 532 nm and 640 nm wavelenghts.

An experimental setup has been built and tested in a fully accessible optical engine. This approach allowed the synchronous use of other optical diagnostic tools such as high-speed imaging, which are not typically available in an all-metal engine, alongside the eTCM input and output data. The engine testing conditions were selected such as to provide a representative sample of optical signals where mixed conditions, with and without blue-flame interference, are present.

The second part of the dissertation concentrates on eTCM as it attempts to extend the domain of applicability of the two color method within the area of strong CO continuum interference.

- First, it provides a means of testing the validity of the conventional two-color method, which can be adversely impacted by the blue-flame interference.
- The second goal is to extract additional information regarding the strength of the radiation associated with the CO flame continuum.

Based on empirical observations of the CO continuum behavior and its relationship with the flame temperature as measured by the two-color method, a reconstruction of the source of interference (CO flame radiation continuum) is proposed. The CO flame continuum empirical model required by eTCM has been developed based on the available experimental data.

The evidence presented in this work suggests that eTCM is capable of temperature and soot optical thickness factor correction under medium and strong blue-flame interference without significant impact on the temperature estimation uncertainty.

The classical implementation of the two-color method (TCM) has arguably become the most successful application of optical diagnostics towards the fundamental understanding of the combustion process in practical combustion systems. The small space required for the fiber optic that is used to collect information from the engine’s cylinder it is a clear advantage. The optical probe could be further miniaturized and used with the proposed extended two-color method (eTCM) as a tool for engine development and calibration.

6.2 Future work

Perhaps the most important direction for future work stemming from the current research is the fundamental investigation and further development of the CO-flame continuum radiation intensity model. The current model relies on empirical data from a relatively small dataset.

The optical engine used in this work is arguably not the best platform to perform such work, which is the main reason why no such attempt has been made at this time. However, other reactors, such as a constant volume optically accessible reactor or a rapid compression machine could provide such data without the confounding effects typically associated with a moving piston. As the pressure effects are not expected to be significant, experimental setups using stationary atmospheric pressure flames could also provide valuable data. Early work by Gaydon and others described briefly the spectral intensity behavior of CO flames, but additional work is required to build a model with accurate predictive capabilities.

Should a reliable CO-flame continuum model become available through such fundamental work, the author envisions the use of such a model for the direct determination of in-cylinder temperatures in absence of soot clouds. The benefits of such a technique are obvious, as it would provide a low-effort means to probe the temperature of low-soot formation combustion modes similar to the HCCI strategy.

Last, but not least, is the application of the currently proposed method (eTCM) to various combustion system with particular emphasis on combustion modes characterized by significant amount of blue-flame radiation, such as PCCI, MK, HCCI, RCCI and others.

REFERENCES

[1] Environmental Protection Agency, U.S. *"Overview of Greenhouse Gases"*. Available from: http://www.epa.gov/climatechange/ghgemissions/gases.html

[2] Environmental Protection Agency, U.S. *"Climate Change Science"*. Available from: http://www.epa.gov/climatechange/science/index.html

[3] Burke, P.J. and Nishitateno, S., *"Gasoline prices, gasoline consumption, and new-vehicle fuel economy: Evidence for a large sample of countries".* Energy Economics, 2013. **36**(0): p. 363-370

[4] Chèze, B., Gastineau, P. and Chevallier, J., *"Forecasting world and regional aviation jet fuel demands to the mid-term (2025)".* Energy Policy, 2011. **39**(9): p. 5147-5158

[5] Cohn, S.M., *"Fuel choice and aggregate energy demand in the residential and commercial sectors".* Energy, 1980. **5**(12): p. 1203-1212

[6] Rauch, P. and Gronalt, M., *"The effects of rising energy costs and transportation mode mix on forest fuel procurement costs".* Biomass and Bioenergy, 2011. **35**(1): p. 690-699

[7] Wadud, Z., Graham, D.J. and Noland, R.B., *"Modelling fuel demand for different socio-economic groups".* Applied Energy, 2009. **86**(12): p. 2740-2749

[8] Environmental Protection Agency, U.S. *"Climate change is happening"*. Available from: http://www.epa.gov/climatechange/basics/

[9] Haines, A., McMichael, A.J., Smith, K.R., Roberts, I., Woodcock, J., Markandya, A., Armstrong, B.G., Campbell-Lendrum, D., Dangour, A.D., Davies, M., Bruce, N., Tonne, C., Barrett, M. and Wilkinson, P., *"Public health benefits of strategies to reduce greenhouse-gas emissions: overview and implications for policy makers".* The Lancet, 2009. **374**(9707): p. 2104-2114

[10] Environmental Protection Agency, U.S. (2004) *"Clean Diesel Combustion – Clean, Efficient, and Cost Effective Technology echnology"*.

[11] Burtscher, H., *"Physical characterization of particulate emissions from diesel engines: a review".* Journal of Aerosol Science, 2005. **36**(7): p. 896-932

[12] Clerc, J.C., *"Catalytic diesel exhaust aftertreatment".* Applied Catalysis B: Environmental, 1996. **10**(1–3): p. 99-115

[13] Güthenke, A., Chatterjee, D., Weibel, M., Krutzsch, B., Kočí, P., Marek, M., Nova, I. and Tronconi, E., *"Current status of modeling lean exhaust gas aftertreatment catalysts"*, in *Advances in Chemical Engineering*, B.M. Guy, Editor. 2007, Academic Press. p. 103-283.

[14] Kittelson, D.B., Watts, W.F., Johnson, J.P., Rowntree, C., Payne, M., Goodier, S., Warrens, C., Preston, H., Zink, U., Ortiz, M., Goersmann, C., Twigg, M.V., Walker, A.P. and Caldow, R., *"On-road evaluation of two Diesel exhaust aftertreatment devices".* Journal of Aerosol Science, 2006. **37**(9): p. 1140-1151

[15] Koltsakis, G.C. and Stamatelos, A.M., *"Catalytic automotive exhaust aftertreatment".* Progress in Energy and Combustion Science, 1997. **23**(1): p. 1-39

[16] Kreuzer, T., Lox, E.S., Lindner, D. and Leyrer, J., *"Advanced exhaust gas aftertreatment systems for gasoline and diesel fuelled vehicles".* Catalysis Today, 1996. **29**(1–4): p. 17-27

[17] Miao, Y., Chen, L.-D., He, Y. and Kuo, T.-w., *"Study of SCR cold-start by energy method".* Chemical Engineering Journal, 2009. **155**(1–2): p. 260-265

[18] Rodríguez-Fernández, J., Tsolakis, A., Cracknell, R.F. and Clark, R.H., *"Combining GTL fuel, reformed EGR and HC-SCR aftertreatment system to reduce diesel NOx emissions. A statistical approach".* International Journal of Hydrogen Energy, 2009. **34**(6): p. 2789-2799

[19] Schejbal, M., Štěpánek, J., Kočí, P., Marek, M. and Kubíček, M., *"Sequence of monolithic converters DOC–CDPF–NSRC for lean exhaust gas detoxification: A simulation study".* Chemical Engineering and Processing: Process Intensification, 2010. **49**(9): p. 943-952

[20] Environmental Protection Agency, U.S. *"Fuel Economy - Regulations and Standards"*. Available from: http://www.epa.gov/fueleconomy/regulations.htm

[21] Akagawa, H., Miyamoto, T., Harada, A., Sasaki, S., Shimazaki, N., Hashizume, T. and Tsujimura, K. *"Approaches to Solve Problems of the Premixed Lean Diesel Combustion"*.

[22] Cracknell, R.F., Head, R.A., McAllister, L.J. and Andrae, J.C.G. *"Octane Sensitivity in Gasoline Fuels Containing Nitro-Alkanes: A Possible Means of Controlling Combustion Phasing for HCCI"*.

[23] Kokjohn, S.L. and Reitz, R.D., *"Investigation of charge preparation strategies for controlled premixed charge compression ignition combustion using a variable pressure injection system".* International Journal of Engine Research, 2010. **11(Compendex)**: p. 257-282

[24] Kook, S., Bae, C., Miles, P.C., Choi, D. and Pickett, L.M. *"The Influence of Charge Dilution and Injection Timing on Low-Temperature Diesel Combustion and Emissions"*.

[25] Ladommatos, N., Abdelhalim, S.M., Zhao, H. and Hu, Z. *"The Dilution, Chemical, and Thermal Effects of Exhaust Gas Recirculation on Diesel Engine Emissions - Part 1: Effect of Reducing Inlet Charge Oxygen"*.

[26] Lee, T. and Reitz, R.D., *"The effect of intake boost pressure on MK (Modulated Kinetics) combustion".* JSME International Journal, Series B: Fluids and Thermal Engineering, 2003. **46(Compendex)**: p. 451-459

[27] Musculus, M.P.B. *"Multiple Simultaneous Optical Diagnostic Imaging of Early-Injection Low-Temperature Combustion in a Heavy-Duty Diesel Engine"*.

[28] Plee, S.L., Ahmad, T. and Myers, J.P. *"Flame Temperature Correlation for the Effects of Exhaust Gas Recirculation on Diesel Particulate and NOx Emissions"*.

[29] Ryan, T.W., Callahan, T.J. and Mehta, D. *"HCCI in a Variable Compression Ratio Engine-Effects of Engine Variables"*.

[30] Sjoberg, M. and Dec, J.E., *"Ethanol Autoignition Characteristics and HCCI Performance for Wide Ranges of Engine Speed, Load and Boost".* SAE Int. J. Engines, 2010. **3**(1): p. 84-106

[31] Splitter, D., Hanson, R., Kokjohn, S. and Reitz, R. *"Reactivity Controlled Compression Ignition (RCCI) Heavy-Duty Engine Operation at Mid-and High-Loads with Conventional and Alternative Fuels"*. SAE 2011-01-0363

[32] Walter, B. and Gatellier, B. *"Development of the High Power NADI™ Concept Using Dual Mode Diesel Combustion to Achieve Zero NOx and Particulate Emissions"*.

[33] Abu-Jrai, A., Rodríguez-Fernández, J., Tsolakis, A., Megaritis, A., Theinnoi, K., Cracknell, R.F. and Clark, R.H., *"Performance, combustion and emissions of a diesel engine operated with reformed EGR. Comparison of diesel and GTL fuelling".* Fuel, 2009. **88**(6): p. 1031-1041

[34] Fang, Q., Fang, J., Zhuang, J. and Huang, Z., *"Influences of pilot injection and exhaust gas recirculation (EGR) on combustion and emissions in a HCCI-DI combustion engine".* Applied Thermal Engineering, 2012. **48**(0): p. 97-104

[35] Hountalas, D.T., Mavropoulos, G.C. and Binder, K.B., *"Effect of exhaust gas recirculation (EGR) temperature for various EGR rates on heavy duty DI diesel engine performance and emissions".* Energy, 2008. **33**(2): p. 272-283

[36] Hussain, J., Palaniradja, K., Alagumurthi, N. and Manimaran, R., *"Effect of Exhaust Gas Recirculation (EGR) on Performance and Emission characteristics of a Three Cylinder Direct Injection Compression Ignition Engine".* Alexandria Engineering Journal, 2012. **51**(4): p. 241-247

[37] Ishida, M., Yamamoto, S., Ueki, H. and Sakaguchi, D., *"Remarkable improvement of NOx–PM trade-off in a diesel engine by means of bioethanol and EGR".* Energy, 2010. **35**(12): p. 4572-4581

[38] Maiboom, A., Tauzia, X. and Hétet, J.-F., *"Experimental study of various effects of exhaust gas recirculation (EGR) on combustion and emissions of an automotive direct injection diesel engine".* Energy, 2008. **33**(1): p. 22-34

[39] Peng, H., Cui, Y., Shi, L. and Deng, K., *"Effects of exhaust gas recirculation (EGR) on combustion and emissions during cold start of direct injection (DI) diesel engine".* Energy, 2008. **33**(3): p. 471-479

[40] Saravanan, N. and Nagarajan, G., *"An experimental investigation on performance and emissions study with port injection using diesel as an ignition source for different EGR flow rates".* International Journal of Hydrogen Energy, 2008. **33**(16): p. 4456-4462

[41] Shi, L., Cui, Y., Deng, K., Peng, H. and Chen, Y., *"Study of low emission homogeneous charge compression ignition (HCCI) engine using combined internal and external exhaust gas recirculation (EGR)".* Energy, 2006. **31**(14): p. 2665-2676

[42] Tsolakis, A., Megaritis, A., Wyszynski, M.L. and Theinnoi, K., *"Engine performance and emissions of a diesel engine operating on diesel-RME (rapeseed methyl ester) blends with EGR (exhaust gas recirculation)".* Energy, 2007. **32**(11): p. 2072-2080

[43] Ying, W. and Longbao, Z., *"Experimental study on exhaust emissions from a multi-cylinder DME engine operating with EGR and oxidation catalyst".* Applied Thermal Engineering, 2008. **28**(13): p. 1589-1595

[44] Zamboni, G. and Capobianco, M., *"Experimental study on the effects of HP and LP EGR in an automotive turbocharged diesel engine".* Applied Energy, 2012. **94**(0): p. 117-128

[45] Zhang, W., Chen, Z., Li, W., Shu, G., Xu, B. and Shen, Y., *"Influence of EGR and oxygen-enriched air on diesel engine NO–Smoke emission and combustion characteristic".* Applied Energy, 2013. **107**(0): p. 304-314

[46] Arcoumanis, C., Bae, C., Nagwaney, A. and Whitelaw, J.H. *"Effect of EGR on Combustion Development in a 1.9L DI Diesel Optical Engine"*.

[47] Environmental Protection Agency, U.S. *"Emission Standards Reference Guide"*. Available from: http://www.epa.gov/otaq/standards/heavy-duty/hdci-exhaust.htm

[48] Beasley, M., Cornwell, R., Fussey, P., King, R., Noble, A., Salamon, T., Truscott, A. and Landsmann, G. *"Reducing Diesel Emissions Dispersion by Coordinated Combustion Feedback Control"*.

[49] Colban, W.F., Kim, D., Miles, P.C., Oh, S., Opat, R., Krieger, R., Foster, D., Durrett, R.P., Manuel, A. and Gonzalez, D., *"A Detailed Comparison of Emissions and Combustion Performance Between Optical and Metal Single-Cylinder Diesel Engines at Low Temperature Combustion Conditions".* SAE Int. J. Fuels Lubr., 2008. **1**(1): p. 505-519

[50] Shiozaki, T., Nakajima, H., Kudo, Y., Miyashita, A. and Aoyagi, Y. *"The Analysis of Combustion Flame Under EGR Conditions in a DI Diesel Engine"*.

[51] Clowater, L., Hamady, F. and Schock, H. *"Fiber Optic Imaging System for Remote Location Flow Visualization Studies"*.

[52] Hall, M.J., Zuzek, P. and Anderson, R.W. *"Fiber Optic Sensor for Crank Angle Resolved Measurements of Burned Gas Residual Fraction in the Cylinder of an SI Engine"*.

[53] He, G., Patania, A., Kluzner, M., Vokovich, D., Astrakhan, V., Wall, T. and Wlodarczyk, M. *"Low-Cost Spark Plug-Integrated Fiber Optic Sensor for Combustion Pressure Monitoring"*.

[54] Jie, M.-S., Lee, S.-H. and Lee, K.-H. *"Flame Propagation Measurement By the Fiber Optic Spark Plug and Ionization Probe"*.

[55] Kawa, T., Ishikawa, T., Yanagihara, S., Koyama, T. and Tsuchiya, K. *"Characteristic of Fiber-Optic Pressure Sensor for Measuring Cylinder Pressure"*.

[56] Kawahara, N., Tomita, E., Ichimiya, M., Takasu, K., Tsuchida, N. and Goto, K. *"Transient Temperature Measurement of Unburned Gas in an Engine Cylinder Using Laser Interferometry with a Fiber-Optic Sensor"*.

[57] Kawahara, N., Tomita, E. and Kamakura, H. *"Transient Temperature Measurement of Gas Using Fiber Optic Heterodyne Interferometry"*.

[58] Kawahara, N., Tomita, E., Ohnishi, K. and Goto, K. *"In-situ Unburned Gas Temperature Measurement in a Spark Ignition Engine Using Laser Interferometry"*.

[59] Lan, C., Caswell, A.W., Kranendonk, L.A., Sanders, S.T., Urata, Y. and Okura, Y. *"19-Color H2O Absorption Spectrometer Applied for Real-Time In-Cylinder Gas Thermometry in an HCCI Engine"*.

[60] Lee, C., Kawahara, N., Tomita, E. and Inoshita, K. *"Gas Temperature Measurement in a DME-HCCI Engine using Heterodyne Interferometry with Spark-Plug-in Fiber-Optic Sensor"*.

[61] Miguel, J. and Higuera, L., *"Handbook of optical fiber sensing technology"*. 2002, West Sussex PO 19 IUD, England: John Wiley & Sons Ltd

ISBN:

[62] Murray, R.T., Cox, E.R., Smith, D.E. and Wright, P.G. *"Fibre Optic Sensors for Automobiles"*.

[63] Nwagboso, C. *"Condition Monitoring of CNG Engine Using Optic Fiber Sensory Systems"*.

[64] Pendlebury, M.A. and Nwagboso, C. *"Fiber Optic Sensors for Engine Combustion Intensity Detection-A Review"*.

[65] Poorman, T.J., Xia, L. and Wlodarczyk, M.T. *"Ignition System-Embedded Fiber-Optic Combustion Pressure Sensor for Engine Control and Monitoring"*.

[66] Roth, K.J., Sobiesiak, A., Robertson, L. and Yates, S. *"In-Cylinder Pressure Measurements with Optical Fiber and Piezoelectric Pressure Transducers"*.

[67] Witze, P.O., Hall, M.J. and Wallace, J.S. *"Fiber-Optic Instrumented Spark Plug for Measuring Early Flame Development in Spark Ignition Engines"*.

[68] Ulrich, O., Wlodarczyk, R. and Wlodarczyk, M.T. *"High-Accuracy Low-Cost Cylinder Pressure Sensor for Advanced Engine Controls"*.

[69] Wlodarczyk, M.T. *"High Accuracy Glow Plug-Integrated Cylinder Pressure Sensor for Closed Loop Engine Control"*. Paper

[70] Wlodarczyk, M.T., Poorman, T., Xia, L., Arnold, J. and Coleman, T., *"In-Cylinder Fiber-Optic Pressure Sensors for Monitoring and Control of Diesel Engines".* 1998

[71] Heywood, J.B., *"Internal combustion engine fundamentals"*. 1988. ISBN:

[72] US, D.o.E., *"Annual Energy Outlook"*. 2006.

[73] U.S. Energy Information Administration. *"U.S. Primary energy consumption by source and sector"*. 2011; Available from: http://www.eia.gov/energyexplained/

[74] Singh, G. *"Overview of the DOE Advanced Combustion Engine R&D"*. 2011; Available from: http://www1.eere.energy.gov/vehiclesandfuels/pdfs/merit_review_2011/adv_combustion/ace00a_singh_2011_o.pdf

[75] Aronsson, U., Chartier, C., Horn, U., Andersson, Ö., Johansson, B. and Egnell, R. *"Heat Release Comparison Between Optical and All-Metal HSDI Diesel Engines"*.

[76] Zhao, H.L., Nicos, *"Engine combustion instrumentation and diagnostics"*. 2001. ISBN: ISBN: 0-7680-0665-1

[77] Steeper, R.R. and Stevens, E.J. *"Characterization of Combustion, Piston Temperatures, Fuel Sprays, and Fuel-Air Mixing in a DISI Optical Engine"*.

[78] De Zilwa, S. and Steeper, R. *"Acquisition of Corresponding Fuel Distribution and Emissions Measurements in HCCI Engines"*.

[79] Higuma, A., Suzuki, T., Yoshida, M., Oguri, Y. and Minoyama, T. *"Improvement of Error in Piezoelectric Pressure Transducer"*.

[80] Rai, H.S., Brunt, M.F.J. and Loader, C.P. *"Quantification and Reduction of IMEP Errors Resulting from Pressure Transducer Thermal Shock in an S.I. Engine"*.

[81] Lee, S., Bae, C., Prucka, R., Fernandes, G., Filipi, Z.S. and Assanis, D.N. *"Quantification of Thermal Shock in a Piezoelectric Pressure Transducer"*.

[82] Patterson, G.J. and Davis, R.S., *"Geometric and Topological Considerations to Maximize Remotely Mounted Cylinder Pressure Transducer Data Quality".* SAE Int. J. Engines, 2009. **2**(1): p. 414-420

[83] Gringer. *"Optical fibre"*. 2008; Available from: http://en.wikipedia.org/wiki/File:Optical-fibre.svg

[84] Yan, J. and Borman, G.L., *"Analysis and In-Cylinder Measurement of Particulate Radiant Emissions and Temperature in a Direct Injection Diesel Engine"*, in *Reprint: Analysis and In-Cylinder Measurement of Particulate Radiant Emissions and Temperature in a Direct Injection Diesel Engine,.* 1988: United States. p. 25p.

[85] Hottel, H.C. and Broughton, F.P., *"Determination of true temperature and total radiation from luminous gas flames".* Industrial and Engineering Chemistry -- Analytical Edition, 1932. **4**(2): p. 166-175

[86] Shakal, J.S. and Martin, J.K. *"Imaging and Spatially Resolved Two-Color Temperature Measurements Through a Coherent Fiberoptic: Observation of Auxiliary Fuel Injection Effects on Combustion in a Two-Stroke DI Diesel"*.

[87] Li, X. and Wallace, J.S. *"In-Cylinder Measurement of Temperature and Soot Concentration Using the Two-Color Method"*.

[88] Struwe, F.J. and Foster, D.E., *"In-Cylinder Measurement of Particulate Radiant Heat Transfer in a Direct Injection Diesel Engine".* SAE 2003-01-0072, 2003

[89] AVL. *"Visiolution - Optical Combustion Analysis Systems"*. 2009; Available from: https://www.avl.com/visiolution-optical-combustion-analysis-systems

[90] Gaydon, A.G., *"The spectroscopy of flames"*. 1974, London; New York: Chapman and Hall; Halsted Press Division, Wiley. ISBN: 0470294337 9780470294338

[91] Zizak, G., *"Flame Emission Spectroscopy: Fundamentals and Applications"*. 2000.

[92] Peters, N., *"Combustion Theory"*. 2010, CEFRC Summer School Princeton.

[93] Uyehara, O.A., Myers, P.S., Watson, K.M. and Wilson, L.A., *"Flame-temperature measurement in internal-combustion engines".* American Society of Mechanical Engineers -- Transactions, 1946. **68**(1): p. 17-28

[94] Zhao, H. and Ladommatos, N., *"Optical diagnostics for soot and temperature measurement in diesel engines".* Progress in Energy and Combustion Science, 1998. **24**(3): p. 221-255

[95] Matsui, Y., Kamimoto, T. and Matsuoka, S. *"A Study on the Time and Space Resolved Measurement of Flame Temperature and Soot Concentration in a D. I. Diesel Engine by the Two-Color Method"*.

[96] Matsui, Y., Kamimoto, T. and Matsuoka, S. *"A Study on the Application of the Two–Color Method to the Measurement of Flame Temperature and Soot Concentration in Diesel Engines"*.

[97] Yu, X., Zha, K., Florea, R. and Jansons, M., *"Comparison of In-Cylinder Soot Evolution in an Optically Accessible Engine Fueled with JP-8 and ULSD".* SAE Int. J. Fuels Lubr., 2012. **5**(2): p. 875-891

[98] Zha, K., Florea, R.-C. and Jansons, M. *"Comparison of soot evolution using high-speed CMOS color camera and two-color thermometry in an optical diesel engine fueled with B20 biodiesel blend and ultra-low sulfur diesel"*. in *ASME 2011 Internal Combustion Engine Division Fall Technical Conference, ICEF 2011, October 2, 2011 - October 5, 2011*. 2011. Morgantown, WV, United states: American Society of Mechanical Engineers

[99] Zha, K., Yu, X., Florea, R. and Jansons, M. *"Impact of Biodiesel Blends on In-cylinder Soot Temperature and Concentrations in a Small-Bore Optical Diesel Engine"*.

[100] Hampson, G.J. and Reitz, R.D. *"Two-Color Imaging of In-Cylinder Soot Concentration and Temperature in a Heavy-Duty DI Diesel Engine with Comparison to Multidimensional Modeling for Single and Split Injections"*.

[101] Musculus, M.P.B. *"Measurements of the Influence of Soot Radiation on In-Cylinder Temperatures and Exhaust NOx in a Heavy-Duty DI Diesel Engine"*.

[102] Bertoli, C., Beatrice, C., di Stasio, S. and Del Giacomo, N. *"In-Cylinder Soot and NOx Concentration Measurements in D.I. Diesel Engine Fed by Fuels of Varying Quality"*.

[103] Bakenhus, M. and Reitz, R.D. *"Two-Color Combustion Visualization of Single and Split Injections in a Single-Cylinder Heavy-Duty D.I. Diesel Engine Using an Endoscope-Based Imaging System"*.

[104] Kobayashi, S., Sakai, T., Nakahira, T., Komori, M. and Tsujimura, K. *"Measurement of Flame Temperature Distribution in D.I. Diesel Engine with High Pressure Fuel Injection"*.

[105] Miyamoto, N., Ogawa, H., Arima, T. and Miyakawa, K. *"Improvement of Diesel Combustion and Emissions with Addition of Various Oxygenated Agents to Diesel Fuels"*.

[106] Winterbone, D.E., Yates, D.A., Clough, E., Rao, K.K., Gomes, P. and Sun, J.H., *"Combustion in high-speed direct injection diesel engines - A comprehensive study".* Proceedings of the Institution of Mechanical Engineers, Part C: Journal of Mechanical Engineering Science, 1994. **208**(4): p. 223-239

[107] Clark, G.L. and Thee, W.C., *"Ultra-Violet Spectroscopy of Flames of Motor Fuels".* INDUSTRIAL AND ENGINEERING CHEMISTRY, 1926. **18**(5): p. 528~531

[108] Pipenberg, K.J. and Pahnke, A.J., *"Spectrometric Investigations of n-Heptane Preflame Reactions in a Motored Engine".* Industrial & Engineering Chemistry, 1957. **49**(12): p. 2067-2072

[109] Ohta, Y. and Furutani, M., *"Identification of cool and blue flames in compression ignition".* Archivum Combustiones, 1991. **11**(1~2): p. 43-52

[110] Lawn, C.J., *"Distributions of instantaneous heat release by the cross-correlation of chemiluminescent emissions".* Combustion and Flame, 2000. **123**(1–2): p. 227-240

[111] Griffiths, J.F. and Whitaker, B.J., *"Thermokinetic interactions leading to knock during homogeneous charge compression ignition".* Combustion and Flame, 2002. **131**(4): p. 386-399

[112] Yao, M.-f., Zheng, Z.-l. and Liang, X. *"Numerical Study on the Chemical Reaction Kinetics of DME/Methanol for HCCI Combustion Process"*.

[113] Arcoumanis, C., Bae, C., Crookes, R. and Kinoshita, E., *"The potential of di-methyl ether (DME) as an alternative fuel for compression-ignition engines: A review".* Fuel, 2008. **87**(7): p. 1014-1030

[114] Kopp, M., Brower, M., Mathieu, O., Petersen, E. and Güthe, F., *"CO*2 chemiluminescence study at low and elevated pressures".* Applied Physics B, 2012

[115] Hottel, H.C., *"Heat Transmission 3rd ed"*, ed. McGraw-Hill. 1954. ISBN:

[116] Siegel, R. and Howell, J.R., *"Thermal Radiation Heat Transfer 3rd edition"*. 1992. ISBN: 0-89116-271-2

[117] Siddall, R.G. and McGrath, I.A., *"The emissivity of luminous flames".* Symposium (International) on Combustion, 1963. **9**(1): p. 102-110

[118] Wahiduzzaman, S., Morel, T., Timar, J. and DeWitt, D.P. *"Experimental and Analytical Study of Heat Radiation in a Diesel Engine"*.

[119] Matsui, Y., Kamimoto, K. and Matsuoka, S. *"A Study on the Time and Space Resolved Measurement of Flame Temperature and Soot Concentration in a Diesel Engine by the Two-Colour Method"*. 790491

[120] Matsui, Y., Kamimoto, K. and Matsuoka, S. *"A Study on the Application of the Two-Colour Method to the Measurement of Flame Temperature and Soot Concentration in Diesel Engines"*. 800970

[121] Yan, J. and Borman, G. *"Analysis and In-Cylinder Measuremnt of Particulate Radiant Emissions and Temperature in a Direct Injection Diesel Engine"*. 881315

[122] Ocean Optics. *"74-UV Collimating lens"*. 2012; Available from: http://www.oceanoptics.com/Products/74series.asp

[123] Edmund Optics. *"UV Fused Silica Plano-Convex (PCX) Lenses"*. 2012; Available from: http://www.edmundoptics.com/optics/optical-lenses/uv-lenses/uv-fused-silica-plano-convex-pcx-lenses/2027

[124] Edmund Optics. *"Dichroic Plate Beamsplitters"*. 2012; Available from: http://www.edmundoptics.com/optics/beamsplitters/plate-beamsplitters/dichroic-plate-beamsplitters/2516

[125] Thorlabs. *"Bandpass Filters"*. 2012; Available from: http://www.thorlabs.com/newgrouppage9.cfm?objectgroup_id=1001

[126] Hamamatsu. *"Photomultiplier Tubes"*. 2012; Available from: http://sales.hamamatsu.com/en/products/electron-tube-division/detectors/photomultiplier-tubes.php

[127] Matlab, *"The language of technical computing".* 1999. **No. 5**

[128] Gaydon, A.G. and Guedeney, F., *"Effect of preheating on the spectra of carbon monoxide diffusion flames".* Transactions of the Faraday Society, 1955. **51**(0): p. 894-900

[129] Kaskan, W.E., *"The source of the continuum in carbon monoxidehydrogen-air flames".* Combustion and Flame, 1959. **3**(0): p. 39-48

[130] Available from: http://www.gaussian.com/

[131] Jansons, M., Brar, A., Estefanous, F., Florea, R., Taraza, D., Henein, N. and Bryzik, W. *"Experimental Investigation of Single and Two-Stage Ignition in a Diesel Engine"*.

[132] Florea, R., *"Optical investigation of ethanol and n-heptane dual-fuel partially premixed combustion in a reciprocating engine"*, in *Mechanical Engineering*. 2012, Wayne State University: Detroit.

[133] Träger, F., *"Springer Handbook of Lasers and Optics"*. 2006: Springer, New York. ISBN: 9780387955797

[134] Taylor, W.E., *"Correlation of the Mohs's scale of hardness with the Vickers' s hardness numbers".* Mineralogical Magazine, 1949. **28**: p. 718

[135] Brown, B. *"catool - Combustion Analysis Tool - User Guide"*. 2010; Available from: http://catool.org

[136] Mueller, C.J., Boehman, A.L. and Martin, G.C., *"An Experimental Investigation of the Origin of Increased NOx Emissions When Fueling a Heavy-Duty Compression-Ignition Engine with Soy Biodiesel".* SAE Int. J. Fuels Lubr., 2009. **2**(1): p. 789-816

[137] O'Connor, J. and Musculus, M., *"Post Injections for Soot Reduction in Diesel Engines: A Review of Current Understanding".* SAE Int. J. Engines, 2013. **6**(1): p. 400-421

[138] O'Connor, J. and Musculus, M., *"Optical Investigation of the Reduction of Unburned Hydrocarbons Using Close-Coupled Post Injections at LTC Conditions in a Heavy-Duty Diesel Engine".* SAE Int. J. Engines, 2013. **6**(1): p. 379-399

ABSTRACT

EXPERIMENTAL INVESTIGATION AND DEVELOPMENT OF AN EXTENDED TWO COLOR METHOD (eTCM) WITH APPLICATION TO INTERNAL COMBUSTION ENGINES

by

ELENA FLOREA

August 2013

Advisor: Dr. Dinu Taraza

Major: Mechanical Engineering

Degree: Doctor of Philosophy

The internal combustion engine is on a continuous path of improvement to reduce exhaust gaseous emissions and improve fuel economy. While recent trends in diesel engine development have lowered the EGR requirements, future regulatory pressure will likely result in a reversed trend in the future.

Given this, it is of interest to improve the application range of diagnostic tools such as the two color method (TCM) typically used in evaluating the properties of engine soot, such as temperature and volume fraction. This optical diagnostic method relies on the use of the light emitted by the soot particles along with a soot emissivity model in order to estimate the temperature T and optical thickness KL characterizing the soot cloud of interest. This assumption is reasonable for the "traditional" diesel combustion, where low degrees of premixed combustion result in very low amounts of blue-flame light emission compared to the soot related radiation. However, for LTC (low temperature combustion) combustion modes this assumption is no longer applicable, especially for combustion strategies characterized by very large premixed combustion phases, such as the Partially-premixed Charge Compression Ignition (PCCI) strategies.

The aim is to obtain more information related to the combustion process and specifically on the soot formation and oxidation process. For this reason, the present research can be divided in two major sections.

The first section focuses on the development of a combustion optical probe and the optical experimental setup necessary for conducting the experimental work. Information regarding the soot formation and oxidation processes may be inferred from the measured signal.

The objective of the second section of the current research is to provide the theoretical background and experimental evidence needed to describe the proposed optical diagnostic tool, the extended two-color method (eTCM). This method attempts to extend the domain of applicability of the classical two color method within the area of strong CO continuum interference as well as providing a method of testing the validity of the conventional two-color method. Further, it provides additional information regarding the strength of the radiation associated with the CO flame continuum.

Towards this goal, the work was conducted on a fully accessible optical engine, which allowed the use of multiple synchronous optical measurements targeted towards the evaluation of the proposed optical diagnostic tool.

The evidence presented in this work suggests that eTCM is capable of temperature and soot optical thickness factor correction under medium and strong blue-flame interference without significant impact on the temperature estimation uncertainty.

Consequently, the currently proposed extended two-color method (eTCM) has the potential for a large-scale impact in the fields of fundamental engine research as well as engine development and calibration.

AUTOBIOGRAPHICAL STATEMENT

Most people can tell you that ever since they were children they wanted to be a teacher or an actor or a doctor. For me it was different, it was a process of discovery. I have not chosen engineering as much as it has chosen me. It was a part of me from the beginning and it started showing in high school when I was more interested in mathematics and physics.

It came naturally for me to continue my education by following a mechanical engineering undergraduate program at Transylvania University of Brasov, Romania and opting for the automotive engineering major.

Towards the end of my undergraduate studies, I received a scholarship at Rheinisch-Westfälische Technische Hochschule Aachen, Germany where I spent the semester working on my graduation thesis. I had the opportunity of working on a “hands on” project that concentrated on upgrading an existing diesel engine to be in conformity with the specifications and regulations for mining applications.

After I graduated from college I knew I didn’t want to bring my education to an end. I was very lucky to receive the position of graduate research assistant at Wayne State University in Detroit, USA. Under the guidance of wonderful professors I started my PhD program working on diesel engines in the Center for Automotive Research group. The research was stimulating and involved working with biofuels on an all metal diesel engine as well as on an optically accessible diesel engine.

On the whole, I look back from where I started, a small town in Romania, and I realize how lucky I was to meet the right people at the right time. They gave me the opportunity to discover what I like and what is a part of me: engineering. I am looking at the future and I am thrilled for the next step in my career as an engineer.